



Spectroscopic Factors with Coupled-Cluster  
Connecting *ab initio* Nuclear Structure to Reactions

Dissertation for the degree of  
philosophiae doctor (PhD)

Øyvind Jensen

November 2, 2010

# Acknowledgements

I would like to thank my advisors Jan S. Vaagen and Gaute Hagen for inspiring discussions and good guidance. During the project I had three visits to Oak Ridge National Laboratory, and spent altogether five months there. For each visit I had a major breakthrough in the particular challenges I was working on, as well as in my own personal understanding of nuclear physics. This happened because of the excellent people at the Physics Division of ORNL, in particular my co-advisor Gaute Hagen, Thomas Papenbrock and David Dean. I am also thankful that they allowed me to use their optimized computer codes, and allocated computer resources.

In november 2008 I moved to Oslo with my family for personal reasons, and I feel greatly indebted to Morten Hjorth-Jensen at the University of Oslo, who offered me a desk, a handful of colleagues, and invited me to take part in the day-to-day activities of his group. The nuclear many-body physics group at the University of Oslo is under the inspiring and ambitious lead of Morten Hjorth-Jensen. It is a very good place to be for a PhD student. I would like to thank my office mates Gustav Jansen and Elise Bergli for fruitful discussions and inspired theory investigations.

Most importantly, I thank my wife, Iselin, for all that she has sacrificed over the last year in order to support me in completing this thesis. Finally, I thank my family (in law as well as in biology) and all friends that have supported me in the long, tough endeavour this has been.

## Abstract

This thesis has two parts. Tools and theory are presented in the first part, and papers with specific applications to nuclear physics are collected in the second part.

A synopsis of theoretical foundations and basic techniques for many body quantum physics is presented in the context of a computer implementation of Wick's theorem for the symbolic algebra system SymPy. A pedagogical introduction to the implemented Python module is presented, and non-trivial aspects of the implemented simplification algorithms are discussed. Computer aided manipulations of second quantization expressions relieves practitioners of laborious and error-prone hand calculations necessary for the derivation of programmable equations.

Theoretical developments of the Coupled-Cluster method (CCM) at Singles-and-Doubles level (CCSD) for the calculation of spectroscopic factors (SF) and radial overlap functions are presented. Algebraic expressions are derived from novel diagram techniques. CCM is one of the most successful methods for accurate numerical quantum mechanical simulations of medium sized many-body systems studied within Chemistry and Nuclear Physics.

The recently developed spherical formulation of CCM is presented and alternative coupling schemes of quantum mechanical angular momentum are discussed in the context of a computer implementation for Racah algebra with SymPy. A pedagogical introduction to this functionality is given and it is used to derive angular momentum coupled expressions for efficient calculation of the spectroscopic factor diagrams.

The first research paper presents a calculation of spectroscopic factors with CCSD. Details of the calculation is presented and convergence properties, as well as the dependence on various model parameters are discussed. Interactions with different cut-offs are employed and the dependence of the SF on the interactions are studied.

In the second paper we employ the angular momentum coupled SF expressions and the spherical formulation of CCM to study the shell closure properties of the neutron rich drip line nucleus  $^{24}\text{O}$ . The article can partly be seen as a response to recent measurements on the isotope and indications that it may be a closed shell nucleus, which would imply a shift of magic numbers near the drip line.

# Contents

<b>1</b>	<b>Introduction</b>	<b>1</b>
1.1	Theoretical Nuclear Physics of Tomorrow . . . . .	1
1.2	Precision and Complexity . . . . .	2
1.3	<i>Ab initio</i> Reactions . . . . .	4
1.4	Outline . . . . .	5
<b>I</b>	<b>Tools and Theory</b>	<b>6</b>
<b>2</b>	<b>Techniques for Nuclear Structure</b>	<b>7</b>
2.1	Quantum Mechanical Description of the Nucleus . . . . .	7
2.1.1	The Fock Space . . . . .	9
2.2	Second Quantization . . . . .	10
2.2.1	The general Hamiltonian in Second Quantization . . . . .	11
2.2.2	Wavefunctions in Second Quantization . . . . .	12
2.2.3	Second Quantization Techniques . . . . .	13
2.2.4	Computer aided Wick's Theorem . . . . .	15
2.3	Second Quantization Algebra with SymPy . . . . .	15
2.3.1	Example: Normal Ordering of the Hamiltonian . . . . .	16
2.3.2	Simplification Strategies . . . . .	18
2.3.3	Implementation in SymPy . . . . .	20
<b>3</b>	<b>Overlap Functions and Spectroscopic Factors</b>	<b>24</b>
3.1	Overlaps in Reaction models . . . . .	24
3.2	Overlap Functions . . . . .	25
3.3	Spectroscopic Factors . . . . .	26
3.3.1	Overlaps in Second Quantization . . . . .	27
3.3.2	Choice of Overlap Definition . . . . .	29
3.4	Non-Hermitian Models . . . . .	30
3.4.1	Spectroscopic Factors . . . . .	30
3.4.2	Radial Overlap Functions . . . . .	31

<b>4</b>	<b>Spectroscopic Factors with Coupled-Cluster</b>	<b>32</b>
4.1	Overview	32
4.1.1	Size Extensivity	33
4.2	Synopsis of the Coupled-Cluster Method	34
4.2.1	Variational Properties	36
4.2.2	Diagram Techniques	36
4.3	Equations-of-Motion Coupled-Cluster (EOM-CC)	38
4.3.1	The Right Eigenvalue Problem	38
4.3.2	The Dual Solutions	40
4.3.3	Particle Removal	41
4.3.4	Normalization	41
4.4	Spectroscopic Factors with Coupled-Cluster	41
4.4.1	Similarity Transformed Operators	42
4.4.2	Diagrams For Spectroscopic Factors	45
<b>5</b>	<b>The Spherical Coupled-Cluster Method</b>	<b>47</b>
5.1	Principles behind the Spherical Coupled-Cluster Formalism	48
5.1.1	Internal Structure of the Amplitudes	48
5.1.2	Factorization of the Geometrical Structure	50
5.1.3	Angular Momentum Coupling of CCM Diagrams	50
5.1.4	Transformation Properties of EOM-CC Operators	52
5.2	Racah Algebra with SymPy	52
5.2.1	The <code>racah</code> Module	52
5.2.2	The <code>braket</code> User Interface Module	54
5.2.3	Coupling Alternatives	55
5.3	Coupling of Spectroscopic Factor Diagrams	60
5.3.1	Example: Coupling of $-\frac{1}{2}l_{ab}^{jk}t_{ik}^{ab}r_j$	61
5.3.2	Verification of the Coupled Expressions	67
<b>II</b>	<b>Applications</b>	<b>70</b>
<b>6</b>	<b>Introduction to Papers and Outlook</b>	<b>71</b>
6.1	Paper 1	71
6.2	Paper 2	72
6.3	Outlook	72
6.3.1	Application of the Tools	72
6.3.2	Application to other Nuclei	73
6.3.3	Tighter Connection with Reactions	73
6.3.4	Detailed Analysis of the Center of Mass	73
<b>A</b>	<b>Angular Momentum Definitions</b>	<b>A1</b>
A.1	The Wigner-Eckart Theorem	A1

<b>B</b>	<b>Coupled Spectroscopic Factor Diagrams</b>	<b>B1</b>
B.1	Diagrams on the Form $\langle A - 1   a_i   A \rangle$ . . . . .	B1
B.2	Diagrams on the Form $\langle A - 1   a_a   A \rangle$ . . . . .	B1
B.3	Diagrams on the Form $\langle A   a_a^\dagger   A - 1 \rangle$ . . . . .	B2
B.4	Diagrams on the Form $\langle A   a_i^\dagger   A - 1 \rangle$ . . . . .	B3

# Chapter 1

## Introduction

### 1.1 Theoretical Nuclear Physics of Tomorrow

The future of theoretical nuclear physics looks bright. The great leaps of progress that has been accomplished in the last decade include *ab initio* calculations for systems up to medium mass nuclei, in particular with the Coupled-Cluster method (CCM) [46, 48] and the Auxiliary Field Diffusion Monte Carlo (AFDMC) [38]. Several *ab initio* methods exist to treat small systems up to 13 particles, e.g. Green's Function Monte Carlo (GFMC) [92, 93] and the No Core Shell Model (NCSM) [33, 82, 84, 85, 81, 87]. The Coupled-Cluster method has also been successfully applied in this region [42], and Recently Lattice Effective Field Theory calculations up to  $^{12}\text{C}$  were reported [30, 31]. The smaller the system, the more *ab initio* methods are available. Reference [63] includes benchmark calculations in  $^4\text{He}$  for even more methods.

These methods apply few-body nucleonic interactions in order to model many-body systems of nucleons. The virtue of *ab initio* methods applied to nuclear physics is to reduce the model dependence of computed results. By means of a recipe for systematic improvements, one can distinguish between parameters of technical and physical character. Whereas a theoretical estimate is expected to depend on physical parameters, it should be insensitive to the technical parameters as the systematic improvements are applied. Since a converged *ab initio* result is independent of the employed method, it is essentially a characterization of the chosen interaction. Ultimately, a converged *ab initio* result may provide a rigorous test of the nuclear interaction model and the physical parameters therein.

In parallel to the progress in *ab initio* theory, there has been a substantial development of Effective Field Theories (EFT) with the goal of deriving scale dependent nuclear interactions from Quantum Chromo Dynamics (QCD) [11, 28, 32, 29, 31, 34, 36, 66, 71, 89]. Chiral EFT provides a deterministic way to derive pion-based nucleonic interactions that are consistent with the underlying QCD, and allows systematic improvements and theoretical error estimates. The expected hierarchy of forces, e.g. that two-body forces are more important than three-body forces, arises

naturally in Chiral EFT, and this is essential for the application to methods that aim to describe the nucleus as a quantum mechanical many-body system. The systematics of EFT also invoke confidence when the interactions are extended to regions where experimental data are sparse or non-existent.

The QCD based EFT interactions cannot provide any *true* or *preferred* nucleonic potential. In order to employ EFT, there are choices that must be made about what should be considered relevant degrees of freedom. For chiral EFT one also chooses a radius of convergence in momentum, a power counting scheme and a regularization method. After all such choices have been made, the EFT interactions become predictable in the sense that the mathematical form of every contribution is given. However, it will include parameters that must be fitted to available experimental data. The resulting QCD-based interaction will typically be suitable to describe processes that play out on the energy scale the interaction was created for. A different physical situation may require a separate derivation leading to a different, but equally correct, interaction.

The modern view on the nuclear interaction is that there is no potential in terms of forces between protons and neutrons that is applicable to all questions in nuclear physics. For instance, for a dilute neutron gas, a low momentum, pion-less EFT interaction could be suitable. For a nucleus, on the other hand, even the assumption that it can be modelled in terms of protons and neutrons, is a bold statement about nature. From simple order-of-magnitude estimates, there are good reasons to expect nucleonic excitations and production of pions to occur frequently in the typical nucleus [36]. This suggests the use of a Chiral EFT instead. So even if the physics of nuclei to a first approximation can be modelled in terms of cold, pointlike nucleons, it should not come as a surprise that accurate calculations may require an approach where the composite nature of the nucleons is taken into account.

There is an intimate relationship between the two developments, as *ab initio* structure calculations are required in order to test various approaches to the QCD based interactions, and elaborate *ab initio* many-body methods would be pointless without good interaction models. The motion towards EFT interactions is partly driven by the observed need for three-body forces [92], and the fact that EFT provides a well defined, systematic way to obtain them. While e.g. Chiral EFT has three-body forces built in from the start, phenomenological potentials must be extended *ad hoc* with phenomenological three-body forces.

## 1.2 Precision and Complexity

Given these developments, and the continually increasing computer power, it is conceivable that nuclear theory can undergo dramatic changes in the not so distant future. We will most certainly see an increased precision of the *ab initio* methods, and an extension to systems that requires more computational effort. Higher precision in the potentials and deeper understanding of the EFT interactions, that may arise from accumulating experience, could lead to well founded predictions with



estimated error bars. This could lead to a development within theoretical nuclear physics that is similar to what the quantum chemistry community has experienced. Namely, that the increased confidence changes the focus from reproduction of data to predictions of properties. An attempt was made in Reference [48] to predict the stability or instability of  $^{28}\text{O}$  with CCM, but the estimated error bars hindered a decision, and it was concluded that three-body forces, i.e. a higher precision potential, was needed.

The sophisticated methods that are propelling this development are complicated. The goal of increased precision often comes with the cost of increased complexity. For instance, the spherical formulation of CCM, that leads to a speedup of several orders of magnitude [46], introduces a substantial amount of angular momentum algebra. In order to increase precision beyond the Coupled-Cluster Singles-and-Doubles (CCSD) approximation, the complexity grows even more. In this context it is natural to consider alternatives to tedious hand derivations and error-prone code punching in order to obtain a numerical implementation.

In this work we present tools that have been developed in order to automate some of the time consuming steps that are needed to obtain increased precision in the sophisticated models. A Python module for the computer algebra system (CAS) SymPy [1] has been implemented, that allows automatic evaluation of Wick's theorem (See Chapter 2). The framework is general, and freely available in an open source CAS, so this tool should have a wide range of possible applications within the greater many-body physics community.

Another tool that was developed in the course of this project consists of a pair of modules for SymPy that allows efficient manipulations of angular momentum algebra expressions. It was successfully applied to the derivation of expressions for spectroscopic factor diagrams in the spherical formulation of the CCM. It is believed that this tool can provide substantial time savings in two regards: (1) complicated expressions can be derived and simplified in minutes, (2) the result is correct if the input was correct. In comparison, Racah algebra calculations by hand are time consuming and error prone.

A third tool, which is not elsewhere presented in this thesis, but which the author was able to develop with funding from Google inc. under the Google Summer of Code programme 2010, is the code generation features of SymPy. The existing code generation features in SymPy were extended to allow the creation of array based Fortran or C code from mathematical expressions obtained with the CAS. The array based code is suitable for numerical implementations of typical many-body quantum physics equations. This functionality has been used together with the aforementioned Wick's theorem framework, to generate Fortran code for all diagrams that enter the CCSDT approximation for a Hamiltonian with a three-body potential. This is, however, a work in progress.

### 1.3 *Ab initio* Reactions

Another frontier within theoretical nuclear physics is to improve the connection between structure and reaction models. It is desirable to make available detailed information from the sophisticated structure models to reaction simulations. Initial developments of *ab initio* reactions have been undertaken for Quantum Monte Carlo [88] and the NCSM [83, 94, 95].

For the Coupled-Cluster method, the extension towards nuclear reactions is still in its infancy. Calculations that employ Coupled-Cluster with a Berggren basis [42, 50] have demonstrated the ability to model open quantum systems with strong couplings to the continuum. The motivation for the work on spectroscopic factors presented in this thesis, was to make closer contact with reaction theory. It is hoped that the calculation of spectroscopic factors with a sophisticated structure model, such as CCM, can provide useful data on the consistency with various reaction models and experimental data. Also the calculation of *ab initio* overlap functions is derived here, and this makes more detailed structure information available for reaction analysis.

Another approach to *ab initio* spectroscopic factors is the Self-Consistent Green's Function (SCGF) method, which has been applied to calculate spectroscopic factors for  $^{56}\text{Ni}$  towards the neighboring nuclei  $A = 55, 57$ , and for Oxygen and Calcium isotopes [6, 4, 5]. In the SCGF formalism, an explicit calculation of the many-body wave function is avoided, and energies and transition matrix elements are used instead as the degrees of freedom.

It should, however, be noted that spectroscopic factors are model dependent quantities, and not observables [3, 35, 37]. Within the EFT-formalism, short-range nucleon properties are not modelled explicitly, but are instead represented by contact terms in the interaction. The contact terms are subject to a fitting procedure, so the short range dynamics will depend on the employed EFT interaction. Quantities that are sensitive to the short-range part of the wavefunctions, may depend strongly on the choice of interaction. This is why even a fully converged *ab initio* calculation of spectroscopic factors with QCD-based interactions must be considered model dependent. However, spectroscopic factors are useful within the context of a given model.

From an experimental point of view, the spectroscopic factor takes the role of an occupation number. It is extracted from experiment by taking the ratio between the observed cross section, and an idealized reaction model that corresponds to an independent particle description. If the observed reaction rates are weaker than suggested by the simulation, it is interpreted as a partial occupation of the single particle state. The single particle state is then said to be *fragmented* [72].

## 1.4 Outline

This thesis consists of two parts, where we will first discuss the tools that have been developed, and the theoretical investigations necessary to calculate spectroscopic factors with the CCM. Chapter 2 introduces the mathematical foundations for many-body quantum mechanics in the context of an introduction to the Second Quantisation module that was written for SymPy. Also the implementation is discussed in some detail.

Chapter 3 introduces overlap functions in the context of stripping and knock-out reactions, and the spectroscopic factor is defined. Different approaches for the definition of the spectroscopic factor are discussed, and a definition that is valid for non-hermitian models is given. Also an expression for *ab initio* overlap functions is given.

The theoretical developments needed for the calculation of spectroscopic factors with the CCM are presented in Chapter 4. The basic ingredients of the CCM are also presented, and the fundamental property of *size extensivity* is explained and discussed here. The development of diagrammatic techniques to handle spectroscopic factors is presented and all diagrams are listed with the corresponding algebraic interpretations.

The recently developed spherical formulation of the CCM is presented in Chapter 5, and the angular momentum structure in the equations is discussed. The Python implementation of Racah algebra for SymPy is presented and various coupling schemes of angular momentum are discussed. Finally, the angular momentum coupling of the spectroscopic factor diagrams within the CAS are explained, and all coupled diagrams are presented in Appendix B

The second part contains the two research papers that were written during this project. Chapter 6 presents the papers, and the discussion of the articles leads naturally to the last section which is the Outlook.

**Part I**

**Tools and Theory**

## Chapter 2

# Techniques for Nuclear Structure

Nuclear structure calculations deal with the physical situation corresponding to an isolated nucleus, and the goal is to understand how the system organizes itself, and to predict its properties.

This chapter serves two purposes. We introduce a general framework for quantum mechanical treatments of the atomic nucleus, and we discuss some fundamental approaches to mathematical modelling of nuclei. This way we introduce notation, and prepare the reader for the discussion of Coupled-Cluster theory in the next chapter. We also demonstrate a second quantization module that was written for the open source computer algebra system SymPy [1]. We believe that this computer code will be in the interest of the reader as it can be used for automatic derivation of equations in the field of many-body physics.

### 2.1 Quantum Mechanical Description of the Nucleus

We will represent the quantum state  $\psi$  of a single nucleon by a *ket*,  $|\psi\rangle$ , which is an element in a Hilbert space  $\mathcal{H}$ . [96]

Quantum operators like the kinetic energy operator or the position operator are considered as linear transformations mapping kets to kets. For an operator  $T$  that acts on states contained in a Hilbert space  $\mathcal{H}$ , we may write

$$T : \mathcal{H} \rightarrow \mathcal{H}. \quad (2.1)$$

The bra states are hermitian conjugates of the kets, and are elements in a dual Hilbert space,

$$\langle\phi| = |\phi\rangle^\dagger \in \mathcal{H}^\dagger. \quad (2.2)$$

The bra states are operators representing linear transformations that map kets to the complex numbers:

$$\langle\cdot| : \mathcal{H} \rightarrow \mathbb{C}. \quad (2.3)$$

Even if the bra  $\langle\cdot|$  is more correctly regarded as an operator, it is common practice to call it a dual *state*. We will also use this terminology.

### Transformation Properties

Transformation properties are categorized as either covariant or contravariant [97]. The former means that the object in question transforms like the basis, while the latter implies inverse transformation properties [52]. The distinction is necessary in order to ensure that physical quantities are independent of basis, i.e. of the mathematical description, and it will have consequences for the angular momentum recouplings in the spherical Coupled-Cluster scheme discussed in Chapter 5. This is the reason why we address the subject here.

For relativistic quantum mechanics it is necessary to keep track of the contravariance and covariance of states and operators, so it is often built into the notation in the form of upper and lower indices. However, in *non-relativistic* formulations, it is seldom employed a notation that distinguishes the transformation properties. Although it is seldom stated explicitly, the norm is to let kets transform covariant, while bras are prescribed contravariant transformation properties. [52] We will also follow this convention.

The canonical example of the difference in transformation properties is the gradient of a function under a rotation of the coordinate system [2]. An equivalent, and in this context, more relevant example is the inner product under an arbitrary transformation of basis. [52, 97] If we represent a general quantum state by  $|\psi\rangle$  and a general bra state by  $\langle\phi|$ , the inner product is defined as the application of the bra state on the ket,

$$\langle\phi|\psi\rangle \in \mathbb{C}. \quad (2.4)$$

If this quantity is to be associated with some observable, e.g. the probability of a transition from state  $|\psi\rangle$  to  $|\phi\rangle$ , it must be independent of the mathematical representation of the states. That is, it must be independent of the basis set. If we represent a basis transformation by an operator  $T$ , the transformation of  $|\psi\rangle$  is written  $|\psi'\rangle = T|\psi\rangle$ . In order for the inner product to be independent of the basis, the bra must transform as  $\langle\phi'| = \langle\phi|T^{-1}$ . This is the *contravariant* transformation. We can then express the invariance of the inner product as,

$$\langle\phi'|\psi'\rangle = \langle\phi|T^{-1}T|\psi\rangle = \langle\phi|\psi\rangle. \quad (2.5)$$

If the transformation is unitary, i.e.  $T^\dagger = T^{-1}$ , it corresponds to a rotation or a reflection [2, 97].

Since we choose to avoid a notation that signals the variance properties explicitly, a word of warning is in place: The variance of composite quantities can not be inferred straightforwardly from the constituents. For instance, we will frequently employ *completeness relations* on the form

$$\sum_{\alpha} |\psi_{\alpha}\rangle \langle\psi_{\alpha}| = \mathbf{1}. \quad (2.6)$$

Here  $\mathbf{1}$  is an identity operator for a Hilbert space  $\mathcal{H}$ . The completeness relation is a statement that the full set of normalized quantum states labelled by  $\alpha$ , spans

that particular Hilbert space. Since the operator  $|\alpha\rangle\langle\alpha|$  contains both contravariant and covariant quantities, one could be fooled to believe that it should have a mixed variance. However, this is clearly not the case, as the identity operator is an isotropic tensor that must be invariant to basis transformations [97]. With a notation geared towards tensor manipulations (index gymnastics) one would represent the completeness relation differently, so that the invariance would be apparent. [52]

### 2.1.1 The Fock Space

To describe quantum mechanically a system with many particles such as the nucleus, we need mathematical structures capable of representing an arbitrary number of particles in a systematic way. This is provided by the Fock space formalism, which unifies the mathematical treatment of quantum systems that differ in the number of particles. The aim is here to present the underlying concepts, but we refer the reader to Reference [96] for a rigorous mathematical treatment.

To distinguish the Hilbert spaces for systems with different number of particles, we rephrase the completeness relation (2.6) as

$$\sum_p |p\rangle\langle p| = \mathbf{1}^{(1)}. \quad (2.7)$$

We have replaced the general state  $\psi$  with a general *single particle state*  $p$ , and the identity operator has been labelled explicitly as the identity of a single particle Hilbert space  $\mathcal{H}^{(1)}$ .

A general quantum system with  $N$  particles is modelled by a *direct product* of single particle states

$$|\psi^{(N)}\rangle = |p \dots q\rangle \equiv \underbrace{|p\rangle \otimes \dots \otimes |q\rangle}_{N \text{ s.p. states}}. \quad (2.8)$$

These states are elements in the Hilbert space constructed as a Cartesian product of single particle Hilbert spaces,

$$|\psi^{(N)}\rangle \in \mathcal{H}^{(N)} = \mathcal{H}^{(1)} \otimes \dots \otimes \mathcal{H}^{(1)}. \quad (2.9)$$

The corresponding completeness relation is written in terms of the identity operation in  $\mathcal{H}^{(N)}$ ,

$$\sum_{p \dots q} |p \dots q\rangle\langle p \dots q| = \mathbf{1}^{(N)}. \quad (2.10)$$

We will also need the Hilbert space  $\mathcal{H}^{(0)}$ , for systems with no particles at all. It contains only elements that are proportional to the vacuum state  $|\rangle$ , so the vacuum completeness is particularly simple:

$$|\rangle\langle| = \mathbf{1}^{(0)}. \quad (2.11)$$

The Fock space can be constructed as a *direct sum* of the Hilbert spaces for 0, 1, ... particles

$$\mathcal{F} = \mathcal{H}^{(0)} \oplus \mathcal{H}^{(1)} \oplus \dots \oplus \mathcal{H}^{(N)} \oplus \dots, \quad (2.12)$$

and the identity operation is defined as

$$\mathbf{1} = \mathbf{1}^{(0)} \oplus \mathbf{1}^{(1)} \oplus \dots \oplus \mathbf{1}^{(N)} \oplus \dots. \quad (2.13)$$

Also the generalization of the inner product is straightforward. We write two states  $|\psi\rangle, |\phi\rangle \in \mathcal{F}$  as

$$|\psi\rangle = \psi_0 | \rangle + |\psi^{(1)}\rangle + \dots + |\psi^{(N)}\rangle + \dots \quad (2.14)$$

$$|\phi\rangle = \phi_0 | \rangle + |\phi^{(1)}\rangle + \dots + |\phi^{(N)}\rangle + \dots. \quad (2.15)$$

Then, the inner product of the Fock space becomes,

$$\langle \phi | \psi \rangle = \phi_0^* \psi_0 + \langle \phi^{(1)} | \psi^{(1)} \rangle + \dots + \langle \phi^{(N)} | \psi^{(N)} \rangle + \dots. \quad (2.16)$$

We have now introduced the mathematical representation of the quantum states we will use throughout this thesis, as well as the structure of the underlying mathematical spaces. Still, there are more mathematical objects we will need to define in order to present a complete discussion of the nuclear physics calculations in the following chapters.

## 2.2 Second Quantization

We now define operators mapping elements in Hilbert spaces  $\mathcal{H}^{(N)}$  to elements in other Hilbert spaces for states with  $N \pm 1$  particles.

$$a_p^\dagger : \mathcal{H}^{(N)} \rightarrow \mathcal{H}^{(N+1)}, \quad (2.17)$$

$$a_p : \mathcal{H}^{(N)} \rightarrow \mathcal{H}^{(N-1)}. \quad (2.18)$$

Here  $p$  is a label that identifies a particular quantum state. The operators will create or annihilate a particle in configuration  $p$ , respectively, and act like step operators in Fock space. For  $n = 0$  we define

$$a_p : \mathcal{H}^{(0)} \rightarrow 0 \quad \forall p. \quad (2.19)$$

In words, if the annihilation operator acts on the particle vacuum, the resulting wavefunction is identically zero.

We denote the action of annihilation and creation operators as in the following examples:

$$a_p^\dagger a_q^\dagger | \rangle = a_p^\dagger | q \rangle = | pq \rangle, \quad (2.20)$$

$$\langle | a_q a_p = \langle q | a_p = \langle pq |. \quad (2.21)$$



Particles can be added to a bra with annihilation operators. When we add a particle it is always placed at the far left, both in the ket and the bra. This ensures that,

$$|pq\rangle^\dagger = \left( a_p^\dagger a_q^\dagger | \rangle \right)^\dagger = \langle | a_q a_p = \langle pq| . \quad (2.22)$$

The formulation of many body quantum physics in terms of creation and annihilation operators is known as second quantization, or occupation number formalism. We will now briefly sketch the basic principles as they will be used extensively in the discussion of the Coupled-Cluster method in Chapter 4.

### 2.2.1 The general Hamiltonian in Second Quantization

As discussed in Chapter 1, there is no single preferred Hamiltonian in terms of protons and neutrons that applies to every nuclear physics calculation. However, the mathematical form of the Hamiltonian can be discussed in some generality. The Hamiltonian can be expressed in occupation number formalism through the following procedure: We start with a Hamiltonian on the form

$$H = \sum_i H_0(i) + V . \quad (2.23)$$

Here  $H_0(i)$  is a Hamiltonian that defines the motion of a single, independent particle, and  $V$  represents residual interactions between particles.  $H_0$  consists of a kinetic energy term and a common shell model potential, providing a first approximation to the nucleus,

$$H_0 = T_{\text{kinetic}} + U . \quad (2.24)$$

Now, we want to express each term in the Hamiltonian  $H$  as a one- two, or three-body term depending on what the term requires. We derive the second quantization operator expression for  $H_0$  by considering the action of  $H_0$  on one of the single particle states  $|q\rangle$ :

$$H_0 |q\rangle = \sum_p \langle p| H_0 |q\rangle |p\rangle \quad (2.25)$$

$$= \left( \sum_p \langle p| H_0 |q\rangle a_p^\dagger a_q \right) |q\rangle . \quad (2.26)$$

We have multiplied from the left with the single particle completeness relation, and exploited the identity  $|p\rangle = a_p^\dagger a_q |q\rangle$ . The total energy of a many body state must include one-body contributions from every occupied orbit, so the total one-body energy operator must include a sum over  $q$  as well. We generalize (2.26) to:

$$H_0 = \sum_{pq} \langle p| H_0 |q\rangle a_p^\dagger a_q = \sum_{pq} h_q^p a_p^\dagger a_q \quad (2.27)$$

Similarly we get for a two-body potential

$$\hat{V} = \frac{1}{4} \sum_{pqrs} V_{rs}^{pq} a_p^\dagger a_q^\dagger a_s a_r \quad (2.28)$$

We have inserted the fraction  $1/4$  to account for the unrestricted summation. We employ the convention that creation (annihilation) operators correspond to upper (lower) indices of the matrix element symbol.

With these formulas in place we might express the Hamiltonian as a sum of one- and two-body operators, regardless of the number of particles in the system,

$$H = \sum_{pq} h_q^p a_p^\dagger a_q + \frac{1}{4} \sum_{pqrs} V_{rs}^{pq} a_p^\dagger a_q^\dagger a_s a_r. \quad (2.29)$$

Higher order terms involving three or more particle interactions follow exactly the same pattern.

Whitehead & al [106] interprets the Hamilton operator in second quantized form as follows: terms like  $\sum_{pq} h_q^p a_p^\dagger a_q$  removes a particle from orbit  $q$ , and creates a particle in orbit  $p$ . Thus, it represents a *flow of particles*, and the matrix element  $h_{pq}$  determines the rate of that flow. If  $h$  is hermitian,  $h_q^p = h_p^{q*}$ , the flow in each direction is equally strong, and the eigenstates of the system are characterized by the relative direction and strength of these currents. Likewise, the density matrix  $\rho_{rs}^{pq} = \langle \psi | a_p^\dagger a_q^\dagger a_s a_r | \psi \rangle$  measures the matter currents in the particular state  $\psi$ .

### 2.2.2 Wavefunctions in Second Quantization

We demonstrate the representation of wave functions in second quantization with a wave on the form used in the Configuration Interaction (CI) method. This corresponds to the wave functions used in nuclear shell model approaches [70, 21].

Let  $|\phi_0\rangle$  be a reference state, representing a particular configuration of  $N$  particles. Let also the indices  $i, j, k \dots$  refer to occupied orbitals and  $a, b, c, \dots$  to unoccupied (virtual) orbitals. This convention will be used throughout this thesis. An excited state can be created by application of second quantization operators on the reference state,

$$|\phi_i^a\rangle = a_a^\dagger a_i |\phi_0\rangle. \quad (2.30)$$

In this notation, lower indices on  $\phi$  represent orbits of particles that have been removed, while upper indices represent orbits of particles that have been created. We will however focus on the operator form, i.e. on the right hand side of equation (2.30).

The general CI wavefunction can be expressed as a linear combination of particle-hole excitation operators. If we truncate the wavefunction so that we can have at most two particles excited simultaneously, we get the approximation known within quantum chemistry as Configuration-Interaction Singles-and-

Doubles (CISD) [8],

$$|\Psi\rangle = \left( c_0 + \sum_{ia} c_i^a a_a^\dagger a_i + \frac{1}{4} \sum_{ijab} c_{ij}^{ab} a_a^\dagger a_b^\dagger a_j a_i \right) |\phi_0\rangle. \quad (2.31)$$

The scalar coefficients  $c_0$ ,  $c_i^a$ , and  $c_{ij}^{ab}$  are weights defining the full state  $|\Psi\rangle$  as a linear combination of all allowed excitations. The advantage of writing the wave function in terms of the occupation formalism operators is that the action of an operator, such as the Hamiltonian can be evaluated in terms of the second quantization operators. Fermionic operators are subject anti-commutation relations that lead to elegant algebraic techniques, and allow explicit evaluation of the expressions [21, 57, 70].

### 2.2.3 Second Quantization Techniques

An efficient way to evaluate a string of second quantization operators is to use Wick's theorem and normal ordering. We will now discuss these concepts with some attention to detail, in order to prepare the reader for the next section where an implementation of a second quantization module for the symbolic algebra library SymPy is presented.

#### Normal Order

A normal ordered sequence of occupation number operators can be defined as a permutation of the sequence such that all *vacuum annihilating operators* are placed to the right. The purpose is to make the action on the vacuum as trivial as possible by maximizing the number of vanishing terms. Normal ordering is always defined with a specific vacuum in mind, and this is why we need to distinguish annihilating operators from the *literal annihilators* defined in the start of section 2.2.

If the problem is formulated with respect to a reference determinant  $|\phi_0\rangle$ , the reference state will play the role of the vacuum, so that the normal ordered form of an operator should maximize the number of vanishing term when applied to  $|\phi_0\rangle$ . If  $i(a)$  refer to an (un)occupied orbit, the reference determinant will vanish upon application of operators  $a_a$  and  $a_i^\dagger$ , while the application of  $a_i$  and  $a_a^\dagger$  will create non-zero elements in the Fock space. Some authors choose to introduce *quasi-particle* operators to camouflage the difference between holes and particles, but we will not follow that approach.

The vacuum expectation value of a normal ordered string of operators will always vanish. This is an essential property and in fact our main motivation for using normal ordering at all. We state the *necessary* condition for normal ordering with respect to a vacuum  $|\phi_0\rangle$ ,

$$\langle \phi_0 | \{ a_a \cdots a_b^\dagger \} | \phi_0 \rangle = 0. \quad (2.32)$$

Here, we have also introduced the curly brackets as a notation for normally ordered operators. Note that this is not a *sufficient* condition.

As suggested by equation (2.32), an operator sequence inside brackets is not necessarily sorted to normal order explicitly. Instead, the curly brackets imply that:

1. All uncontracted operators should be arranged to normal order before the operator sequence is applied to a state, and
2. All uncontracted operators within the brackets (anti-)commute.

The assertion of anti-commutation applies to fermionic systems, and commutation applies to bosonic systems. For fermionic systems, the order within the brackets is important, as it determines the sign of the final normal ordered expression.

### Contracted Operators

The contraction of a pair of second quantization operators  $a_p^\dagger a_p$  is defined as

$$\overline{a_p^\dagger a_q} = a_p^\dagger a_q - \{a_p^\dagger a_q\} \quad (2.33)$$

To evaluate the contraction, it is necessary to explicitly write the operators to the vacuum dependent normal order. Orbits below and above the Fermi surface must be considered separately.

$$\overline{a_i^\dagger a_j} = a_i^\dagger a_j - \{a_i^\dagger a_j\} = a_i^\dagger a_j + a_j a_i^\dagger = \delta_{ij} . \quad (2.34)$$

$$\overline{a_a a_b^\dagger} = a_a a_b^\dagger - \{a_a a_b^\dagger\} = a_a a_b^\dagger + a_b^\dagger a_a = \delta_{ab} . \quad (2.35)$$

In these cases, the contraction reduces to the anticommutator. Otherwise, if the operators are already normally ordered, the contraction evaluates to zero,

$$\overline{a_b^\dagger a_a} = \overline{a_j a_i^\dagger} = 0 . \quad (2.36)$$

Contractions between hole and particle states will always vanish since the operators always anticommute.

The contraction is equal to the expectation value of the pair in vacuum, some authors even define it by this property,

$$\overline{a_p^\dagger a_q} = \langle \phi_0 | a_p^\dagger a_q | \phi_0 \rangle . \quad (2.37)$$

Together with (2.32), this property can be viewed as a simple case of the so-called Wick's theorem.

### 2.2.4 Computer aided Wick's Theorem

Wick's theorem provides a method to rewrite a sequence of second quantization operators into normally ordered form. The theorem can be stated as

$$\begin{aligned}
 ABC \dots XYZ &= \{ABC \dots XYZ\} \\
 &+ \sum_{singles} \left\{ \overline{ABC \dots XYZ} \right\} \\
 &+ \sum_{doubles} \left\{ \overline{\overline{ABC \dots XYZ}} \right\} \\
 &+ \sum_{triples} \dots \dots
 \end{aligned} \tag{2.38}$$

The summation over “singles” includes a term for every possible single contraction, “doubles” refers to all combinations of two contractions and so on.

The systematic structure of the right hand side expression in equation (2.38) lends itself naturally to symbolic evaluation with a computer. A number of implementations exist to exploit this, and the pioneering work was done in the early seventies, although the first implementations were based on diagram formulations [91]. The first known implementation of Wick's theorem is the command interpreter SQSYM [59], that was reported in 1991. A modern approach is provided by the Tensor Contraction Engine [58], which is also capable of generating optimized and parallelized Fortran code. Other recent accomplishments are the work of Engels-Putzka and Hanrath [27, 51], and Kállay, Surján and Gauss [62, 61]. Bochevarov and Sherrill have an approach based directly on Goldstone diagrams instead of Wick's theorem [16].

In order to manipulate second quantization expressions from within a computer algebra system (CAS), a fermionic second quantization framework and a Wick's theorem function for the open source Python package SymPy [1] was implemented by this author. The code was submitted to the SymPy project, and has been included in the official distribution since version 0.6.6. The following section provides a brief introduction to the framework.

## 2.3 Second Quantization Algebra with SymPy

SymPy [1] is a Python package for general purpose symbolic algebra. The source code is organized with a core that defines the basic objects and handles the interpretation of Python code as symbolic math expressions, and several modules that specializes the functionality for various applications. The physics module contains a second quantization submodule for which this author has written the functionality for fermionic systems, including the implementation of Wick's theorem and the functions to simplify the resulting expressions.

---

```

from sympy import symbols, latex, WildFunction, collect
from sympy.physics.secondquant import F, Fd, wicks, \
    AntiSymmetricTensor, substitute_dummies, NO

# Summation indices are distinguished by the dummy attribute
p, q, r, s = symbols('p q r s', dummy=True)

# Setup a general two body Hamiltonian
t = AntiSymmetricTensor('t', (p,), (q,))
10 v = AntiSymmetricTensor('v', (p, q), (r, s))
ham = t*Fd(p)*F(q) + v*Fd(p)*Fd(q)*F(s)*F(r)/4

# Rewrite to normal order
ham_normal = wicks(ham, simplify_kronecker_deltas=True)

# Insert indices according to our convention
index_rule = {
    'below': 'kl',
    'above': 'cd',
20 'general': 'pqrs'
}
ham_normal = substitute_dummies(ham_normal,
    new_indices=True, pretty_indices=index_rule)

# Obtain latex expression
print latex(ham_normal)

```

---

Listing 2.1: Python script for normal ordering of a two-body Hamiltonian

We demonstrate the implementation by rewriting the general two-body Hamiltonian to normal ordered form using SymPy.

### 2.3.1 Example: Normal Ordering of the Hamiltonian

The calculation is done with the script presented in Listing 2.1. The keyword argument `dummy=True` on line 6 informs SymPy that the symbols are summation indices, so the Hamiltonian defined on line 11 corresponds to

$$H = \sum_{pq} t_q^p a_p^\dagger a_q + \frac{1}{4} \sum_{pqrs} v_{rs}^{pq} a_p^\dagger a_q^\dagger a_s a_r. \quad (2.39)$$

Compiling the output from the script with a  $\text{\LaTeX}$ -interpreter gives the following expression,

$$\frac{1}{2} v_{lk}^{lk} + t_q^p \left\{ a_p^\dagger a_q \right\} + v_{kq}^{kp} \left\{ a_p^\dagger a_q \right\} + \frac{1}{4} v_{sr}^{qp} \left\{ a_q^\dagger a_p^\dagger a_r a_s \right\} + t_k^k. \quad (2.40)$$

With implicit summation of repeated indices, the expression is correct and can be verified against a multitude of references, see for instance [57, 21]. On a technical

note, all indices in this expression are recognized by SymPy as summation indices, even though dummy variables are not marked as such in the  $\text{\LaTeX}$  output.

All terms with occupation number operators have been written in normal order, but still the Hamiltonian does not obey equation (2.32) which should hold for normally ordered operators. We have instead

$$E_0 \equiv \langle \phi_0 | H | \phi_0 \rangle = \sum_i t_i^i + \frac{1}{2} \sum_{ij} V_{ij}^{ij},$$

where we have introduced the vacuum energy  $E_0$ . By subtracting the reference state energy, thus shifting the energy levels, we get the proper normal ordered Hamiltonian

$$H_N = H - E_0 = \left( t_q^p + v_{iq}^{ip} \right) \left\{ a_p^\dagger a_q \right\} - \frac{1}{4} v_{rs}^{pq} \left\{ a_p^\dagger a_q^\dagger a_r a_s \right\}, \quad (2.41)$$

with the desired property (2.32),

$$\langle \phi_0 | H_N | \phi_0 \rangle = 0.$$

Continuing the SymPy script in Listing 2.1, we can get the expression for  $E_0$  and  $H_N$  by issuing the commands

---

```
E0 = wicks(ham_normal, keep_only_fully_contracted=True)
ham_normal = ham_normal - E0
print latex(ham_normal)
```

---

This time we called the `wicks` routine with a keyword argument to indicate that we were only interested in the fully contracted terms. This is how `wicks` is used to evaluate a vacuum expectation value. The output is again a  $\text{\LaTeX}$ -expression, namely,

$$t_q^p \left\{ a_p^\dagger a_q \right\} + v_{kq}^{kp} \left\{ a_p^\dagger a_q \right\} + \frac{1}{4} v_{sr}^{qp} \left\{ a_q^\dagger a_p^\dagger a_r a_s \right\}. \quad (2.42)$$

Clearly this expression is equivalent to (2.41), although it is not yet on exactly the same form. However, since SymPy is a general purpose CAS, we can rewrite the expression easily with the following commands:

---

```
w = WildFunction('w')
ham_normal = collect(ham_normal, NO(w))
print latex(ham_normal)
```

---

The result is as expected,

$$\left( t_q^p + v_{kq}^{kp} \right) \left\{ a_p^\dagger a_q \right\} + \frac{1}{4} v_{sr}^{qp} \left\{ a_q^\dagger a_p^\dagger a_r a_s \right\}. \quad (2.43)$$

The object of type `WildFunction` acts like a wildcard that matches any expression. Here we use it to instruct `collect` to collect coefficients for all instances of normally ordered products (represented by `NO()` in SymPy).

By going through this example, we have demonstrated some key points about the implementation. It has been shown how a simple calculation can be performed, and in particular the central role of the `wicks` routine. Moreover, we also witnessed the benefit that comes from doing the calculations in a general purpose CAS, with rich support for expression manipulation. Included in the official SymPy distribution [1] is an example script that derives the equations for Coupled-Cluster Singles and Doubles (See Chapter 4). The module has also been used to derive Coupled-Cluster equations at the level of Triple excitations for a three-body interaction, as well as Fortran code for the several hundred diagrams. This is an ongoing project, that will hopefully lead to publications in the coming year.

### 2.3.2 Simplification Strategies

The difficult and most time consuming part of a computer based symbolic calculation lies often not in the steps that constitute the central algorithm, but rather in the analysis and manipulations that are needed to rewrite and simplify the expressions. See Reference [20] for a discussion about general simplification procedures. Equations of manageable complexity provide a much better basis for numerical implementations, so it is important to have robust simplification routines. In this respect it is particularly fruitful to employ a CAS, as much of the expression manipulations can be done with general utility functions, that are subject to testing and optimization in a broad range of applications.

The expressions that arise in a second quantization framework have a structure that is difficult to attack with standard Symbolic Algebra techniques such as a canonical form of all expressions and subexpressions. Engels-Putzka [27] pursues a canonical form, and details a way to achieve a robust canonization procedure by imposing restrictions that specialize the method to Coupled-Cluster calculations. In the end, however, she concludes the discussion of canonization by choosing a different approach based on graphs. That way she avoids the restriction to Coupled-Cluster applications. The graphs employed by Engels-Putzka are used to represent and analyze the contraction structure of a term, i.e. the topology of the corresponding diagram.

Hirata [58] uses canonization as the primary simplification method, but employs a more thorough check for terms where canonization fails. The problematic terms are those with a cyclic contraction structure, e.g.

$$\sum_{pqrstu} A_{rs}^{pq} B_{pq}^{tu} C_{tu}^{rs} . \quad (2.44)$$

It is easy to see why a *local canonization* scheme fails for such terms. We assume that (2.44) is on canonical form and examine first what happens when a local canonization scheme succeeds. For the purpose of this discussion, we define a simple local canonization scheme, where an indexed object has the symmetry property

$$A_{rs}^{pq} = -A_{rs}^{qp} = -A_{sr}^{pq} = A_{sr}^{qp} . \quad (2.45)$$



The canonical form is determined by alphabetical ordering of upper and lower indices, such that of the alternatives in equation (2.45), the canonical form is the first,  $A_{rs}^{pq}$ . The order of factors is also determined alphabetically and lexically such that equation (2.44) is on canonical form. The canonization consist of two steps that are performed in the given order:

1. Indices are ordered alphabetically as allowed by the symmetry of the indexed object.
2. Factors are ordered alphabetically. The letters of an indexed object are read in the sequence: stem, upper indices (left to right), lower indices (left to right).

We exemplify this by considering a term that is equivalent to Equation (2.44) with a permutation of summation indices  $u$  and  $t$ ,

$$\sum_{pqrsut} A_{rs}^{pq} B_{pq}^{ut} C_{ut}^{rs}. \quad (2.46)$$

Using the symmetry (2.45) of  $B$  and  $C$  each of them can be rewritten to canonical form by permuting  $u$  and  $t$  and taking the signs into account. In this case, the canonization of each factor results in the canonization of the entire term, i.e. *the local canonization implies a global canonization*.

If we instead permute  $s$  and  $t$ , the situation is more complex,

$$\sum_{pqrtsu} A_{rt}^{pq} B_{pq}^{su} C_{su}^{rt}. \quad (2.47)$$

According to the canonization scheme we have introduced so far, this expression is already on canonical form. But the equivalence with (2.44) is not obvious, and a computer will not be able to detect it without processing the term further. We can try to remedy this by imposing canonization rules that apply to the entire term. Hirata uses relabelling of all summation indices, so we state another rule for this demonstration:

3. The summation indices should be relabelled such that the first occurrence of any summation index across the term from left to right, appear in alphabetical order.

Applying this rule to expression (2.47) leads again to the canonical form (2.44).

But let's consider yet another complication. If  $A = B$ , expression (2.44) becomes

$$\sum_{pqrstu} B_{rs}^{pq} B_{tu}^{rs} C_{pq}^{tu}. \quad (2.48)$$

According to our scheme, the factors should be ordered alphabetically. Here, this implies that the order of the two leftmost factors depends on the summation indices. It is easy to construct examples where this leads to a conflict with rule 3 about the

order of summation indices. Consider for instance a permutation of  $p$  and  $s$ . Steps 1 and 2 give,

$$\sum_{pqrstu} B_{rp}^{sq} B_{tu}^{rp} C_{sq}^{tu} \stackrel{1}{=} \sum_{pqrstu} B_{pr}^{qs} B_{tu}^{pr} C_{qs}^{tu} \stackrel{2}{=} \sum_{pqrstu} B_{tu}^{pr} B_{pr}^{qs} C_{qs}^{tu}. \quad (2.49)$$

The application of step 3 proceeds like,

$$\sum_{pqrstu} B_{tu}^{pr} B_{pr}^{qs} C_{qs}^{tu} \stackrel{3}{=} \sum_{pqrstu} B_{rs}^{pq} B_{pq}^{tu} C_{tu}^{rs}. \quad (2.50)$$

Again, we have reached a canonical form, for which the equivalence with the original expression, Equation (2.48), is obfuscated by the summation index labels. Clearly, the problem arises because the factor order happens to depend on the dummy indices.

### 2.3.3 Implementation in SymPy

The second quantization framework of SymPy employs a mixture of local canonization and canonization based on the contraction structure. The local canonization consists of

1. All upper and lower indices are sorted to an arbitrary canonical order with particle indices < hole indices < general indices.
2. Factors are sorted to an arbitrary canonical order

These steps are performed immediately, to the extent that it is impossible to create non-canonized expressions. Step 1 is built into the anti-symmetric indexed objects, while 2 is an inherent property of SymPy. In order to canonize the summation index labels, we employ a more elaborate procedure.

#### Strategy for Identification of Equivalent Terms

To identify and combine terms that differ only because of summation index labels, the employed strategy is to relabel indices consistently across terms. This may be viewed as a *global canonization* step. A consistent relabeling is achieved by analysis of the contraction structure in each term. This information is encoded, and each summation index in a term is assigned a descriptive key. The key is inferred exclusively from the two factors in which the index is present, and is constructed to be fully independent of the index label or the label of any other summation index.

We will first introduce a notation that will be used in the following discussion. The key generation procedure will be denoted by an operator  $K$ , that will map a given combination of an index and its term, to the corresponding key,

$$K : (\text{index}, \text{term}) \rightarrow \text{key}. \quad (2.51)$$

For example, the key for an index  $i$  in a term  $f(i, j)$  will be denoted  $K(i, f(i, j))$ .

The keys are required to be independent of the current labels of the summation indices. This implies that two equivalent terms  $f(i, j)$  and  $f(k, l)$  that differ only because of dummy labels will give rise to exactly the same set of keys, e.g.

$$\{K(x, f(i, j)) | x \in \{i, j\}\} = \{K(x, f(k, l)) | x \in \{k, l\}\}. \quad (2.52)$$

Where the curly brackets are used to denote a mathematical set. In fact, we can make a stronger, more general statement:

Equivalent terms will have the same *multiplicity* of each key.

From relation (2.52) it follows that, if all keys in a term are unique, we can identify corresponding summation indices in an equivalent term by comparing the keys. By consistent relabelling of corresponding indices, the computer algebra system can easily combine terms as appropriate. What remains to discuss is the treatment of ambiguities.

### Treatment of Ambiguous Keys

It may happen that not all generated keys are unique, so that for a term  $f(i, j)$ ,

$$K(i, f(i, j)) = K(j, f(i, j)). \quad (2.53)$$

Here,  $i$  and  $j$  have identical keys, so that those indices cannot be relabelled consistently in an unambiguous way. A more elaborate procedure is needed for terms that give rise to non-unique keys. There are two possible cases:

1. At least one index has been assigned a unique key.
2. No index has a unique key.

In case 1, we have identified at least one index that can be consistently relabelled in all equivalent terms. The strategy is then to substitute those indices consistently, using non-dummy indices, and then generate new keys for the remaining ambiguous indices. The new keys may be unique for some, or all, of the ambiguous summation indices, so that they can be used in another round of consistent relabelling. This procedure is repeated as many times as necessary. Eventually, we will either obtain a full set of unique keys, so that all summation indices can be canonized, or we will encounter case 2.

Let us now turn to the more difficult case 2. This situation will not occur in the standard Coupled-Cluster equations, [27] and a proper treatment of this is not implemented in SymPy. However, for completeness, we propose a way to handle the global canonization of such terms. Because every equivalent term will face this situation, what we need is a way to get out of it such that the equivalence can be detected. A possible approach is to

1. Construct all terms that correspond to permutations of the ambiguous dummies.

2. Employ a reliable method to compare the alternative terms.
3. Pick the “largest”.

The comparison method is arbitrary as long as *transitivity* is fulfilled, that is

$$a < b \wedge b < c \implies a < c. \quad (2.54)$$

For instance, one could compare the string representations of the terms using Python’s built in string comparison functionality. After this procedure, all ambiguous terms would be rewritten to the “largest” form, which would be identical for equivalent terms.

### Implementation

The key assigned to a summation index consists of the following information

1. Index range (below or above the Fermi surface, or both).
2. Both factors that contain the key as they appear with all summation indices masked according to range. The masked factors are sorted alphabetically
3. The position of the index in the first factor as they are ordered in 2. Either “upper” or “lower”.
4. The position of the index in the second factor as they are ordered in 2. Either “upper” or “lower”.

The index position information in items 3 and 4 will distinguish only between upper and lower indices, and not the exact index positions. This is because the internal order in the upper and lower indices is determined by canonization, so it contains a dependence on the actual summation index labels. If we included more information in items 3 and 4, we would violate the assumption that the keys are independent of the existing dummy labels. In addition, it is assumed in steps 3 and 4 that the two factors involved in the contraction can be ordered unambiguously. This is not always the case for a general expression, as demonstrated in the discussion of (2.49) and (2.50). If this situation arises, items 3 and 4 are left out of the key.

It would be inefficient to identify equivalent terms by comparing keys term for term. For an expression containing  $n$  terms, this approach would require  $\frac{1}{2}n(n-1)$  comparisons and not scale very well. Instead, we sort the dummies in each term according to the assigned keys. If all keys in the term are unique, the summation indices can be ordered unambiguously. Then (2.52) guarantees that all equivalent terms will have corresponding summation indices at the same position in the sorted list. When a uniquely sorted list of summation indices have been obtained, the summation indices are relabelled according to the position in the sorted list.

The code checks whether any keys are identical. In that case a routine is called to determine the order nevertheless. We create an auxiliary expression which is identical to the original term, except that all indices with unique keys have been replaced by fixed indices. The auxiliary term is then used in a recursive call to generate new keys for each group of ambiguous indices. The interested reader is referred to the source code [1].

## Chapter 3

# Overlap Functions and Spectroscopic Factors

### 3.1 Overlaps in Reaction models

There is no universal model for reactions, only particular models depending on beam energy, target and what the essential degrees of freedom are. In general both structure and reaction theories must be carefully picked and the combination of the two perspectives is non-trivial.

If the reaction happens fast, it may be sufficient to model the complex interactions between target and projectile as a *direct reaction*. The concept of direct reactions is not uniquely defined, but is instead loosely associated with reactions that turn out to be well described by particularly simple reaction models, where few degrees of freedom are involved. Typically the term is used for a fast reaction that is characterized by a small transfer of energy, and where the cross section varies slowly with the energy transfer [3, 98].

Overlap functions arise naturally in the Distorted Wave Born Approximation (DWBA) for pickup and stripping reactions with light ions, e.g. the frequently studied  $B(p, d)A$  and  $A(d, p)B$  reactions. The reaction (transition) amplitude for  $A(d, p)B$  is essentially given in its simplest standard approximation as

$$T_{BA}^{DWBA} = \sqrt{B} \left\langle \chi_p^{(-)} \Psi_p \Psi_B \left| v_{np} \right| \Psi_d \Psi_A \chi_d^{(+)} \right\rangle \quad (3.1)$$

Here  $\chi$  are the incoming and outgoing distorted waves while the  $\Psi$  are the internal wavefunctions of the participating nuclear systems. The integration goes over internal coordinates and the necessary relative coordinates, taking the relative coordinates (channel radii) to be  $r_{dA}$  and  $r_{pB}$  (projectile/ejectile coordinates before and after the reaction). These will also be the coordinates used as argument for the  $\chi$  functions. The interaction  $v_{np}$  is assumed dependent only on the relative coordinate between the proton and the neutron transferred to  $A$ . It is in other words independent of the internal coordinates of nuclei  $A$ , and we may slip the  $\Psi_A$  past

the interaction operator and carry out the integration over the internal coordinates,  $\xi$ . This introduces the overlap  $O_A^B(\mathbf{x}_{nA})$  in the reaction amplitude integral:

$$T_{BA}^{DWBA} = \sqrt{B} \left\langle \chi_p^{(-)} \Psi_p O_A^B \middle| v_{np} \middle| \Psi_d \chi_d^{(+)} \right\rangle \quad (3.2)$$

The coordinate for the picked-up neutron,  $\mathbf{x}_{nA}$ , which is not integrated over, is the only coordinate important for the interaction. Thus, the overlap provides all the nuclear structure information which has any influence on the transfer amplitude connecting states  $A$  and  $B$ .

The internal wavefunction for the deuteron depends on the relative coordinate  $\mathbf{x}_{np}$  and the spin coordinates. Clearly, these coordinates must be of importance to the neutron-proton interaction, and  $\psi_d$  can not slip past the interaction operator. The internal proton wavefunction on the other hand, will only depend on the spin coordinate  $\sigma$ . If we assume the interaction to be spin independent, the proton function can slip past the interaction and give an overlap on the right hand side,

$$O_p^d(\mathbf{x}_{np}) = \sum_{\sigma_p} \Psi_p(\sigma_p) \Psi_d(\mathbf{r}_{np}, \sigma_n, \sigma_p). \quad (3.3)$$

The reaction amplitude becomes

$$T_{BA}^{DWBA} = \sqrt{B} \left\langle \chi_p^{(-)} O_A^B \middle| v_{np} \middle| O_p^d \chi_d^{(+)} \right\rangle. \quad (3.4)$$

Again the proton deuteron overlap provides all the structure information needed about the deuteron, to determine the reaction amplitude.

### 3.2 Overlap Functions

The general overlap function between given states of two nuclei with  $A$  and  $B = A + 1$  nucleons respectively is defined as [3]

$$O_A^B(\mathbf{x}_1) \equiv \sqrt{B} \int d\xi \Psi_A^*(\xi) \Psi_B(\mathbf{x}_1, \xi). \quad (3.5)$$

Here,  $\xi$  represents intrinsic (e.g. Jacobian) coordinates for  $A$  nucleons, and  $\mathbf{x}_1 = (\mathbf{r}, \sigma)$  is the coordinate from the center of mass of nucleus  $A$  to an external point particle at position  $\mathbf{r}$  with spin coordinate  $\sigma$ . The overlap function  $O_A^B(\mathbf{x}_1)$  can then be interpreted as the wavefunction of the external particle as if it was attached to nucleus  $A$ . The purpose is to integrate out the irrelevant degrees of freedom so that the essential structure information is represented in a condensed form, and spectator particles that do not play an active role in the reaction can be neglected. We notice that, if  $\Psi_A$  and  $\Psi_B$  are both translation invariant wave functions, the overlap is also translation invariant. The parity  $\Pi_{AB}$  of the overlap is given by the the product of the parities, [3]

$$\Pi_{AB} = \Pi_A \cdot \Pi_B.$$

We denote the angular momentum quantum labels associated with the transferred particle by  $j$  and  $m$  for the magnitude and projection respectively. If the systems  $A$  and  $B$  have angular momenta  $J_A, M_A$  and  $J_B, M_B$ , the projection of the transferred particle must obey [3],

$$m + M_A = M_B. \quad (3.6)$$

On the other hand, the magnitude of the angular momentum  $j$  may take several values. It is restricted by the triangular inequality [3],

$$|J_A - J_B| \leq j \leq J_A + J_B. \quad (3.7)$$

This implies that the single particle overlap function in Equation (3.5) cannot in general be associated with the transfer of a well defined angular momentum.

In order to obtain overlap functions corresponding to the transfer of a well defined angular momentum, we write the general overlap function as a sum, where each term is assumed to have single particle angular momentum magnitude  $j$ .

$$O_{AJ_A M_A}^{BJ_B M_B}(\mathbf{x}) = \sum_j (J_A M_A j m | J_B M_B) O_{Ajm}^B(\mathbf{x}). \quad (3.8)$$

Here, we have expressed each term as a product of a Clebsch-Gordan coefficient and a wave function. We note that this form guarantees the requirements (3.6) and (3.7).

The overlap functions associated with the transfer of a well defined angular momentum can be written with spin-orbital spherical harmonics,

$$O_{Ajm}^B(\mathbf{x}) = O_A^B(lj; r) Y_{lm}(\hat{x}). \quad (3.9)$$

### 3.3 Spectroscopic Factors

The *spectroscopic factor* is the norm of the radial overlap function,

$$S_A^B(lj) = \int dr r^2 O_A^B(lj; r)^* O_A^B(lj; r). \quad (3.10)$$

From the discussion in the preceding sections, we understand that the radial overlap function  $O_A^B(lj; r)$  measures to what extent state  $B$  can be described as state  $A$  with a particle attached in the orbit  $l, j$ , as a function of the distance  $r$ . Correspondingly, the interpretation of the spectroscopic factor, is that it measures the probability that system  $B$  can be obtained by the addition of a particle in the orbit  $l, j$  to system  $A$ .

The experimental extraction of spectroscopic factors employs pick-up or stripping reactions where a single nucleon is transferred from one nucleus to another. A popular procedure for extraction of spectroscopic factors is the so-called well depth prescription (WDP) [3]. Then the radial shape of the overlap function is approximated with a unit normalised phenomenological solution calculated for a



well, where the depth is adjusted so that the relevant single particle separation energy and an assumed physical node number is reproduced. That single particle wave contains all structure information that enters the calculation. The norm of the overlap function, i.e. the spectroscopic factor, is then determined by a fit to the measured cross sections.

The idea is that the norm of the overlap can be calculated independently by a more sophisticated structure model, and compared with the experimentally extracted values. With the WDP, the structure models are not required to reproduce correct asymptotic behaviours, as the radial dependence is approximated phenomenologically. This is beneficial as it allows testing of a broad range of structure models, the flip side is that it introduces another set of parameters to the analysis, and thus increases the model dependence.

It is important to keep in mind that spectroscopic factors are model dependent, and do not represent physical (observable) properties of the nucleus directly [35, 37]. Still, it is a useful and meaningful concept for interpretations within a given model. For instance, through knock-out reactions, spectroscopic factors can be used to estimate shell closure properties (See Paper 2 of this thesis). These can then be used to evaluate an array of structure models, and this information is valuable, even given the model dependence.

### 3.3.1 Overlaps in Second Quantization

To formulate the overlap with creation operators, we want an expression which measures the extent to which the wavefunctions  $\Psi_A$  and  $\Psi_{B=A+1}$  can be related to each other by the application of simple creation operators. Thus, the relevant expression is  $\langle B | a^\dagger(\mathbf{x}) | A \rangle$ , where  $a^\dagger(\mathbf{x})$  is a creation operator for a point particle at position  $\mathbf{r}$  and with spin  $\sigma$ . The field theoretical expression for the overlap is derived rigorously in Reference [3],

$$O_A^B(\mathbf{x}) = \langle B | a^\dagger(\mathbf{x}) | A \rangle^* = \sum_{ljm} \langle B | a_{ljm}^\dagger(r) | A \rangle^* Y_{ljm}(\hat{x}). \quad (3.11)$$

Where  $a^\dagger(\mathbf{x})$  has been substituted by

$$a^\dagger(\mathbf{x}) = \sum_{ljm} a_{ljm}^\dagger(r) Y_{ljm}^*(\hat{x}). \quad (3.12)$$

Again, we see that the projection  $m$  can only take the value consistent with the projections of system  $A$  and  $B$ ,  $M_A + m = M_B$ . Also the parity of system  $B$  must be matched by the combined parity of system  $A$  and the added particle  $(-1)^l$ , so the triple sum is reduced to a single sum over  $j$ :

$$O_A^B(\mathbf{x}) = \sum_j \langle B | a_{ljm}^\dagger(r) | A \rangle^* Y_{ljm}(\hat{x}). \quad (3.13)$$

Comparing this with equations (3.8) and (3.9), we see that the radial overlap function obeys the equation,

$$(J_A M_A j m | J_B M_B) O_A^B(lj; r) = \langle B | a_{ljm}^\dagger(r) | A \rangle^* . \quad (3.14)$$

This can be viewed as an application of the Wigner-Eckart theorem, where the overlap  $O_A^B(lj; r)$  is the reduced matrix element,

$$O_A^B(lj; r) = \langle B || a_{lj}^\dagger(r) || A \rangle^* . \quad (3.15)$$

See Appendix A for a definition of the reduced matrix element we employ.

In order to work with a single particle energy basis, we can expand the radial point particle creation operator in orbital wave functions, viz.

$$a_{ljm}^\dagger(r) = \sum_n a_{nljm}^\dagger \phi_{nljm}(r) . \quad (3.16)$$

The creation operator  $a_{nljm}^\dagger$  represents the action of populating an orbit characterized by the quantum labels  $n, l, j$  and  $m$ . Note that when the occupation number formalism is related to such a shell model like description, the coordinates are not translation invariant. While (3.5) is written in terms of intrinsic coordinates, a many-body wavefunction in terms of Slater determinants have one coordinate associated with each particle. This overdetermines the system, and implies a loss of translation invariance.

The spectroscopic factor has a particularly simple interpretation if both systems  $A$  and  $B$  are represented by Slater determinants. Let's assume, in a simple picture, that the states  $A$  and  $B$  are pure product states of the same set of single particle orbits  $|p\rangle$ , and let  $|b\rangle$  be the particular orbit which is present in  $B$  but not in  $A$ . Then  $\Psi_A$  and  $\Psi_B$  would have the simple relation  $\langle \Psi_B | a_p^\dagger | \Psi_A \rangle = \delta_{pb}$ . In other words, we could produce the state  $B$  by simply attaching a particle to  $A$  in the well defined orbit  $b$ .

This is not the case for realistic applications. This is in part due to the limitations of the single particle picture: As the particles are not independent of each other, the motion of the attached particle will be influenced by the residual particles and cannot be fully described by a simple single particle orbit. In addition, the attached particle is also expected to disturb the internal organisation of the remaining  $A$  particles. It is clear that the overlap  $\langle \Psi_B | a_p^\dagger | \Psi_A \rangle$  in this case is determined both by

- How much the internal organization of  $A$  is affected by the added particle, and
- Whether the attached particle can be described by the single particle wave functions used in the model.

In total, the spectroscopic factor measures inter-dependencies of all particles with respect to an assumed motion of one of them.

### 3.3.2 Choice of Overlap Definition

As we have seen, the radial overlap function  $O_A^B(lj; r)$  can be expressed in terms reduced matrix element. In this thesis the chosen form of the Wigner-Eckart theorem is given in appendix A. The reduced matrix elements used by other authors may differ by a factor determined by the angular momentum values.

For overlap functions, there is yet another arbitrary decision that will influence the value of the calculated results. Employing the Wigner-Eckart theorem on  $\langle B|a_{ljm}^\dagger(r)|A\rangle^*$  we can choose between two paths:

- We can reproduce equation (3.15),

$$\langle B|a_{ljm}^\dagger(r)|A\rangle^* = (J_A M_A j m | J_B M_B) \langle B||a_{lj}^\dagger(r)||A\rangle^* \quad (3.17)$$

Note that the spherical overlap function is represented by a complex conjugated reduced matrix element. This overlap function may be associated with particle addition to system  $A$ .

- We can evaluate the complex conjugation before employing the Wigner-Eckart theorem:

$$\begin{aligned} \langle B|a_{ljm}^\dagger(r)|A\rangle^* &= \langle A|a_{ljm}(r)|B\rangle \\ &= (-)^{j-m} \langle A|\tilde{a}_{lj-m}(r)|B\rangle \\ &= (-)^{j-m} (J_B M_B j -m | J_A M_A) \langle A||\tilde{a}_{lj}(r)||B\rangle \end{aligned} \quad (3.18)$$

Here, we have introduced the spherical annihilation operator,  $\tilde{a}_{ljm}(r) = (-1)^{j+m} a_{lj-m}$ . This time, the spherical overlap corresponds to a reduced matrix element without complex conjugation, and we may associate it with particle removal from system  $B$ .

The difference between the reduced matrix elements involves more than a complex conjugation. Using symmetry properties of Clebsch-Gordan coefficients, we find the relation,

$$(J_B M_B j -m | J_A M_A) = (-)^{1-m+J_A-J_B} \frac{\hat{J}_A}{\hat{J}_B} (J_A M_A j m | J_B M_B) .$$

Here, we have used the notation  $\hat{J} = \sqrt{2J+1}$ . Clearly, the different paths lead to different normalizations of the reduced matrix elements, which implies different spectroscopic factors. Equating the two alternatives, we see that

$$\langle B||a_{lj}^\dagger(r)||A\rangle^* = (-)^{J_A+J-J_B} \frac{\hat{J}_A}{\hat{J}_B} \langle A||\tilde{a}_{lj}(r)||B\rangle . \quad (3.19)$$

The corresponding spectroscopic factors are related by a factor

$$\frac{\hat{J}_A^2}{\hat{J}_B^2} .$$

We conclude that the overlap functions can be defined in several ways, even for a given reduced matrix element definition. Different variants are encountered in the literature, and this must be taken into account when results are compared. In this work, we will use the second alternative. The spectroscopic factors will then be between 0 and 1 for particle removal from a system with  $J = 0$ .

### 3.4 Non-Hermitian Models

As we will see in Chapter 4, the calculation of spectroscopic factors with Coupled-Cluster will be done with left and right solutions of a non-hermitian eigenvalue problem. We will now derive a definition that accounts for this.

#### 3.4.1 Spectroscopic Factors

As we have seen, the spectroscopic factor can be written

$$S_A^B(lj) = \int dr r^2 O_A^B(lj; r)^* O_A^B(lj; r). \quad (3.10)$$

In the second quantization formulation, it was easy to see that  $O_A^B(lj; r)$  is actually a reduced matrix element, and in the preceeding section we discussed two alternatives for the relation of  $O_A^B(lj; r)$  to a reduced matrix element. We will in the following abandon the original overlap definition, Equation (3.15), and use Relation (3.18) between the overlap functions and the reduced matrix elements.

Employing Relation (3.18) we see that the two factors in the integrand of Equation (3.10), can be written

$$O_A^B(lj; r) = \langle A | [\tilde{a}_{lj}(r)] | B \rangle = (-)^{j-m} \frac{\langle A | a_{ljm}(r) | B \rangle}{(J_B M_B j - m | J_A M_A)}, \quad (3.20)$$

$$O_A^B(lj; r)^* = \langle A | [\tilde{a}_{lj}(r)] | B \rangle^* = (-)^{j-m} \frac{\langle B | a_{ljm}^\dagger(r) | A \rangle}{(J_B M_B j - m | J_A M_A)}. \quad (3.21)$$

Using the relations

$$a_{ljm}^\dagger(r) = \sum_n a_{nljm}^\dagger \phi_{nljm}(r), \quad (3.22)$$

$$a_{ljm}(r) = \sum_n a_{nljm} \phi_{nljm}^*(r). \quad (3.23)$$

and the orthogonality  $\int dr r^2 \phi_{n'ljm}^*(r) \phi_{nljm}(r) = \delta_{nn'}$ , the representation of (3.10) in a single particle basis  $\phi_{nljm}(r)$  of energy eigenstates can now be written,

$$S_A^B(lj) = \sum_n \frac{\langle B | a_{nljm}^\dagger | A \rangle \langle A | a_{nljm} | B \rangle}{(J_B M_B j - m | J_A M_A)^2}. \quad (3.24)$$

An alternative way to write the spectroscopic factor that will prove to be convenient for the calculation of spectroscopic factors with spherical Coupled-Cluster theory (see Chapter 5) follows if equations (3.20) and (3.21) written as

$$O_A^B(lj; r) = \sum_{mM_A} (-)^{j-m} \langle A | a_{ljm}(r) | B \rangle (J_B M_B j - m | J_A M_A) , \quad (3.25)$$

$$O_A^B(lj; r)^* = \sum_{mM_A} (-)^{j-m} \langle B | a_{ljm}^\dagger(r) | A \rangle (J_B M_B j - m | J_A M_A) . \quad (3.26)$$

Here we have applied the orthogonality relations for Clebsch-Gordan coefficients and the fact that the overlap functions are reduced matrix elements, and therefore independent of the projections. Again we can use the orthogonality of the single particle basis to obtain

$$\begin{aligned} S_A^B(lj) &= \sum_n \left( \sum_{mM_A} (-)^{j-m} (J_B M_B j - m | J_A M_A) \langle B | a_{nljm}^\dagger | A \rangle \right) \\ &\quad \times \left( \sum_{mM_A} (-)^{j-m} (J_B M_B j - m | J_A M_A) \langle A | a_{nljm} | B \rangle \right) . \end{aligned} \quad (3.27)$$

We will return to this expression in Chapter 5.

### 3.4.2 Radial Overlap Functions

We may also consider the radial shape of the overlap functions, as this provides a more detailed description of the model wavefunction. So instead of integrating out the radial coordinate  $r$ , we choose now to take a close look at the integrand. From equations (3.10), (3.22) and (3.23), we find that the integrand of interest is

$$|R_A^B(lj; r)|^2 = O_A^B(lj; r)^* O_A^B(lj; r) \quad (3.28)$$

$$= \sum_{nn'} \frac{\langle B | a_{n'ljm}^\dagger | A \rangle \langle A | a_{nljm} | B \rangle}{(J_B M_B j - m | J_A M_A)^2} \phi_{n'ljm}^*(r) \phi_{nljm}(r) \quad (3.29)$$

We note that there is a double sum over the single particle nodal quantum number, and recall that previously, this sum was reduced to a single summation by the orthogonality of the single particle basis functions. Here, we will delay the integration, and instead evaluate the double sum. The identity,

$$S_A^B(lj) = \int dr r^2 |R_A^B(lj; r)|^2 , \quad (3.30)$$

provides a convenient check of the overlap functions. We will briefly return to these objects in the outlook, Chapter 6.3

## Chapter 4

# Spectroscopic Factors with Coupled-Cluster

The purpose of this chapter is to explain how spectroscopic factors can be calculated within the Coupled-Cluster method (CCM). In order to do that, we see it as necessary to present briefly the Coupled-Cluster method and discuss some of its properties. The extension to Equations-of-Motion Coupled-Cluster is also central in the calculation of spectroscopic factors, so the fundamental ideas for that will also be presented. Here, we will provide more details than in Paper 1 [60].

### 4.1 Overview

The Coupled-Cluster formalism was originally formulated by Coester [18], and Coester & Kümmel [19] in 1960. Later Čížek and Paldus developed the method further for applications to Chemistry. Čížek is credited as the first to write down the explicit Coupled-Cluster equations [104, 105], and Paldus did the first *ab initio* calculation with the method [90]. Other contributors in the early phase are Bartlett & Purvis [9, 7] and Bishop & Lührmann [15, 12].

Despite the fact that Coester and Kümmel originally developed the CCM for applications to nuclear physics, the method has seen a much wider deployment in the Quantum Chemistry community. Since the pioneering work in the sixties the method has grown a plethora of variations and is today textbook material for quantum Chemists [21, 56, 100]. In the mid seventies, Coupled-Cluster was applied to nuclear physics in several papers by the Bochum group [68]. Later, the Manchester group have used Coupled-Cluster with translation invariant coordinates in position space [14, 13, 79]. This is an interesting approach, but is restricted to only the lightest nuclei due to the computationally tough challenge of antisymmetrization. Nuclear applications of translation variant Coupled-Cluster method resurfaced in 1999 with Mihaila and Heisenberg's papers [53, 77, 78, 76].

In order to advance beyond sporadic applications of CCM to nuclear physics, Dean and Hjorth-Jensen declared the start of a systematic program for applications

of Coupled-Cluster to nuclear physics in 2003 [23, 24]. This has led to a series of articles with a multitude of applications to various nuclei, [65, 107, 40, 42, 43, 46, 48, 50, 47] and theory development for challenges particular to nuclear physics [42, 49, 45, 60]. This thesis can be seen as a contribution to this line of research.

#### 4.1.1 Size Extensivity

One of the inherent benefits of CCM compared to the Configuration Interaction method (CI, see section 2.2.2) employed for instance in shell model approaches, is the size extensivity of CCM. This is a term borrowed from thermodynamics [41], and it refers to the property of linear scaling with respect to the number of particles in a system. In thermodynamics, the number of particles is assumed to be very large, so one might wonder why size-extensivity could be relevant for systems as small as nuclei, with only a few hundred particles. But it is well known that the binding energy per particle for nuclei is fairly stable across the nuclear chart [86], and only the lightest nuclei deviate from this rule. In other words, the empirical binding energy of nuclei behaves as an extensive quantity, even though the systems are tiny in a thermodynamical context.

For an *ab initio* method that aims to predict binding energies systematically over a wide range of nuclei, it is important that the theory reproduces the empirical properties across the nuclear chart. In particular, since we must limit the interaction to few-body terms, correct scaling of the binding energy with particle number must be built into the method *a priori*. This is guaranteed by the fact that no *unlinked diagrams* enter the Coupled-Cluster equations [8, 100, 67].

There is an intimate relationship between Coupled-Cluster and many body perturbation theory (MBPT). In fact, one can accurately describe CCM as the summation of selected MBPT diagrams to infinite order. By comparing the MBPT wavefunction with the CCM wavefunction, one can study the correspondence of terms [67]. Since MBPT is size extensive, provided that only linked diagrams enter the approximation, this must also hold for Coupled-Cluster.

The relation between size extensivity and unlinked diagrams can be understood with intuitive arguments. In MBPT we consider a Hamilton operator,

$$H = H_0 + V. \quad (4.1)$$

where  $V$  is the perturbation. The exact energy is approximated up to  $N$ -th order as

$$E_{MBPT} = E_0 + E^{(1)} + E^{(2)} + \dots + E^{(N)}. \quad (4.2)$$

Without going into more details, we recall that the  $n$ -th order contribution to the energy applies the perturbation operator,  $V$ , to the reference state  $n$  times. We assume that as higher order corrections are added we will eventually converge to the exact energy,  $E$ . That is,

$$E_{MBPT} \rightarrow E, \quad N \rightarrow \infty \quad (4.3)$$

If the exact energy has a certain scaling with respect to some parameter  $\lambda$ , the approximated energy *must* reproduce this scaling as  $N \rightarrow \infty$ , and it *should* reproduce the scaling for finite  $N$ , so that we can have confidence in an approximate calculation. This implies that the leading contributions in the approximation should have a scaling with  $\lambda$  that is identical to the physical behaviour. Other terms may have a weaker scaling with  $\lambda$ , and the contributions from these terms would become negligible as  $\lambda \rightarrow \infty$ . For instance, if we consider the exact energy and some term,  $f$ , that is important for large  $\lambda$ , as functions of  $\lambda$ , we must require,

$$\frac{f(\lambda)}{E(\lambda)} = C, \quad \lambda \rightarrow \infty. \quad (4.4)$$

Here  $C$  represents a finite constant.

We are now ready to demonstrate the problem that arises if unlinked diagrams are included in  $E_{MBTP}$ . Let's assume that the term  $f(\lambda)$  contributes to the second order correction,  $E^{(2)}$ , and that the particular scaling behaviour is linear, i.e.  $E \propto \lambda$  and  $f(\lambda) = c\lambda$  with  $c$  constant. If unlinked diagrams were allowed, the same term would reappear in  $E^{(4)}$ , but this time to the second power, i.e. as  $f(\lambda)^2 = c^2\lambda^2$ . Clearly, this contribution would scale differently, and stronger than  $E$  with respect to the parameter  $\lambda$ . For large  $\lambda$ , it would disrupt the scaling of the approximate calculation.

The practical consequence of the unphysical scaling that may arise due to unlinked diagrams, is that a method, and a set of physical parameters, that work well in one end of the scaling parameter, e.g. for small systems, may not reproduce properties of larger systems. CI methods, such as shell model approaches will suffer from the lack of size extensivity, unless the full order of excitations are included [8]. CCM on the other hand does not include unlinked diagrams, so that the correct scaling is built into the method also when the excitations are limited.

## 4.2 Synopsis of the Coupled-Cluster Method

In this section we give a brief overview of the Coupled-Cluster method. We apply concepts and techniques that were discussed in Chapter 2.

The fundamental idea behind the Coupled-Cluster method is that the many body wavefunction can be approximated efficiently with the ansatz,

$$|\psi\rangle = e^T |\phi_0\rangle, \quad (4.5)$$

where  $|\phi_0\rangle \in \mathcal{H}^{(A)}$  is an antisymmetrized product state of  $A$  single particle wavefunctions. The idea is to introduce excitations in the wavefunction through a so-called cluster operator,

$$T : \mathcal{H}^{(A)} \rightarrow \mathcal{H}^{(A)}. \quad (4.6)$$

It is on the form,

$$T = T_1 + T_2 + \dots + T_A, \quad (4.7)$$



where  $T_n$  is an  $n$ -particle- $n$ -hole excitation operator,

$$T_n = \left( \frac{1}{n!} \right)^2 \sum_{\substack{a_1, \dots, a_n \\ i_1, \dots, i_n}} t_{i_1 \dots i_n}^{a_1 \dots a_n} a_{a_1}^\dagger \cdots a_{a_n}^\dagger a_{i_n} \cdots a_{i_1} . \quad (4.8)$$

Note that, since  $T_n$  contains only annihilators below Fermi level and creators above, all  $T_n$  commute with each other,

$$[T_n, T_m] = 0 . \quad (4.9)$$

The ground state wave function (4.5) for a particular Hamilton operator is determined by solving the non-linear set of equations,

$$\langle \phi_i^a | \bar{H} | \phi_0 \rangle = 0 , \quad (4.10)$$

$$\langle \phi_{ij}^{ab} | \bar{H} | \phi_0 \rangle = 0 , \quad (4.11)$$

$\vdots$

Here,  $|\phi_i^a\rangle$  is a particle-hole excited Slater determinant, and we have introduced the similarity transformed Hamilton operator,

$$\bar{H} = e^{-T} H e^T . \quad (4.12)$$

Once the  $T$  operator has been determined, the ground state energy is given by,

$$E = \langle \phi_0 | \bar{H} | \phi_0 \rangle . \quad (4.13)$$

We choose to set up the equations as a similarity transform of the Hamilton operator, because this lets us rewrite the transformation to an exact closed form.  $\bar{H}$  can be expanded with the Campbell-Baker-Hausdorff formula, [21, 8, 100]

$$e^{-T} H e^T = H + [H, T] + \frac{1}{2!} [H, T]^2 + \frac{1}{3!} [[H, T], T] + \cdots \quad (4.14)$$

For a given Hamiltonian operator, this equation has a finite number of terms, and constitutes a closed form of the similarity transformation. It is the form of  $T_n$  in Eq. (4.8) that leads to a natural truncation of this expression.

If Wick's theorem (See Section 2.2.4) is used to rewrite the commutators in Eq. (4.14), the terms with no contractions cancel because  $T_n$  has an even number of operators. Therefore, a commutator involving the  $T$  operator, leads to a sum where every term has at least one contraction. For the nested commutators in Eq. (4.14), one pair of operators is contracted at each nesting level. If the nesting level exceeds the maximum number of contractions between  $H$  and the cluster operators, the term vanishes. Consequently, the expansion has a finite number of terms.

To emphasize the closed form of the similarity transform, Eq. (4.14) is often denoted with a different notation, viz.

$$e^{-T} H e^T = (H e^T)_C . \quad (4.15)$$

The subscript  $C$  indicates that only “connected” terms should be included in the expansion, that is, only terms for which every factor from the cluster operator  $T_1$ ,  $T_2$ , etc., has at least one contraction with the Hamilton operator. The equivalence with Eq. (4.14) follows since  $T$  contains no operator that vanishes when applied to the vacuum  $|\phi_0\rangle$ . The only way to obtain non-zero contractions that involve the operators in  $T_n$ , is when  $T_n$  is placed to the *right* of any vacuum annihilating operators. This property can be stated in terms of Wick’s theorem,

$$\left\{ a_{a_1}^\dagger \cdots a_{a_n}^\dagger a_{i_n} \cdots a_{i_1} \right\} \left\{ a_p^\dagger \cdots a_q \right\} = \left\{ a_{a_1}^\dagger \cdots a_{a_n}^\dagger a_{i_n} \cdots a_{i_1} a_p^\dagger \cdots a_q \right\}. \quad (4.16)$$

Here, we have positioned the operators  $T_n$  on the *left*, and it is clear that no contractions are possible. For a single commutator this leads to the relation,

$$[H, T] = HT - TH = (HT)_C. \quad (4.17)$$

The generalization to Eq. (4.15) follows since  $T$  cannot contract with another  $T$ , so that the nested commutators can be written as,

$$[[H, T], T] = ((HT)_c T)_c = (HT^2)_C.$$

Approximations are introduced to Coupled-Cluster calculations by truncation of the  $T$  operator. Clearly, without a truncation of  $T$ , the number of amplitudes would quickly become unmanageable. A truncation to (S)ingle, (D)ouble, (T)riple, ..., excitations in  $T$  is described with acronyms CCS, CCSD, CCSDT, .... This nomenclature is employed widely within quantum chemistry, and also used adopted here.

### 4.2.1 Variational Properties

From the form of the excitation operators  $T_n$ , Eq. (4.8), and the exponential ansatz, Eq. (4.5), it follows that  $\bar{H}$  is non-hermitian. In turn this implies that the Coupled-Cluster energy is non-variational. The energy calculated with an approximate  $T$  (e.g. a truncation to CCSD) does not give an upper bound of the exact energy. However, considerable experience with CCM applied to quantum chemistry and gradually also to nuclear physics, suggest that the convergence toward the correct energy with respect to truncations in  $T$  follows a pattern which appears to be *effectively variational* for most applications. The error will typically be reduced by one order of magnitude for each level of excitations included in the  $T$  operator [54, 55].

### 4.2.2 Diagram Techniques

A diagram formalism for CCM provides a convenient method to determine Wick contractions in equations (4.10), (4.11) and (4.13). Since we will develop the diagram technique further for spectroscopic factors, we summarize the basic concepts, but we refer the reader to Refs. [21, 100] for pedagogical introductions to the Coupled-Cluster diagrams and for the rules of algebraic interpretations.

$$\begin{array}{ll}
 \begin{array}{c} \text{Diagram 1: A vertex with two outgoing lines labeled } q \text{ and } p. \end{array} & \sum_{pq} f_q^p \{a_p^\dagger a_q\} \\
 \begin{array}{c} \text{Diagram 2: A vertex with four lines. Two incoming lines labeled } r \text{ and } s, \text{ and two outgoing lines labeled } p \text{ and } q. \end{array} & \frac{1}{4} \sum_{pqrs} v_{rs}^{pq} \{a_p^\dagger a_q^\dagger a_s a_r\} \\
 \begin{array}{c} \text{Diagram 3: A vertex with two lines. One incoming line labeled } i \text{ and one outgoing line labeled } a. \end{array} & \sum_{ia} t_i^a a_a^\dagger a_i \\
 \begin{array}{c} \text{Diagram 4: A vertex with four lines. Two incoming lines labeled } i \text{ and } j, \text{ and two outgoing lines labeled } a \text{ and } b. \end{array} & \frac{1}{4} \sum_{ijab} t_{ij}^{ab} a_a^\dagger a_b^\dagger a_j a_i
 \end{array}$$

Figure 4.1: Components in the diagrammatic representation of the Coupled-Cluster equations and the corresponding algebraic interpretation. Note that the pointed lines with general indices  $p, q, r, \dots$  can be rotated freely. If the arrow points upwards or downwards, the index corresponds to a particle or hole orbit respectively. The lines annotated with indices restricted to be above or below the Fermi level,  $a, b$  or  $i, j$  respectively, are required to point in the direction indicated. Note that all creation operators are represented by lines pointing out of a vertex, while annihilators point inwards. Second quantization operators attached to the same interaction line are normal ordered. The fractions  $1/4$  are included to account for the unrestricted summations.

$$\begin{array}{c}
 \begin{array}{c} \text{Diagram 1: A loop with two vertices. The left vertex has an incoming line labeled } i \text{ and an outgoing line labeled } a. \text{ The right vertex has an incoming line labeled } a \text{ and an outgoing line labeled } i. \end{array} \\
 f_a^i t_i^a
 \end{array}
 +
 \begin{array}{c}
 \begin{array}{c} \text{Diagram 2: Two separate loops. The left loop has an incoming line labeled } i \text{ and an outgoing line labeled } a. \text{ The right loop has an incoming line labeled } j \text{ and an outgoing line labeled } b. \end{array} \\
 \frac{1}{2} v_{ab}^{ij} t_i^a t_j^b
 \end{array}
 +
 \begin{array}{c}
 \begin{array}{c} \text{Diagram 3: Two separate loops. The left loop has an incoming line labeled } i \text{ and an outgoing line labeled } a. \text{ The right loop has an incoming line labeled } j \text{ and an outgoing line labeled } b. \end{array} \\
 \frac{1}{4} v_{ab}^{ij} t_{ij}^{ab}
 \end{array}$$

Figure 4.2: Coupled-Cluster energy in diagrammatic representation and the corresponding algebraic interpretation.

Fig. 4.1 lists the basic constituents of the Coupled-Cluster diagrams and Fig. 4.2 demonstrates how the energy equation (4.13) can be written diagrammatically for CCSD with a two-body interaction. The algebraic interpretation of the diagrams is,

$$E = f_a^i t_i^a + \frac{1}{2} v_{ab}^{ij} t_i^a t_j^b + \frac{1}{4} v_{ab}^{ij} t_{ij}^{ab}. \quad (4.18)$$

This expression can also be derived using the techniques discussed in Chapter 2, in particular Wick's theorem.

The diagrams can be viewed as simply a bookkeeping system for Wick contractions. Whenever there is a connection between interaction lines, it corresponds to a Wick contraction in the equations. Lines with an arrow pointing up and down correspond to particle and hole states respectively. A diagram in which every directed line has been connected, corresponds to the vacuum expectation value of the operators in the expression. The phase is determined by counting the number of loops  $n_l$ , and the number of hole lines  $n_h$  in the diagram, and calculated as

$$(-1)^{n_h + n_l}. \quad (4.19)$$

The factor is determined by including a fraction 1/2 for each pair of *equivalent lines* and for each pair of *equivalent vertices*. The second term in (4.18) has one pair of equivalent vertices, and the third term has two pairs of equivalent lines.

### 4.3 Equations-of-Motion Coupled-Cluster (EOM-CC)

In order to develop a Coupled-Cluster expression for the spectroscopic factor, we will need to circumvent the non-hermitian nature of CCM, and also to model the odd neighbours of the spherical closed (sub-)shell nucleus. Solutions to both of these challenges are provided by the method known as Equations-of-Motion Coupled-Cluster [8, 22, 26, 39, 80, 101]. For the spectroscopic factors we will need both left and right solutions for the closed shell system with  $A$  nucleons as well as the system with one less particle. Algebraic and diagrammatic forms of the solutions are given in Figure 4.3. The interpretation is as discussed in the caption to Figure 4.1.

#### 4.3.1 The Right Eigenvalue Problem

The reference determinant ket is, by construction, the ground state of the similarity transformed Hamiltonian,  $\bar{H}$ . If we want to study excited states we need a more general state. Such a state is written in the EOM-CCM approximation as <sup>1</sup>

$$R_k |\psi_0\rangle = R_k e^T |\phi_0\rangle \quad (4.20)$$

<sup>1</sup>We use the notation from reference [21] where  $|R_k\rangle = R_k |\phi_0\rangle$  is an eigenstate of  $\bar{H}$ . This differs from the notation of reference [8] where  $|R_k\rangle = R_k e^T |\phi_0\rangle$  is an eigenstate of  $H$ .

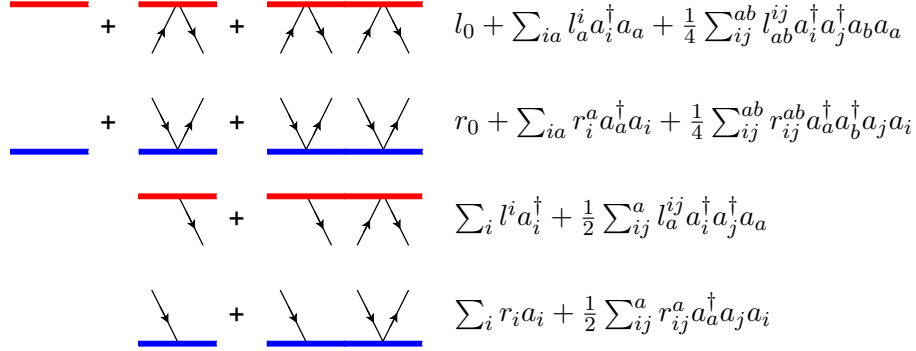


Figure 4.3: The diagrammatic representation of the left and right EOM solutions for  $A$ -body and  $A - 1$ -body states. See caption of Figure 4.1 for interpretation rules.

where  $R_k$  is a general operator exciting the Coupled-Cluster ground state,  $|\psi_0\rangle = e^T |\phi_0\rangle$  to the state  $k$ .  $R_k$  consist of terms  $R_k = r_0 + R_1 + R_2$  where  $r_0$  is a scalar and,

$$R_1 = \sum_{ia} r_i^a a_a^\dagger a_i, \quad R_2 = \frac{1}{4} \sum_{ijab} r_{ij}^{ab} a_a^\dagger a_b^\dagger a_j a_i. \quad (4.21)$$

Thus, we make a linear combination of particle-hole excited states and restrict the number of excitations to two. The solutions are expected to be eigenstates of  $H$ , so they should solve the eigenvalue problem,

$$H R_k |\psi_0\rangle = E_k R_k |\psi_0\rangle. \quad (4.22)$$

Comparing with the ground state energy eigenproblem,

$$H |\psi_0\rangle = E_0 |\psi_0\rangle, \quad (4.23)$$

we see that we can write

$$[H, R_k] |\psi_0\rangle = (E_k - E_0) R_k |\psi_0\rangle. \quad (4.24)$$

This is the “equation of motion”. Left multiplying with  $e^{-T}$  and using the fact  $[R_k, T] = 0$ , we can rewrite the EOM as operators acting on the reference determinant:

$$[\bar{H}, R_k] |\phi_0\rangle = (E_k - E_0) R_k |\phi_0\rangle. \quad (4.25)$$

Note that, we have here the similarity transformed Hamiltonian. For practical computations, it may be desirable to construct this operator explicitly and store it for the solution of several forms of the EOM state operator. A computationally effective form of  $\bar{H}$  is given in reference [40].

We now rewrite the left hand side to normal order with Wicks theorem. The form of  $R_k$ , Equation (4.21), leads again to the property (4.16), so that only fully connected terms survive,

$$(\bar{H} R_k)_C |\phi_0\rangle = \omega_k R_k |\phi_0\rangle. \quad (4.26)$$

Here, we have also introduced the relative excitation energy

$$\omega_k = E_k - E_0. \quad (4.27)$$

Assuming the amplitude equations have been solved,  $\bar{H}$  is known and the right eigenvalue problem is reduced to finding the coefficients  $R_0, r_i^a$  and  $r_{ij}^{ab}$ . If we project on excited bras, we get linear equations for the coefficients,

$$\langle \phi_i^a | (\bar{H} R_k)_C | \phi_0 \rangle = \omega_k r_i^a, \quad (4.28)$$

$$\langle \phi_{ij}^{ab} | (\bar{H} R_k)_C | \phi_0 \rangle = \omega_k r_{ij}^{ab}. \quad (4.29)$$

By solving these equations we determine the coefficients  $r_i^a$  and  $r_{ij}^{ab}$  which define the eigenstates of the system. The amplitude for no excitations,  $r_0$ , is also included in  $R_k$ , so that the general expression also allows for the ground state. The ground state must be identical to the Coupled-Cluster solution, so in that case  $r_0 = 1$  and  $r_i^a = r_{ij}^{ab} = 0$ .

The left hand sides of Eqs. (4.28 and 4.29) can be evaluated diagrammatically. We refer the reader to Reference [8] for a discussion of EOM diagrams. Note that the similarity transformed Hamiltonian can have three-body forces even though the bare Hamiltonian has only two-body forces. Diagrammatically this happens when one couples the two-body interaction with the  $T_2$  operator. (See Figure 4.1)

### 4.3.2 The Dual Solutions

Since  $\bar{H}$  is non-hermitian, there is also a corresponding left eigenvalue problem for which the solutions are not simply the conjugated of the right hand solutions. The ground state bra is not the hermitian conjugated ground state ket. Instead we try to write it as a linear combination of dual excited Slater determinants. The left eigenstates of  $\bar{H}$  can be written with the operator  $L_k$

$$\langle L_k | = \langle \phi_0 | L_k \quad (4.30)$$

where  $L_k$  is a deexcitation operator acting to the left, leading to excited bra configurations. It is constructed in a way similar to  $R_k$ , viz.

$$L_k = l_0 + L_1 + L_2. \quad (4.31)$$

Here,

$$L_1 = \sum_{ia} l_a^i a_i^\dagger a_a, \quad L_2 = \frac{1}{4} \sum_{ijab} l_{ab}^{ij} a_i^\dagger a_j^\dagger a_b a_a. \quad (4.32)$$

Since  $L_k$  creates particles with hole-indices, and destroys particle-indices it is clearly a deexcitation operator, so unlike the excitation operators, it does not commute with  $T$ .

As for the right eigenvalue case, we define the eigenbra  $\langle L_k |$  as an eigenvector of the transformed Hamiltonian,  $\bar{H}$ . The eigenvalue problem

$$\langle L_k | \bar{H} = \langle L_k | E_k \quad (4.33)$$

can be projected on singly or doubly excited kets to give the two equations

$$\langle \phi_0 | (l_0 + L_1 + L_2) \overline{H} | \phi_i^a \rangle = E_k l_a^i \quad (4.34)$$

and

$$\langle \phi_0 | (l_0 + L_1 + L_2) \overline{H} | \phi_{ij}^{ab} \rangle = E_k l_{ab}^{ij}. \quad (4.35)$$

Where the coefficients  $l_a^i$  and  $l_{ab}^{ij}$  define the eigenstates. Note, however, that this expression does not involve the commutator, so that the  $L$ -operators may contribute with diagrams not connected to the Hamiltonian. This is also the reason why it is natural to use  $E_k$  instead of  $\omega_k$  in the expression above. The relative excitation energy  $\omega_k$  can easily be obtained through relation (4.27).

Again the coefficient equations can be written down diagrammatically. These excitation operators are now to the left of the Hamiltonian. In the diagrams this corresponds to having the excitation operators (from  $l_a^i$  and  $l_{ab}^{ij}$ ) at the top. The loose directed lines should now extend downwards corresponding to the excited kets. Again the  $\overline{H}_3$  three-body force enters the diagrams even though the bare Hamiltonian is restricted to a two-body interaction [8].

### 4.3.3 Particle Removal

If the particle conserving operators  $R_k$  and  $L_k$  are replaced with particle removal operators, the formalism is known as particle-removal equation-of-motion (PR-EOM). The solutions will represent neighbours of the nucleus modelled as the Coupled-Cluster solution. We use this technique to generate the final wavefunctions we need for the spectroscopic factor calculation. See Fig. 4.3 for explicit expressions of the operators.

### 4.3.4 Normalization

The left and right ground state solutions are *bi-normalized* against each other, i.e.

$$\langle L_k | R_{k'} \rangle = \delta_{kk'}. \quad (4.36)$$

Note that this requirement does not uniquely define a normalization for the left and right solutions separately. For any scaling  $\alpha$  of  $|R_{k'}\rangle$ , the normalization condition can be recovered by a corresponding scaling  $1/\alpha$  for  $\langle L_k|$ . This ambiguity must be taken into account when EOM solutions are used to calculate derived quantities such as spectroscopic factors.

## 4.4 Spectroscopic Factors with Coupled-Cluster

In order to calculate spectroscopic factors with the Coupled-Cluster method, we need to start with an expression that is well defined also for eigenstates to the non-hermitian operator  $\overline{H}$ . Using the EOM-CCSD solutions for the right and left

eigenvalue problems for the  $A$  and the  $A - 1$  systems, we must take care to employ the eigenstates of  $H$ , not those of  $\bar{H}$ . If  $R_k$  and  $L_k$  parametrize right and left EOM-CCSD solutions respectively, the corresponding eigenstates of  $H$  are given by  $e^T R_k |\phi_0\rangle$  and  $\langle\phi_0| L_k e^{-T}$ . By inserting the appropriate solutions, Equation (3.24) can be written,

$$S_{A-1}^A(lj) = \sum_n \frac{\langle\phi_0| L_0^A \overline{a_{nljm}^\dagger} R_\mu^{A-1} |\phi_0\rangle \langle\phi_0| L_\mu^{A-1} \overline{a_{nljm}} R_0^A |\phi_0\rangle}{(J_A M_{Aj-m} | J_{A-1} M_{A-1})^2}. \quad (4.37)$$

This is how we define the spectroscopic factors within coupled-cluster theory. We have introduced the similarity-transformed creation and annihilation operators,

$$\overline{a_p^\dagger} \equiv e^{-T} a_p^\dagger e^T = \left( a_p^\dagger e^T \right)_C, \quad (4.38)$$

$$\overline{a_p} \equiv e^{-T} a_p e^T = \left( a_p e^T \right)_C. \quad (4.39)$$

Again we have used property (4.16) of the  $T$  operator to write the similarity transformation as a sum of connected terms.

If we did not define the SF using both left and right solutions as in Eq. (4.37), we would not be able to determine a unique normalization due to the ambiguity discussed in section 4.3.4. The chosen form removes this ambiguity as both left and right solutions are present in the same factor. A scaling of a pair of left and right solutions does not change the expression in (4.37).

#### 4.4.1 Similarity Transformed Operators

Evaluating the Hausdorff expansion of the similarity transformed creation operator, we get

$$\overline{a_p^\dagger} = a_p^\dagger + [a_p^\dagger, T] + \text{vanishing terms} \quad (4.40)$$

$$= a_p^\dagger + \sum_{ib} t_i^b [a_p^\dagger, a_b^\dagger a_i] + \frac{1}{4} \sum_{ijbc} t_{ij}^{bc} [a_p^\dagger, a_b^\dagger a_c^\dagger a_j a_i] \quad (4.41)$$

$$= a_p^\dagger - \sum_{ib} t_i^b a_b^\dagger \delta_{ip} + \frac{1}{2} \sum_{ijbc} t_{ij}^{bc} a_b^\dagger a_c^\dagger a_i \delta_{jp} \quad (4.42)$$

Thus, the form of  $\overline{a_p^\dagger}$  depends on whether  $p$  is a particle index ( $a, b, \dots$ ) or a hole index ( $i, j, \dots$ ),

$$\overline{a_a^\dagger} = a_a^\dagger \quad (4.43)$$

$$\overline{a_i^\dagger} = a_i^\dagger - \sum_b t_i^b a_b^\dagger - \frac{1}{2} \sum_{kbc} t_{ik}^{bc} a_b^\dagger a_c^\dagger a_k. \quad (4.44)$$



Similarly

$$\overline{a_p} = a_p + [a_p, T] + \text{vanishing terms} \quad (4.45)$$

$$= a_p + \sum_{ib} t_i^b [a_p, a_b^\dagger a_i] + \frac{1}{4} \sum_{ijbc} t_{ij}^{bc} [a_p, a_b^\dagger a_c^\dagger a_j a_i] \quad (4.46)$$

$$= a_p + \sum_{ib} t_i^b a_i \delta_{bp} + \frac{1}{2} \sum_{ijbc} t_{ij}^{bc} a_c^\dagger a_j a_i \delta_{bp}. \quad (4.47)$$

and

$$\overline{a_i} = a_i \quad (4.48)$$

$$\overline{a_a} = a_a + \sum_i t_i^a a_i + \frac{1}{2} \sum_{ijc} t_{ij}^{ac} a_c^\dagger a_j a_i. \quad (4.49)$$

### Diagram Representation

The regular diagram rules for CCM [8, 21] do not specify how to treat a second quantization operator present in the matrix element. The index  $p$  in the operators  $a_p^\dagger$  and  $a_p$  is not summed over, and we need to use a diagrammatic representation which prevents us from introducing a summation. Also, we want to keep in line with the convention that creation operators go out of interaction lines, while annihilators go into them. We accomplish both of these requirements by representing the creation operator as a line coming out of a small open circle and the annihilation operator as a line going into a small open circle. The “bare” operators will then be represented as

$$a_a^\dagger = \text{diagram of a line exiting a small open circle} \quad (4.50)$$

$$a_i^\dagger = \text{diagram of a line exiting a small open circle} \quad (4.51)$$

$$a_a = \text{diagram of a line entering a small open circle} \quad (4.52)$$

$$a_i = \text{diagram of a line entering a small open circle}. \quad (4.53)$$

Clearly, this notation allows the diagrammatic contraction of the outgoing creation operators with inwards pointing annihilators in other diagram components, and vice versa for the annihilator diagrams. The small open circle marks this operator line as the unsummable index.

The diagram representation of  $\overline{a_p^\dagger}$  follows from the connection requirement stated in Equations (4.38) and (4.39). Obviously, a single second quantization operator cannot be connected to more than one term of the  $T$  operator. The possible

CCSD diagrams for the creation operator are,

$$\overline{a_a^\dagger} = \text{diagram}, \quad (4.54)$$

$$\overline{a_i^\dagger} = \text{diagram} + \text{diagram} + \text{diagram}. \quad (4.55)$$

As expected, the creation operator can only be contracted with  $T$  if the index refers to an orbit below the Fermi surface. The transformed annihilator  $\overline{a_p}$  will be represented as,

$$\overline{a_a} = \text{diagram} + \text{diagram} + \text{diagram}, \quad (4.56)$$

$$\overline{a_i} = \text{diagram}. \quad (4.57)$$

It is the annihilator with a particle index that can be contracted with the  $T$  operator.

As a check, we perform the algebraic interpretation of these diagrams according to the standard rules. For operator diagrams, all external directed lines are summed over. This must also be the case here, except for lines that are connected to the bare second quantization operator, which is explicitly defined without summation. The index label order in the diagram corresponds exactly to the order on the amplitude, and we associate incoming lines with subscript indices and outgoing lines with superscript indices. However, the index order in the operator string is different in the diagram and the algebraic representation: Outgoing lines correspond to creation operators and appear in the same order, while inwards pointing lines are annihilators that appear in reversed order.

The interpretations of (4.54) and (4.57) are trivial, and according to the rules discussed above, we may interpret (4.55) and (4.56) as

$$\overline{a_i^\dagger} = a_i^\dagger + n_1 \sum_a t_i^a a_a^\dagger + n_2 \frac{1}{2} \sum_{abj} t_{ij}^{ab} a_a^\dagger a_b^\dagger a_j, \quad (4.58)$$

$$\overline{a_a} = a_a + m_1 \sum_i t_i^a a_i + m_2 \frac{1}{2} \sum_{bij} t_{ij}^{ab} a_b^\dagger a_j a_i. \quad (4.59)$$

We have inserted factors  $\frac{1}{2}$  in order to avoid overcounting due to the unrestricted summation. The coefficients  $n_\nu$  and  $m_\mu$  represent the sign and possibly a factor that must be determined. Note that the fixed second quantization operator is attached to the  $T_2$  diagrams on the leftmost end in diagram expressions (4.55) and (4.56). This corresponds to a contraction with the operators in  $T_2$  that are on the extreme ends, as is also apparent in the equations above. This is necessary if an algebraic interpretation of the operators is desired.<sup>2</sup>

<sup>2</sup>When the operator is used in matrix elements the unsummable index can be placed anywhere as the interpretation rules for matrix elements will compensate for it by the phase determined from the number of loops.

The algebraic sign of an operator diagram is determined by the contraction structure of the diagram when all external directed lines, have been stripped off. We may see the second and third terms in (4.55) and (4.56) as partially contracted operators, the rule can also be stated that signs and factors from already contracted operators must be included in the algebraic interpretation. The internal hole lines in Equation (4.55) lead to a phase  $-1$  for each term, and we conclude that,

$$n_1 = n_2 = -1, \quad (4.60)$$

$$m_1 = m_2 = +1. \quad (4.61)$$

Thus, Equations (4.44) and (4.49) are reproduced.

#### 4.4.2 Diagrams For Spectroscopic Factors

Equation (4.37) can be represented by diagrams where the similarity transformed creation and annihilation operators are represented by the above diagrams. The EOM-CCSD solutions are represented diagrammatically as displayed in Figure 4.3. At the bottom and top of the diagrams, we should have the reference determinant, which corresponds to no loose directed arrows. The spectroscopic factor diagrams are found by considering all terms in the products of the involved operators. The products that must be evaluated can now be written in diagrammatic form,

$$\langle A - 1 | a_i | A \rangle = \left( \text{red line} + \text{red line with two arrows} \right) \circ \left( \text{blue line} + \text{blue line with two arrows} + \text{blue line with four arrows} \right) \quad (4.62)$$

$$\langle A - 1 | a_a | A \rangle = \left( \text{red line} + \text{red line with two arrows} \right) \quad (4.63)$$

$$\times \left( \text{hole line} + \text{hole line with two arrows} + \text{hole line with four arrows} \right) \left( \text{blue line} + \text{blue line with two arrows} + \text{blue line with four arrows} \right)$$

$$\langle A | a_a^\dagger | A - 1 \rangle = \left( \text{red line} + \text{red line with two arrows} + \text{red line with four arrows} \right) \circ \left( \text{blue line} + \text{blue line with two arrows} \right) \quad (4.64)$$

$$\langle A | a_i^\dagger | A - 1 \rangle = \left( \text{red line} + \text{red line with two arrows} + \text{red line with four arrows} \right) \quad (4.65)$$

$$\times \left( \text{hole line} + \text{hole line with two arrows} + \text{hole line with four arrows} \right) \left( \text{blue line} + \text{blue line with two arrows} \right)$$

Only those terms that are fully contracted will survive and contribute with a term to the overlap. The diagrams that give non-zero contributions are displayed in Figure 4.4 with the algebraic interpretations.

$\langle A-1 a_i A\rangle$		$l^i r_0$ $l_a^{ij} r_j^a$
$\langle A-1 a_a A\rangle$		$l^i t_i^a r_0$ $l^i r_i^a$ $\frac{1}{2} l_b^{ij} t_{ij}^{ab} r_0$ $l_b^{ij} t_i^a r_j^b$ $\frac{1}{2} l_b^{ij} r_{ij}^{ab}$
$\langle A a_a^\dagger A-1\rangle$		$l_a^i r_i$ $\frac{1}{2} l_{ab}^{ij} r_{ij}^b$
$\langle A a_i^\dagger A-1\rangle$		$l^0 r_i$ $l_a^j r_{ij}^a$ $-l_a^j t_i^a r_j$ $-\frac{1}{2} l_{ab}^{jk} t_i^a r_{jk}^b$ $-\frac{1}{2} l_{ab}^{jk} t_{ik}^{ab} r_j$

Figure 4.4: Diagram representation of the overlap expressions; repeated indices implies a summation. If the closed-shell system is in the ground state, diagrams involving either  $r_i^a$  or  $r_{ij}^{ab}$  vanish. The individual components of these diagrams are explained in Figures 4.1 and 4.3.

## Chapter 5

# The Spherical Coupled-Cluster Method

The angular momentum coupled Coupled-Cluster formalism was recently developed by Hagen and Papenbrock at the Oak Ridge National Laboratory. [46, 47] It leads to a tremendous speed-up compared to an  $m$ -scheme implementation as demonstrated in several applications [45, 46, 48, 50, 47]. The increased efficiency has two sources.

1. Using a spherical model, the number of single particle basis states is much smaller than with the  $m$ -scheme basis. This is due to the redundancy of the single particle projection label. However, for product states, we must instead introduce combined quantum labels  $J$  and  $M$  for the total angular momentum and its projection.
2. In the spherical formulation of CCM, one can employ the Wigner-Eckart theorem to factorize the geometrical structure out of the amplitude equations.

In this chapter we will briefly explain the principles of the spherical Coupled-Cluster method. Quantum mechanical angular momentum algebra is a field that has matured to the extent that it has gone past science. The application of angular momentum algebra is straightforward and the techniques are regarded as a set of standard tools for quantum physicists [17, 25, 99, 103]. However, the mathematical expressions that are involved are often complex, and hand calculations are laborious and error prone. This author preferred to automate the angular momentum algebra by implementing a Racah-algebra module for the computer algebra system SymPy. This work will also be presented.

## 5.1 Principles behind the Spherical Coupled-Cluster Formalism

In this section, we discuss the basic principles and assumptions inherent in the angular momentum coupled formulation of Coupled-Cluster.

### 5.1.1 Internal Structure of the Amplitudes

The underlying idea is to express the amplitudes  $t_i^a, t_{ij}^{ab}, \dots$  in the cluster operator  $T$  as defined in (4.8) as matrix elements in the form of expectation values,

$$\langle a|T|i\rangle \equiv t_i^a \quad (5.1)$$

$$\langle ab|T|ij\rangle \equiv t_{ij}^{ab} \quad (5.2)$$

$$\vdots \quad (5.3)$$

The expectation value notation displays the amplitudes in a form that allows a conceptually different interpretation. While the amplitudes have so far been considered simply as scalar unknowns to be determined, this notation reveals an internal structure. The cluster operator  $T$  maps kets to kets. For A-body states in a Hilbert space  $\mathcal{H}^{(A)}$ ,

$$T : \mathcal{H}^{(A)} \rightarrow \mathcal{H}^{(A)}. \quad (5.4)$$

As discussed in section 2.1, the bra state  $\langle ab|$  is also an operator, but with the complex plane as the range:

$$\langle ab| : \mathcal{H}^{(A)} \rightarrow \mathbf{C}. \quad (5.5)$$

The amplitudes of  $T$  can be seen as two operators acting on a quantum state  $|ij\rangle$ , first the cluster operator  $T$  and then the dual state  $\langle ab|$ . We will exploit the properties of these components, in particular the transformation properties under rotation. (See discussion in Section 2.1.)

### Properties of the Cluster Operator

The transformation properties of the ket and the bra can safely be assumed known, as they depend solely on the form of the single particle basis waves. We are in control of these objects, and can decide to use eigenstates of total angular momentum, that are known to transform like spherical tensors. The cluster operator  $T$ , however, is different in this regard. A representation of the operator is given by Eqs. (4.7) and (4.8), but the form of  $T$  does not in itself guarantee well defined rotational properties.

However, it is empirically known that all even-even nuclei have ground states with zero angular momentum. Some nuclei are also believed to have a spherical shape, and this is said to correspond to closed shell configurations. For efficient modelling of these nuclei, we may choose to impose a restriction on the cluster

amplitude, namely that the operator must transform like a scalar under rotations, i.e. like a spherical tensor of rank 0. Thus, we require [70, 99],

$$[\hat{J}_{\pm}, T] = [\hat{J}_z, T] = 0. \quad (5.6)$$

Here  $\hat{J}_{\pm}$  are ladder operators for the angular momentum projection and  $\hat{J}_z$  is the operator that probes the projection quantum number.

When spherical tensor operators are multiplied, the product will in general have components of various ranks, but the possible ranks are limited by the triangular addition rule for angular momenta. When two angular momenta  $\mathbf{j}_1$  and  $\mathbf{j}_2$  are added to form a new angular momentum  $\mathbf{J} = \mathbf{j}_1 + \mathbf{j}_2$ , the requirement is that

$$|j_1 - j_2| \leq J \leq j_1 + j_2.$$

When the Coupled-Cluster equations (4.10, 4.11, ...) are solved iteratively, the interaction and the Fock term are used as starting amplitudes for  $T_1$  and  $T_2$  respectively. Since all terms in the Hamiltonian have zero rank, the iterations involve only products of zero rank tensors. The triangular requirement implies that a cluster operator  $T$  generated with this procedure, can also be expected to have zero rank. However, in order to make  $T$  obey conditions (5.6) *a priori*, each term in the cluster operator can be explicitly coupled to zero angular momentum.

To take advantage of the inherent symmetries in the spherical Coupled-Cluster scheme, the excitation amplitudes used in  $m$ -scheme need to be replaced with corresponding coupled amplitudes. The spherical cluster operators take the form [47],

$$T_1 = \sum_{ia} \tilde{t}_i^a [a_a^\dagger \otimes \tilde{a}_i]^0 \quad (5.7)$$

Here,  $a$  and  $i$  are labels for degenerate orbits with angular momentum magnitudes  $j_a$  and  $j_i$ , that is, the single particle projections are excluded. As usual  $a, b, \dots$  runs over all orbits above Fermi level while  $i, j, \dots$  runs below. The  $T_2$  amplitudes, take the form

$$T_2 = \sum_{ijabJ} \tilde{t}_{ij}^{ab}(J) \left[ [a_a^\dagger \otimes a_b^\dagger]^J \otimes [\tilde{a}_j \otimes \tilde{a}_i]^J \right]^0. \quad (5.8)$$

Note that the  $T_2$  amplitude includes a sum over the intermediate two-particle angular momentum  $J$ .

We have used the tilde to distinguish the amplitudes in the spherical expression. The form of the cluster operators (5.7) and (5.8) implies that  $T$  becomes a spherical tensor of rank zero per definition, and also that the number of degrees of freedom is reduced dramatically. Numerous applications to nuclei with a closed shell structure [45, 46, 48, 50, 47] have demonstrated that these systems do not require the  $m$ -scheme degrees of freedom for a satisfactory description with the CCM.

### 5.1.2 Factorization of the Geometrical Structure

The Wigner-Eckart theorem applies to matrix elements composed of three spherical tensors. The ket, the operator, and the bra must all transform like spherical tensors. The exact transformation properties that are required for each of them, depends on the definition of the reduced matrix element. We will as in Chapter 3 use the Wigner-Eckart theorem on the form, (For reference this relation is repeated in Appendix A)

$$\langle IN | T_m^{(j)} | JM \rangle = (JMjm | IN) \langle I || T^{(j)} || J \rangle . \quad (5.9)$$

Here,  $(\cdot | \cdot)$  is a Clebsch-Gordan coefficient and  $\langle \cdot || \cdot || \cdot \rangle$  denotes the *reduced matrix element*.  $I$ ,  $j$  and  $J$  are angular momenta, and  $N$ ,  $m$  and  $M$  the respective projections. The relation in (5.9) displays exactly how the geometry, i.e. the projection dependence, is factorized out from the *three-tensor matrix element*.

Eq. (5.9) also displays the assumed transformation property of the spherical tensor operator. Clebsch-Gordan coefficients are defined such that they couple objects with the same transformation properties, i.e. the same *variance*. Therefore, since the Clebsch-Gordan coefficient in (5.9) couples the operator and the ket, it is implicitly assumed that  $T_m^{(j)}$  and  $|JM\rangle$  are both covariant quantities.

Since both  $T$  and the Hamiltonian operator,  $H$ , is of zero rank, the Wigner-Eckart theorem takes a particularly simple form when used with the Coupled-Cluster equations (5.7, 5.8). This Clebsch-Gordan coefficient has a well known analytical form [17, 25, 99, 70],

$$(jm00 | JM) = \delta_{Jj} \delta_{Mm} . \quad (5.10)$$

So, in this case, the geometric factor is trivial and the Wigner-Eckart theorem simply confirms the form of  $T_1$  and  $T_2$ . However, we will see that for the spectroscopic factor diagrams, the geometric factor will contribute in a less trivial way.

### 5.1.3 Angular Momentum Coupling of CCM Diagrams

Working equations can be derived from the  $m$ -scheme equations. By a straightforward coupling of the  $m$ -scheme  $T$  operator, we can relate the  $m$ -scheme amplitudes to the spherical equivalents by,

$$t_{ij}^{ab} = \sum_{JM} (j_a m_a j_b m_b | JM) (j_i m_i j_j m_j | JM) \langle (ab)J || t || (ij)J \rangle . \quad (5.11)$$

Here, we have coupled the bra and the ket to states with well defined total angular momentum, and the Wigner-Eckart theorem is applied to the resulting three-tensor matrix element. The inverse relation is found using the orthogonality relations for Clebsch-Gordan coefficients,

$$\tilde{t}_{ij}^{ab}(J) \equiv \langle (ab)J || t || (ij)J \rangle = \sum_{m_a m_b m_i m_j} (j_a m_a j_b m_b | JM) (j_i m_i j_j m_j | JM) t_{ij}^{ab} . \quad (5.12)$$



We now demonstrate the angular momentum coupling of a term in the energy equation (4.18), and we start with the algebraic representation of the diagram that connects the interaction  $V$  and the  $T_2$  amplitude. The term reads (in m-scheme),

$$\frac{1}{4} v_{ab}^{ij} t_{ij}^{ab}. \quad (5.13)$$

The coupled form of the interaction factor is

$$v_{ab}^{ij} = \sum_{J'M'} (j_a m_a j_b m_b | J' M') (j_i m_i j_j m_j | J' M') \langle (ij) J' || v || (ab) J' \rangle \quad (5.14)$$

We have used the Wigner-Eckart theorem and the fact that the potential is also a rank zero spherical tensor. Clearly it does not couple states of different  $J$  or  $M$ . When the coupling expressions (5.11) and (5.14) are combined in the diagram, we can use the orthogonality relations of Clebsch-Gordan coefficients. Recall that there is an implicit sum over all repeated m-scheme indices  $i, j, a$  and  $b$ , so that there is also an implicit sum over all projections  $m_i, m_j, m_a$  and  $m_b$ . Since the matrix elements (reduced or not) are expressed in the coupled basis, there is no dependence on the single particle projections except the Clebsch-Gordan coefficients. This means that we can apply the orthogonality relations to write,

$$\frac{1}{4} v_{ab}^{ij} t_{ij}^{ab} = \frac{1}{4} \sum_{J(ab)(ij)} (2J+1) \langle (ij) J || v || (ab) J \rangle \langle (ab) J || t || (ij) J \rangle \quad (5.15)$$

The parenthesized summation indices indicates that the single particle orbits must be consistent with the total angular momentum  $J_{ab} = J_{ij} = J$ . That is, the triangular inequalities,

$$|j_a - j_b| \leq J_{ab} \leq j_a + j_b, \quad (5.16)$$

$$|j_i - j_j| \leq J_{ij} \leq j_i + j_j, \quad (5.17)$$

must be obeyed. The summation over single particle orbitals is the remnant of the implicit summation in the original  $m$ -scheme diagram. For clarity we choose to write the summations explicitly in the final expression. Since the expression is independent of the total projection, the sum over  $M$  can be evaluated, and this gives the factor  $(2J+1)$ .

We have introduced the coupled amplitudes (5.11) by combining incoming and outgoing indices to a total  $JM$ . For diagram (5.15) discussed above, this works efficiently. But there are other diagrams in the CC equations that connect the operators in such a way that better efficiency is achieved with a different coupling scheme. An example of such a diagram is the T2 diagram

$$t_{ik}^{ac} v_{cj}^{kb} = \langle ac | t | ik \rangle \langle kb | v | cj \rangle. \quad (5.18)$$

The contracted indices are  $k$  and  $c$ , so an element with the coupling given by Eq. (5.11) needs to be *decoupled* before the sum can be evaluated. Another approach is to *recouple* it to a so called cross-coupled matrix element [69]. We will return to different coupling schemes in section 5.2.3.

<code>ClebschGordanCoefficient</code>	Represents a Clebsch-Gordan coefficient
<code>ThreeJSymbol</code>	Represents a $3j$ -symbol.
<code>SixJSymbol</code>	Represents a $6j$ -symbol.
<code>AtomicSphericalTensor</code>	Represents a Spherical Tensor.
<code>CompositeSphericalTensor</code>	Represents a Spherical Tensor that is constructed by coupling other Spherical Tensors.

Table 5.1: Classes that represent mathematical objects in the `racah` module.

### 5.1.4 Transformation Properties of EOM-CC Operators

For the coupling of the spectroscopic factors, we also need to consider the transformation properties of the states generated with the EOM-CC formalism. The general EOM solution is allowed to have non-zero angular momentum. We denote this dependence explicitly with an argument to the wave operators, i.e.  $R^A(J, M)$ ,  $L^A(J, M)$ , etc. If the system identifier, e.g.  $A$ , is indicated by the angular momentum quantum labels, we will sometimes suppress the superscript.

The transformation properties of the EOM wave operators are taken to be consistent with the rotational properties of the states they create. The operators that produce right eigenstates of  $\bar{H}$  transform like a tensor,

$$T_m^{(j)}. \quad (5.19)$$

The left eigenstate operators are assumed to transform like

$$(-1)^{j-m} T_{-m}^{(j)}, \quad (5.20)$$

where  $T_{-m}^{(j)}$  is a spherical tensor.

## 5.2 Racah Algebra with SymPy

In order to calculate the coupled expressions of the spectroscopic factor diagrams in Figure 4.4, a computer program was created in the form of modules for the computer algebra system SymPy [1] (See also Chapter 2.3). In order to facilitate a flexible treatment of the available coupling schemes in the computer implementation, a strict separation between logic and interface was enforced, and implemented in two separate Python modules. The `braket` module contains objects to set up states and matrix elements in different coupling schemes, while the workhorse of the computer implemented angular momentum recoupling is the `racah` module.

### 5.2.1 The `racah` Module

The most important classes that are used to represent mathematical objects in the `racah` module are listed in Table 5.1. These are all subclasses of appropriate

<code>apply_orthogonality</code>	Identifies pairs of Clebsch-Gordan coefficients or $3j$ -symbols that can be reduced to Kronecker delta functions by means of orthogonality relations.
<code>convert_cgc2tjs</code>	Converts all Clebsch-Gordan coefficients in an expression to $3j$ -symbols.
<code>convert_tjs2cgc</code>	Converts all $3j$ -symbols in an expression to Clebsch-Gordan coefficients.
<code>evaluate_sums</code>	Evaluates summations that are particularly simple because of Kronecker delta functions.
<code>refine_phases</code>	Simplifies the phase of an expression. Information from the angular momentum symbols in the expression, as well as assumptions about half-integer and integer variables are used in the simplification.
<code>refine_tjs2sjs</code>	Identifies four compatible $3j$ -symbols and rewrites them to a $6j$ -symbol. This function will also ensure that the resulting expression is independent of the projection variables.

Table 5.2: Functions in the `racah` module that are used to manipulate expressions. Most of these functions take optional parameters that modify the behaviour.

SymPy base classes, which implies that the interpretation of Python code as mathematical statements is handled by the SymPy core. The goal of the `racah` module, is to implement methods to perform expression manipulations that are particular to angular momentum algebra. The most important functions for this purpose, are presented in Table 5.2. The usage of these functions will be demonstrated in section 5.3.

The implementation employs symmetry relations of the various angular momentum symbols to enforce a canonical form of all objects, except the Clebsch-Gordan coefficients. These are allowed to be on any form for the convenience of the user. Internally, however, they are converted to  $3j$ -symbols whenever a canonical form is required.

SymPy has recently gained a relatively rich assumption framework, which is also extensible. In order to simplify expressions containing symbols that are known to be half-integer, i.e. of the form  $n/2$  where  $n$  is odd, it was necessary to define and implement handlers for a new `half_integer` assumption. The rules listed in Table 5.3 are implemented through various assumption handlers in the `racah` module.

<code>integer</code>	$\Rightarrow$	<code>¬half_integer</code>
<code>integer+half_integer</code>	$\Rightarrow$	<code>half_integer</code>
<code>half_integer+half_integer</code>	$\Rightarrow$	<code>integer</code>
<code>half_integer*odd</code>	$\Rightarrow$	<code>half_integer</code>
<code>half_integer*even</code>	$\Rightarrow$	<code>integer</code>
<code>2*half_integer*odd</code>	$\Rightarrow$	<code>odd</code>
<code>2*half_integer*even</code>	$\Rightarrow$	<code>even</code>

Table 5.3: Inference rules for the `half_integer` assumption implemented in the `racah` module.

<code>SphericalTensorOperator</code>	Represents an operator transforming as a spherical tensor $T_m^{(j)}$ .
<code>DualSphericalTensorOperator</code>	Represents an operator transforming as $(-1)^{(j-m)}T_{-m}^{(j)}$ .
<code>SphFermKet</code>	Represents a fermionic ket.
<code>SphFermBra</code>	Represents a fermionic bra.
<code>MatrixElement</code>	Base class and factory for the specialized matrix elements below.
<code>DirectMatrixElement</code>	Represents an uncoupled ( $m$ -scheme) matrix element.
<code>ReducedMatrixElement</code>	Represents a reduced matrix element.
<code>ThreeTensorMatrixElement</code>	Represents a <i>reducible</i> matrix element.

Table 5.4: Classes that are implemented in the `braket` module. These classes are used to represent coupling orders. Upon request, the coupling can be returned as an expression with Clebsch-Gordan coefficients. This coupling expression will be suitable for manipulations with the functions defined in the `racah` module. This provides a convenient user interface to the Racah machinery.

### 5.2.2 The `braket` User Interface Module

The mathematical expressions that must be given as input to the `racah` module in order to derive the coupled expressions, are already quite complicated. To type in the coupling expressions for each diagram by hand would be a tedious and error prone task. The `braket` module was created instead, to allow input in the form of matrix elements with a specified coupling order. Upon request, the `braket` module will provide expressions for the full decoupling of a matrix element, and optionally relations between different coupling schemes. The output is specifically intended for further processing with the `racah` module.

The most important classes of the `braket` module are listed in Table 5.4. These classes provide a convenient way to set up different coupling schemes for matrix elements. The only function of interest that is implemented in the `braket` module, is called `rewrite_coupling`. Given an expression with matrix ele-

ments, and the requested coupling order, it will return an expression where the matrix elements have been rewritten to the requested form.

In the following section we demonstrate how different coupling schemes can be set up using the `braket` module.

### 5.2.3 Coupling Alternatives

The  $m$ -scheme matrix element,

$$\langle ab|v|cd\rangle ,$$

can be viewed as a composition of 5 independent spherical tensors,

$$\langle a| \langle b| v |c\rangle |d\rangle . \quad (5.21)$$

The conventional coupling of such an element starts with the creation of spherical basis states  $\langle(ab)JM|$  and  $|(cd)J'M'\rangle$ . Then the Wigner-Eckart theorem can be used on the resulting three spherical tensors. The coupling of basis states to construct a spherical two-particle basis for the matrix elements is in a sense arbitrary. We may instead choose to couple the factors in a different order.

By coupling a single particle ket to a single particle bra, we get *cross-coupled* matrix elements. A slightly different approach involves also a reformulation of the matrix element through a redefinition of the vacuum. This latter approach leads to *particle-hole coupled* matrix elements. The `braket` module is implemented so that it can handle all these alternatives. The coupling schemes presented in the following sections are extracted from Reference [69], and listed here for demonstration purposes.

#### Coupling of Dual States

When employing different coupling schemes for the matrix elements, it is crucial to treat correctly the rotational transformation properties of all involved quantities. The contravariant nature of a bra  $\langle j_a m_a|$ , means that the geometry, as probed by rotations, is identical to that of  $(-1)^{j_a-m_a} |j_a-m_a\rangle$ . In addition, one must decide upfront the rotational properties of the coupled state. The effective coefficient for coupling  $|c\rangle$  and  $\langle a|$  to a new *covariant* spherical tensor is

$$(-1)^{j_a-m_a} (j_c m_c j_a - m_a | J_{ca} M_{ca}) .$$

If we couple two dual states with each other to form a new dual state, we can get away with ignoring such phases and reflections. This is easily demonstrated by calculating it properly, treating all bra states as spherical tensors with the correct

rotation properties. The coupled dual state can then be rewritten [69]

$$\langle (ab)J_{ab}M_{ab} | = (-1)^{J_{ab}-M_{ab}} [\langle a | \otimes \langle b |]_{-M_{ab}}^{J_{ab}} \quad (5.22)$$

$$= (-1)^{J_{ab}-M_{ab}} \sum_{m_a m_b} (-1)^{j_a-m_a} (-1)^{j_b-m_b} \times (j_a-m_a j_b-m_b | J_{ab}-M_{ab}) \langle a | \langle b | \quad (5.23)$$

$$= \sum_{m_a m_b} (j_a m_a j_b m_b | J_{ab} M_{ab}) \langle a | \langle b | . \quad (5.24)$$

When the coupled state is written as a tensor product in (5.22), the rotation properties are explicitly displayed through the phase and the inverted projection. Also the operands,  $\langle a |$  and  $\langle b |$ , of the tensor product must be treated according to their properties as spherical tensors, which leads to (5.23). Then the addition rule for projections  $m_a + m_b - M_{ab} = 0$  and the symmetry relations of Clebsch-Gordan coefficients gives (5.24).

With the `braket` module, a coupled dual state is constructed by the statements

---

```
a = SphFermBra('a')
b = SphFermBra('b')
ab = SphFermBra('ab', a, b)
print latex(ab)
print latex(ab.as_direct_product())
```

---

The coupled bra is printed as,

$$\langle ab(a \curvearrowright b) | . \quad (5.25)$$

The coupling order is indicated by the curved arrow. When the coupled state is written in terms of the direct product state, the expression is,

$$\sum_{m_a m_b} (j_a m_a j_b m_b | J_{ab} M_{ab}) \langle a | \langle b | . \quad (5.26)$$

### Cross-Coupled Matrix Elements

Above, we saw that the symmetry properties of Clebsch-Gordan coefficients ensures that a straightforward “ket-like” coupling of two dual states results in a coupled bra,  $\langle JM |$ , that transforms correctly as the tensor  $(-1)^{J-M} T_{-M}^J$ . For the cross coupled matrix element we cannot expect the same simplification, so we need to calculate it by including all phases and reflections.

$$\begin{aligned} \langle ab|v|cd \rangle &= \sum_{J_{db} M_{db}} \sum_{J_{ca} M_{ca}} \langle \overline{ab|v|cd} \rangle \\ &\times (-1)^{J_{ca}-M_{ca}} (-1)^{j_a-m_a} (j_c m_c j_a-m_a | J_{ca}-M_{ca}) \\ &\times (-1)^{j_b-m_b} (j_d m_d j_b-m_b | J_{db} M_{db}) \end{aligned} \quad (5.27)$$

This may be taken as the definition of a cross coupled matrix element. Notice that while  $|d\rangle$  and  $\langle b|$  are coupled to form a ket, we have coupled  $|c\rangle$  and  $\langle a|$  so that they will form a state with the transformation properties of a bra. Note that we have defined the coupling from right to left, i.e.  $c$  to  $a$  and  $d$  to  $b$ , this was an arbitrary decision.

The two spherical tensors we have constructed above are

$$[|d\rangle \otimes \langle b|]_{M_{db}}^{J_{db}}$$

and

$$(-1)^{J_{ca}-M_{ca}} [|c\rangle \otimes \langle a|]_{-M_{ca}}^{J_{ca}}.$$

The reason we take care to construct tensors corresponding to one ket and one dual state, is because we are interested in a *scalar*, hence isotropic, matrix element. If we had constructed tensors corresponding to two kets or two dual states, the resulting expression could not have been coupled further to an isotropic scalar form. The decision to couple  $ca$  to a dual state instead of  $db$  was completely arbitrary, and because the matrix element is isotropic, it should not depend on this choice.

We fail to find an equivalent expression that uses two ket-like couplings as we could for the coupled dual state in (5.24). Equation (5.27) can be rewritten to

$$\begin{aligned} \langle ab|v|cd\rangle &= \sum_{J_{db}M_{db}} \sum_{J_{ca}M_{ca}} \langle \overline{ab}|v|cd\rangle (-1)^{-2m_c} \\ &\times (-1)^{j_c-m_c} (j_c-m_c j_a m_a | J_{ca} M_{ca}) \\ &\times (-1)^{j_b-m_b} (j_d m_d j_b -m_b | J_{db} M_{db}) \end{aligned} \quad (5.28)$$

The phase  $(-1)^{-2m_c}$  displays the breaking of isotropy if we insist on using two ket-like couplings.

With the `braket` module, we can also achieve this coupling order:

---

```
a = SphFermBra('a')
b = SphFermBra('b')
c = SphFermKet('c')
d = SphFermKet('d')
V = SphericalTensorOperator('V', 'J', 'M')
ca = SphFermBra('ca', c, a)
db = SphFermKet('db', d, b)
matel = MatrixElement(ca, V, db)
```

---

The cross-coupled element is represented as

$$\langle ca(|c\rangle \curvearrowright a)|V(J, M)|db(d \curvearrowright \langle b|)\rangle \quad (5.29)$$

And when it is expressed in the uncoupled form, the  $\text{\LaTeX}$  output is,

$$\begin{aligned} (-1)^{j_a-m_a} (-1)^{J_{ca}-M_{ca}} (-1)^{j_b-m_b} \sum_{m_a m_b m_c m_d} \\ (j_c m_c j_a -m_a | J_{ca} -M_{ca}) (j_d m_d j_b -m_b | J_{db} M_{db}) \\ \langle a, b|V(J, M)|c, d\rangle. \end{aligned} \quad (5.30)$$

### Particle-Hole Coupled Matrix Elements

There is yet another procedure we can follow to obtain a different coupling structure in the matrix elements. The matrix element in a particular basis must be independent of the way we choose to label it. Specifically, the partition of single particle states into holes and particles is purely technical and can not have any physical significance. So we should be able to switch perspective by viewing particle orbitals as holes in a different vacuum. Examples of matrix relabelling are

$$\langle ab|v|cd\rangle_{v_0} = \langle a|v|cdb^{-1}\rangle_{v_1} = \dots = \langle c^{-1}d^{-1}|v|a^{-1}b^{-1}\rangle_{v_n}, \quad (5.31)$$

where the subscript indicates that we have changed the vacuum definition.<sup>1</sup> Despite the different appearance of the matrix element, it is not affected by these redefinitions. For all vacua, the actual matrix element describes the correlated transition of particles from configurations  $c, d$  to  $a, b$ . By redefining the vacuum before coupling, we can employ the regular coupling scheme, and still obtain several different coupling structures of the matrix element.

The Pauli principle implies that

$$\langle ab|v|cd\rangle = \langle a|v|cdb^{-1}\rangle = -\langle b|v|cda^{-1}\rangle, \quad (5.32)$$

because in order to absorb an orbit into the vacuum, the corresponding operator needs to be adjacent to the vacuum state, i.e. at the rightmost position. If this process involves an odd number of permutations we get a negative sign due to the antisymmetrized interaction. The absorbed orbit will always show up as a hole immediately next to the other vacuum, i.e. as the rightmost label in the other state.

Before we consider coupling of the relabeled matrix elements, we will determine the rotational transformation properties of the newly introduced hole states. Considering that  $\langle jm| = \langle |a_{jm}$  for some vacuum, we may associate the tensorial characteristics of a single particle state with the generating operator. For another vacuum the same operator creates a hole in the empty ket state,  $a_{jm} | \rangle = |(jm)^{-1}\rangle$ , but the geometric structure should be identical in both cases. Accordingly,  $|(jm)^{-1}\rangle$  transforms like,

$$Q_m^j = (-1)^{j-m} T_{-m}^j. \quad (5.33)$$

This quantity characterizes any hole state on the ket side, and represents the *covariant transformation of a hole state*. Applying here the relation between spherical tensors and their hermitian conjugates [25, 69], we find that  $\langle (jm)^{-1}|$  should transform like,

$$(-1)^{j-m} Q_{-m}^j = (-1)^{j-m} (-1)^{j+m} T_m^j = (-1)^{2j} T_m^j. \quad (5.34)$$

So, whenever a dual hole state  $\langle (jm)^{-1}|$  is coupled, it should be treated like a quantity of the form  $(-1)^{2j} T_m^j$ , where  $T_m^j$  is a spherical tensor. This property

<sup>1</sup>Elsewhere in this work we drop the subscript signalling the change of vacuum.



defines the *contravariant transformation of a hole state*. For fermions, the phase  $(-1)^{2j}$  implies a change of sign.

Applying the above transformation properties to the coupling of a vacuum-shifted matrix element, we can write

$$\begin{aligned} \langle ab|v|cd\rangle &= \langle ac^{-1}|v|db^{-1}\rangle = -\langle c^{-1}a|v|db^{-1}\rangle \\ &= -\sum_{JM} \langle (c^{-1}a)|v|(db^{-1})\rangle (-1)^{J-M} \end{aligned} \quad (5.35)$$

$$\begin{aligned} &\times (-1)^{j_a-m_a} (-1)^{j_b-m_b} (-1)^{2j_c} \\ &\times (j_c m_c j_a - m_a | J-M) (j_d m_d j_b - m_b | JM) \\ &= -\sum_{JM} \langle (c^{-1}a)JM|v|(db^{-1})JM\rangle \\ &\times (-1)^{j_c-m_c} (j_c-m_c j_a m_a | JM) \\ &\times (-1)^{j_b-m_b} (j_d m_d j_b - m_b | JM) \end{aligned} \quad (5.36)$$

Evidently, the ph-matrix element can be coupled according to the same recipe as the conventionally coupled matrix elements (5.24), where also the bra state is coupled ket-like. The only difference is that hole states on both sides must rotate like  $(-1)^{j-m} T_{-m}^j$ . The phase  $(-1)^{2j_c}$ , introduced by the bra side hole state  $c^{-1}$ , repairs the broken isotropy observed in Equation (5.28) when we tried a ket-like coupling for the cross coupled matrix element.

Apart from a possible sign due to the Pauli principle (5.32), the ph-matrix elements can be related to cross coupled matrix elements by

$$\langle \overline{ab}|v|\overline{cd}\rangle = (-1)^{2j_c} \langle (ac^{-1})|v|(db^{-1})\rangle. \quad (5.37)$$

The coupled matrix elements are related with a phase for each hole state in the bra. The coupling direction is assumed to be the same in both forms.

In order to represent particle-hole coupled matrix elements with the `braket` module, the following statements can be used:

---

```
a = SphFermBra('a')
b = SphFermKet('b')
c = SphFermBra('c')
d = SphFermKet('d')
ca = SphFermBra('ca', -c, a)
db = SphFermKet('db', d, -b)
matel = MatrixElement(ca, V, db)
```

---

Here, we have formed the coupled ket from two single particle kets, where one of them, i.e. `b` is negated. This is interpreted as a hole state. The same applies to the coupled bra, where `c` is a hole state. The notation used for particle-hole coupled matrix elements is,

$$\langle ca(-c \curvearrowright a)|V(J, M)|db(d \curvearrowright -b)\rangle. \quad (5.38)$$

The coupling of hole states is implemented according to the conclusion that a ket-like coupling expression is valid. In terms of the uncoupled matrix element, we get,

$$\begin{aligned}
 & - (-1)^{j_b - m_b} (-1)^{j_c - m_c} \sum_{m_a m_b m_c m_d} \\
 & (j_c - m_c j_a m_a | J_{ca} M_{ca}) (j_d m_d j_b - m_b | J_{db} M_{db}) \\
 & \langle a, -c | V(J, M) | d, -b \rangle . \quad (5.39)
 \end{aligned}$$

We may also request the expression in terms of the direct matrix element in the original vacuum.

---

```
matel.as_direct_product(only_particle_states=True)
```

---

The (slightly rearranged) L<sup>A</sup>T<sub>E</sub>X output is now,

$$\begin{aligned}
 & \sum_{m_a m_b m_c m_d} - (-1)^{j_b - m_b} (-1)^{j_c - m_c} \\
 & (j_d m_d j_b - m_b | J_{db} M_{db}) (j_c - m_c j_a m_a | J_{ca} M_{ca}) \\
 & \langle a, b | V(J, M) | c, d \rangle . \quad (5.40)
 \end{aligned}$$

This concludes the presentation of the `braket` module. The author hopes to have have conveyed an impression that it provides a convenient user interface, for feeding a variety of angular momentum coupling structures to the computer algebra system. Clearly, once the coupling information is in the computer memory, represented by some data structure, it is available for further processing. In the next section, we will see how the `braket` module and the `racah` module fit together in an application to angular momentum coupled spectroscopic factor diagrams.

### 5.3 Coupling of Spectroscopic Factor Diagrams

We will now demonstrate how the SymPy modules can be used to derive the angular momentum coupled form of the spectroscopic factor diagrams discussed in section 4.4 and summarized in Figure 4.4. We will demonstrate the procedure only for a single diagram. All resulting equations are given in appendix B.

Whereas the form (4.37) of the spectroscopic factor, was convenient for the calculation of spectroscopic factors in the  $m$ -scheme formulation, we choose another form in the spherical implementation. As before, the spectroscopic factor is defined by equation (3.10), and adapted to a non-hermitian model by a suitable representation of the Overlap functions. However, as we will employ angular

$T, V, F$	$T^{(0)}$
$a_{jm}^\dagger, R^A(j, m), R^{A-1}(j, m)$	$T_m^{(j)}$
$a_{jm}, L^A(j, m), L^{A-1}(j, m)$	$(-1)^{j-m} T_{-m}^{(j)}$

Table 5.5: Transformation properties of all operators contributing to the spectroscopic factor diagrams. The operators are listed on the left and the assumed transformation property on the right. The transformation properties are presented in terms of a general spherical tensor  $T_m^{(j)}$  that exemplifies the rotational behaviour of the corresponding operators.

momentum algebra techniques, we express the spectroscopic factor on the form,

$$S_A^B(lj) = \sum_n \left( \sum_{mM_A} (-)^{j-m} (J_B M_B j-m | J_A M_A) \langle B | a_{nljm}^\dagger | A \rangle \right) \quad (3.27)$$

$$\times \left( \sum_{m'M'_A} (-)^{j-m'} (J_B M'_B j-m' | J_A M'_A) \langle A | a_{nljm'} | B \rangle \right).$$

The angular momentum algebra is unaffected by the nodal quantum number  $n$ , so we can treat each term separately. In addition, the two factors are calculated independent from each other, so the angular momentum coupling of each factor can be done separately. We recall that in Chapter 3,  $B$  denoted the system with largest number of particles, while  $A$  represented the system with one less particle. Here, the systems are denoted  $A$  and  $A-1$  respectively.

Inserting the appropriate EOM-CCSD solutions the expressions that need to be rewritten for spherical Coupled-Cluster are:

$$\sum_{mM_A} (-)^{j-m} (J_A M_A j-m | J_{A-1} M_{A-1}) \langle \phi_0 | L_0(J_A) \overline{a_{nljm}^\dagger} R_\mu(J_{A-1}) | \phi_0 \rangle, \quad (5.41)$$

and,

$$\sum_{mM_A} (-)^{j-m} (J_A M_A j-m | J_{A-1} M_{A-1}) \langle \phi_0 | L_\mu(J_{A-1}) \overline{a_{nljm}} R_0(J_A) | \phi_0 \rangle. \quad (5.42)$$

We will see that this form of the reduced matrix elements is useful when we rewrite the coupled diagrams to simpler forms.

### 5.3.1 Example: Coupling of $-\frac{1}{2} l_{ab}^{jk} t_{ik}^{ab} r_j$

The script in Listing 5.1 shows what objects need to be set up in order to use the `braket` and the `racah` module to couple the diagram,

---

```

from sympy import Symbol, Assume, latex
from sympy.physics.racahalgebra import (
    refine_phases, refine_tjs2sjs, convert_cgc2tjs,
    evaluate_sums, apply_orthogonality,
    ASigma, ClebschGordanCoefficient )
from sympy.physics.braket import (
    MatrixElement, ReducedMatrixElement, Dagger,
    SphFermKet, SphFermBra, SphericalTensorOperator,
    DualSphericalTensorOperator, rewrite_coupling,
10    braket_assumptions )

# Create the single particle states
i, j, k, a, b = map(SphFermKet, 'ijkab')

# Angular momenta for the spherical tensor operators
J_A = Symbol('J_A', nonnegative=True)
M_A = Symbol('M_A')
J_Aml = Symbol('J_Aml', nonnegative=True)
M_Aml = Symbol('M_Aml')
20

# Register the assumptions
braket_assumptions.add(Assume(J_A, 'integer'))
braket_assumptions.add(Assume(M_A, 'integer'))
braket_assumptions.add(Assume(J_Aml, 'half_integer'))
braket_assumptions.add(Assume(M_Aml, 'half_integer'))

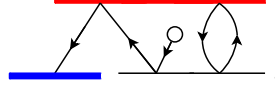
# Create spherical tensor operators
T = SphericalTensorOperator('T', 0, 0)
RAml = SphericalTensorOperator('R', J_Aml, M_Aml)
30 LA = DualSphericalTensorOperator('L', J_A, M_A)

# Create all matrix elements
l_abjk = MatrixElement((Dagger(j), Dagger(k)), LA, (a, b))
l_abjk_sph = ReducedMatrixElement(
    SphFermBra('jk', Dagger(j), Dagger(k)),
    LA, SphFermKet('ab', a, b))
t_abik = MatrixElement((Dagger(a), Dagger(b)), T, (i, k))
t_abik_sph = ReducedMatrixElement(
    SphFermBra('ab', Dagger(a), Dagger(b)),
40    T, SphFermKet('ik', i, k))
r_j = MatrixElement(0, RAml, j)
r_j_sph = ReducedMatrixElement(0, RAml, j)

```

---

Listing 5.1: First part of a Python script for the coupling of the spectroscopic factor diagram  $-\frac{1}{2}l_{ab}^{jk}t_{ik}^{ab}r_j$ . Both the  $m$ -scheme matrix elements and the reduced matrix elements that represent the solution amplitudes in the spherical formulation are set up, and this provides enough information that the full coupling expressions can be extracted. All classes that are used in this part of the script come from the `braket` module.



It corresponds to the term  $-\frac{1}{2}t_{ab}^{jk}t_{ik}^{ab}r_j$  in the algebraic expression.

After the import statements, we construct objects of the type `SphFermKet` to represent the single particle states on line 13. The name of the class is an abbreviation for “spherical fermionic ket”. Each instance of `SphFermKet` will automatically create symbols for the angular momentum quantum labels, and register the necessary assumptions so that these symbols are recognized as half-integers. The state label is used as a subscript so that it is easy to distinguish the angular momentum values that belong to a particular single particle state. For instance, a state labelled by  $i$  will register assumptions about the symbols  $j_i$  and  $m_i$ .

The `SphericalTensorOperator` and `DualSphericalTensorOperator` classes do not automatically register assumptions about the rank and projection symbols, so this must be done manually. This is the purpose of lines 15-30. The  $A$ -body system is assumed to have integer angular momentum, and the  $A - 1$ -body system has half-integer angular momentum. It is important to inform SymPy about these assumptions as this allows simplifications of the phases that will arise when we rewrite the expressions. The constructors for the spherical tensor operator objects take a label as well as the rank and projection symbols as arguments.

The matrix elements that are set up on lines 32-42, corresponds to the following (in order):

- $\langle jk|L^A|ab\rangle$ ,
- $\langle (jk)J_{jk}||L(J_A)|| (ab)J_{ab}\rangle$ ,
- $\langle ab|T|ik\rangle$ ,
- $\langle (ab)J_{ab}||T||(ik)J_{ik}\rangle$ ,
- $\langle |R^{A-1}|j\rangle$ ,
- $\langle ||R(J_{A-1})||j\rangle$ .

We have used `SphFermKet` again, as well as its dual counterpart, `SphFermBra`. This time, however, the states are composite, and the objects are used primarily as a data structure to represent the coupling order used in the matrix element. Here, we do not use *cross-coupled* or *particle-hole coupled* elements so the interpretation of the composite states is straightforward. `SphFermKet('ab', a, b)` creates the spherical two-body state,

$$|(ab)J_{ab}M_{ab}\rangle = \sum_{m_a m_b} (j_a m_a j_b m_b | J_{ab} M_{ab}) |ab\rangle .$$

On the bra side we use `Dagger` to obtain dual single particle states, from which the composite bra can be constructed. That is,

`SphFermBra('jk', Dagger(j), Dagger(k))` represents

$$\langle(jk)J_{jk}M_{jk}| = \sum_{m_j m_k} (j_j m_j j_k m_k | J_{jk} M_{jk}) \langle jk| .$$

The `ReducedMatrixElement` class contains information about the Wigner-Eckart theorem it is defined for. It has a method that will return the correct geometrical factor and the corresponding `ThreeTensorMatrixElement`. This, in turn, carries information about the applied coupling scheme. Altogether, the objects defined in Listing 5.1 contains everything that is needed in order to extract the complete coupling structure of the diagram. This concludes the initialization and we are ready to start working with actual mathematical expressions.

The script continues with the lines:

---

```
# Setup the reduction factor
j_i = Symbol('j_i', nonnegative=True)
m_i = Symbol('m_i')
sf_reduction = ASigma(M_A, m_i)*(-1)**(j_i - m_i) \
    *ClebschGordanCoefficient(
        J_A, M_A, j_i, -m_i, J_Aml, M_Aml)

# Setup the uncoupled expression
expr_msc = ASigma('m_a', 'm_b', 'm_j', 'm_k') \
53      *l_abjk*t_abik*r_j*sf_reduction
```

---

The coupling coefficient from Equation (5.41) is created and stored as the variable `sf_reduction` before it is included in the final uncoupled expression. The `ASigma` class is used to input and store information about summation variables. Note that we include summations over the projections  $m_a$ ,  $m_b$ ,  $m_j$  and  $m_k$ . These summations have been implicit elsewhere in this thesis, but the `racah` module requires that all summations over projection labels must be stated explicitly. Using the  $\text{\LaTeX}$  printing facilities of SymPy, we obtain the following (slightly rearranged) output for the  $m$ -scheme expression:

$$\sum_{M_A m_i} \sum_{m_a m_b m_j m_k} (-1)^{j_i - m_i} (J_A M_A j_i - m_i | J_{Aml} M_{Aml}) \langle a, b | T(0, 0) | i, k \rangle \langle j, k | L(J_A, M_A) | a, b \rangle \langle | R(J_{Aml}, M_{Aml}) | j \rangle . \quad (5.43)$$

In order to obtain an expression in terms of the amplitudes in the spherical formulation of Coupled-Cluster and EOM-CCSD, we use `rewrite_coupling`.

---

```
# Rewrite it to spherical form
expr_sph = rewrite_coupling(expr_msc,
    [t_abik_sph, l_abjk_sph, r_j_sph])
```

---

We have supplied the uncoupled expression and a list of matrix elements with the desired coupling. The expression is searched for matrix elements that may

be rewritten into the requested form, and the necessary coupling coefficients are determined.

$$\begin{aligned}
& \sum_{M_A m_i} \sum_{m_a m_b m_j m_k} \sum_{J_{ab} J_{ik} M_{ab} M_{ik}} \sum_{J_{ab} J_{jk} M_{ab} M_{jk}} (-1)^{J_A - M_A} (-1)^{j_i - m_i} \\
& (J_A M_A j_i - m_i | J_{Am1} M_{Am1}) (j_a m_a j_b m_b | J_{ab} M_{ab}) (j_a m_a j_b m_b | J_{ab} M_{ab}) \\
& (j_j m_j j_k m_k | J_{ik} M_{ik}) (j_j m_j J_{Am1} M_{Am1} | 00) (j_j m_j j_k m_k | J_{jk} M_{jk}) \\
& (J_{ab} M_{ab} J_A - M_A | J_{jk} M_{jk}) (J_{ik} M_{ik} 00 | J_{ab} M_{ab}) \langle \| R(J_{Am1}) \| j \rangle \\
& \langle ab(a \curvearrowright b) \| T(0) \| ik(i \curvearrowright k) \rangle \langle jk(j \curvearrowright k) \| L(J_A) \| ab(a \curvearrowright b) \rangle . \quad (5.44)
\end{aligned}$$

The expression bears clear signs of the brute force approach that has been taken, but gives also a clear impression of the complexity that may arise from seemingly simple expressions. It thus provides ample motivation for the creation of computer code to handle the symbolical manipulations that are required to simplify it.

The reduced matrix elements indicate the coupling order with a curved arrow. What appears as a double summation over the same variable,  $J_{ab}$ , is actually two separate summations. This is due to the fact that the latex printer does not distinguish dummy variables from each other. Internally, the two  $J_{ab}$  are actually different variables and if we would need to distinguish them in the  $\text{\LaTeX}$  output, we could easily accomplish that with a substitution. However, this is only an intermediate step in the calculation, and we have no intention of using the expression as it is. We choose to accept it at this point, and we will see that the final result has no such cosmetic issues.

We start the expression simplification by invoking the orthogonality relations of the two Clebsch-Gordan coefficients that couple  $a$  and  $b$ .

---

```
expr_sph = apply_orthogonality(expr_sph, ['m_a', 'm_b'])
```

---

The result is

$$\begin{aligned}
& \sum_{M_A m_i m_j m_k J_{ab} J_{ik} J_{jk} M_{ab} M_{ab} M_{ik} M_{jk}} (-1)^{J_A + j_i - M_A - m_i} \delta_{J_{ab}, J_{ab}} \delta_{M_{ab}, M_{ab}} \\
& (J_A M_A j_i - m_i | J_{Am1} M_{Am1}) (j_i m_i j_k m_k | J_{ik} M_{ik}) (j_j m_j J_{Am1} M_{Am1} | 00) \\
& (j_j m_j j_k m_k | J_{jk} M_{jk}) (J_{ab} M_{ab} J_A - M_A | J_{jk} M_{jk}) (J_{ik} M_{ik} 00 | J_{ab} M_{ab}) \\
& \langle \| R(J_{Am1}) \| j \rangle \langle ab(a \curvearrowright b) \| T(0) \| ik(i \curvearrowright k) \rangle \langle jk(j \curvearrowright k) \| L(J_A) \| ab(a \curvearrowright b) \rangle . \quad (5.45)
\end{aligned}$$

As expected, the summation over  $m_a$  and  $m_b$  is gone, and two Clebsch-Gordan coefficients have been replaced with the appropriate delta functions. (Here we see clearly that  $J_{ab}$  and  $M_{ab}$  are different variables internally, since the delta functions have not been evaluated to 1.) The orthogonality relation can only be applied if the expression does not depend on  $m_a$  or  $m_b$  except in the orthogonal Clebsch-Gordan coefficients. The function `apply_orthogonality` checks that this is indeed the case, and tries to rewrite the phase if it contains any of the summation variables.

The next step is to convert the Clebsch-Gordan coefficients to  $3j$ -symbols, as this also implies an automatic evaluation of any trivial coupling coefficients.

---

```
expr_sph = convert_cgc2tjs(expr_sph)
```

---

The expression is now rather complex, and the reader has already an impression about how the calculations are performed, so there is no need to display it here. Clearly, the delta functions that arise from the coupling coefficients zero angular momentum values, can be used to simplify the expression considerably. Such simplifications are performed in the next statement,

---

```
expr_sph = evaluate_sums(expr_sph, all_deltas=True)
```

---

This function evaluates summations that are trivial due to Kronecker delta functions in the expression. The keyword `all_deltas` is used to indicate that delta functions that cannot be removed by evaluation of the summations, should nevertheless be used to make sure that the expression contains only one of the indices. The expression is now:

$$\begin{aligned}
& \sum_{M_A m_i m_k J_{ab} J_{jk} M_{ab} M_{jk}} \sqrt{1 + 2J_{ab}} (1 + 2J_{jk}) \delta_{J_{Am1}, j_j} \\
& (-1)^{J_{Am1} + M_{Am1}} (-1)^{J_A + J_{Am1} + j_i} (-1)^{J_A + M_{Am1} - j_i} (-1)^{-J_A + J_{ab} + M_{jk}} \\
& (-1)^{J_{Am1} + j_k + J_{jk}} (-1)^{j_i - j_k + M_{ab}} (-1)^{J_{Am1} - j_k + M_{jk}} (-1)^{J_A + j_i - M_A - m_i} \\
& \langle \|R(J_{Am1})\|j \rangle \langle ab(a \curvearrowright b) \|T(0) \|ik(i \curvearrowright k) \rangle \langle jk(j \curvearrowright k) \|L(J_A) \|ab(a \curvearrowright b) \rangle \\
& \begin{pmatrix} J_A & J_{Am1} & j_i \\ M_A & -M_{Am1} & -m_i \end{pmatrix} \begin{pmatrix} J_A & J_{ab} & J_{jk} \\ M_A & -M_{ab} & M_{jk} \end{pmatrix} \\
& \begin{pmatrix} J_{Am1} & j_k & J_{jk} \\ M_{Am1} & -m_k & M_{jk} \end{pmatrix} \begin{pmatrix} j_i & j_k & J_{ab} \\ m_i & m_k & -M_{ab} \end{pmatrix} \quad (5.46)
\end{aligned}$$

The phase is unnecessary complex, and the remedy is,

---

```
expr_sph = refine_phases(expr_sph)
```

---

The word “refine” is in SymPy used to signal that assumptions will be taken into account. `refine_phases` invokes not only algebraic rearrangements of the phases, but also the assumptions that have been registered about the angular momentum symbols. In addition, the triangular relations and the projection label requirements implied by the angular momentum symbols in the expression are used in the search for a simpler phase. The expression appears much more friendly as soon as the



phase has been rewritten,

$$\begin{aligned}
& \sum_{M_A m_i m_k J_{ab} J_{jk} M_{ab} M_{jk}} (-1)^{-M_A - j_k - m_i + J_{ab} + J_{jk} + M_{ab}} \\
& \quad \sqrt{1 + 2J_{ab}} (1 + 2J_{jk}) \delta_{J_{Am1}, j_j} \langle \|R(J_{Am1})\|j \rangle \\
& \quad \langle ab(a \curvearrowright b) \|T(0)\|ik(i \curvearrowright k) \rangle \langle jk(j \curvearrowright k) \|L(J_A)\|ab(a \curvearrowright b) \rangle \\
& \quad \begin{pmatrix} J_A & J_{Am1} & j_i \\ M_A & -M_{Am1} & -m_i \end{pmatrix} \begin{pmatrix} J_A & J_{ab} & J_{jk} \\ M_A & -M_{ab} & M_{jk} \end{pmatrix} \\
& \quad \begin{pmatrix} J_{Am1} & j_k & J_{jk} \\ M_{Am1} & -m_k & M_{jk} \end{pmatrix} \begin{pmatrix} j_i & j_k & J_{ab} \\ m_i & m_k & -M_{ab} \end{pmatrix}. \quad (5.47)
\end{aligned}$$

In the end, what remains is to rewrite the four  $3j$ -symbols into a  $6j$ -symbol, if that is possible.

---

```
expr_sph = refine_tjs2sjs(expr_sph, verbose=True)
```

---

We include the keyword argument `verbose` in order to get useful feedback in case the algorithm fails to rewrite the expression. This functionality proved to be helpful when the `racah` module was used to couple all 14 diagrams for the spectroscopic factors. Here, however, the preliminary steps we have already discussed are sufficient, and the call to `refine_tjs2sjs` succeeds. It returns the expression,

$$\begin{aligned}
& \sum_{J_{ab} J_{jk}} (-1)^{-j_i - j_k + J_{ab}} \frac{\sqrt{1 + 2J_{ab}}}{1 + 2J_{Am1}} (1 + 2J_{jk}) \delta_{J_{Am1}, j_j} \\
& \quad \langle \|R(J_{Am1})\|j \rangle \langle ab(a \curvearrowright b) \|T(0)\|ik(i \curvearrowright k) \rangle \\
& \quad \langle jk(j \curvearrowright k) \|L(J_A)\|ab(a \curvearrowright b) \rangle \left\{ \begin{matrix} J_A & j_i & J_{Am1} \\ j_k & J_{jk} & J_{ab} \end{matrix} \right\} \quad (5.48)
\end{aligned}$$

We see that the phase have been rewritten so that the projection variables that are present in expression (5.47) have been removed. This is a necessary condition for the success of the `refine_tjs2sjs` function. If the resulting expression cannot be written without projection symbols associated with the angular momentum magnitudes in the  $6j$ -symbol, the assumption that the total expression is independent of the projections is violated. In that case the four  $3j$ -symbols cannot be written as a  $6j$ -symbol and this will cause an exception in the refinement function.

This concludes the example where we demonstrate how the `racah` and `braket` modules can be used to manipulate angular momentum expressions, and in particular to derive coupled expressions for spectroscopic factors with Coupled-Cluster. In Appendix B we report the coupled version of all spectroscopic factor diagrams, but only the final results are be presented there.

### 5.3.2 Verification of the Coupled Expressions

We will now discuss briefly the procedure that was used in order to verify the coupled expressions listed in Appendix B. The `racah` and `braket` modules have

been developed with a focus on unit testing [10], so there is a substantial amount of tests for the basic symbolic manipulations. This is necessary so that we can have confidence in the algebraic rearrangements, and this policy is rigidly enforced throughout the SymPy source code. However, in order to use the coupled expressions for scientific publications, we prefer to have an additional and independent verification.

The coupled expressions have been implemented as an addition to the Fortran code developed for spherical Coupled-Cluster calculations by Thomas Papenbrock and Gaute Hagen at Oak Ridge National Laboratory. The numerical implementation can be used to test against the  $m$ -scheme code for which the expressions are much simpler (Figure 4.4).

The testing of the coupled diagrams is displayed schematically in Figure 5.1. The coupled diagrams were tested one by one against the corresponding  $m$ -scheme diagram as follows:

1. The arrays representing the operators,  $T$ ,  $R_A$ ,  $R_{A-1}$ ,  $L_A$ ,  $L_{A-1}$  in the spherical code was assigned random elements.
2. All arrays was copied and transformed to corresponding  $m$ -scheme arrays.
3. The  $m$ -scheme arrays was used to calculate the overlap function with a specific diagram in the  $m$ -scheme code.
4. The arrays of the spherical code was used to calculate the overlap function with the corresponding coupled diagram.
5. The results was reduced to scalars according to equations (3.24) and (3.27) for the  $m$ -scheme and spherical overlaps respectively, and then compared.

This automated testing scheme was implemented before the coupled diagrams, so that it could be used also during the development process. Since each diagram could be tested separately, the testing framework contributed to a remarkably smooth development process. Ultimately, the successful coupling of the spectroscopic factor diagrams also verifies the `racah` and `braket` modules.

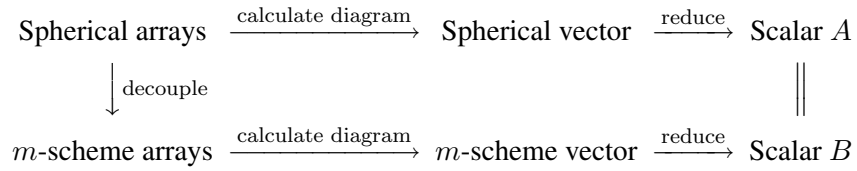


Figure 5.1: Testing scheme used to verify the coupled diagrams. By “decouple” we refer to the transformation from a spherical formalism to  $m$ -scheme. The term “reduce” refers to the nodal sum in equations (3.24) and (3.27) for  $m$ -scheme Coupled-Cluster and spherical Coupled-Cluster respectively. The scalars  $A$  and  $B$  should be equal by this procedure. This scheme allows testing diagram by diagram, which is very useful under code development. It has been used to verify the spectroscopic factor diagrams listed in appendix B.

# **Part II**

## **Applications**

## Chapter 6

# Introduction to Papers and Outlook

In this chapter we present the steps that have been taken towards the goal of *ab initio* reaction calculations. The chronological presentation of the papers leads naturally to the outlook section at the end of this chapter.

### 6.1 Paper 1

Computation of spectroscopic factors with the coupled-cluster method

In the first article we present the theory developments for the calculation of spectroscopic factors in the  $m$ -scheme Coupled-Cluster formalism, and examine how the results depend on the technical parameter  $\hbar\omega$  for different model spaces and different interactions. The purpose was to get a first impression of how our results would depend on model parameters, and to verify that expected properties could be reproduced.

By testing dependence on the momentum cut-off in the two-body interaction, we exemplified how strongly *ab initio* spectroscopic factors can vary for interactions of the same quality, i.e. that are equally well fitted to available two-body scattering data. This is important information as it provides data on the uncertainties related to the choice of nucleon-nucleon interaction. This uncertainty increases the tolerance for what can be considered acceptable errors related to other uncertainties, such as the approximation to CCSD.

We found that the dependence on the interaction is stronger than the model space dependence even with fairly small model spaces. The  $m$ -scheme calculations are computationally expensive compared to the spherical formulation, so we did not pursue convergence of energy in these calculations. Nevertheless it was deemed relevant to display the energy data graphically in order to provide information about the calculations. The calculations were performed with an intrinsic Hamiltonian, which depends on a mass parameter. Due to the definition of

the spectroscopic factor within Coupled-Cluster, we cannot employ a Hamiltonian that is intrinsic to both the  $A$ -body system and the  $A - 1$  system. It was found that also the dependence on the mass parameter was negligible in comparison with the dependence on the interaction.

## 6.2 Paper 2

Closed-shell properties of  $^{24}\text{O}$  with *ab initio* coupled-cluster theory

At the time of writing, the second paper is a preprint, and it has not yet been submitted for publication. In this article we apply the angular momentum coupled form of the spectroscopic factor diagrams to evaluate the shell closure properties of  $^{24}\text{O}$ . The drip line of the Oxygen isotopes has been a subject of extensive studies, and the emerging consensus is that  $^{24}\text{O}$  seems to be the heaviest stable Oxygen isotope. This paper is partly a response to the experimental result in Reference [64], where experimental indications of the closed shell structure were reported.

It is found that the CCM calculation of the  $^{24}\text{O}$  model predicts occupation numbers that correspond to filled single particle states, i.e. a closed shell structure. Moreover, the values calculated with our *ab initio* method were within the error bars of the spectroscopic factors extracted from the measurements in Reference [64].

## 6.3 Outlook

### 6.3.1 Application of the Tools

The tools that have been developed for efficient derivation of many-body physics equations in the course of this project, are of limited value if they are not used in future applications. The detailed description of the functionality that has been presented in this work, was done with the hope that also others may see the benefits of the automated approach and be tempted to use it. The second quantization framework is already part of SymPy, which is open source and freely available. It can be run on any platform for which a working Python interpreter exists. At the time of writing, the Racah algebra functionality is not yet submitted to the official SymPy distribution, but this will be done in the near future. If it is accepted for inclusion, there is hope that it will continue to be a useful tool, also for applications in other fields.

The tools can lead to fast theory developments for a number of remaining tasks in the context of Coupled-Cluster (CCM). Some possible applications are

1. In order to increase precision of the CCM implementation, and at the same time allow full treatment of a three-body interaction, thereby reducing the

error bars related to the interaction, there is need for code that handles a 3-body Hamiltonian with CCSDT. Steps have already been taken towards this goal, but the outcome is not yet clear.

2. Spectroscopic factors for particle attachment needs to be implemented. The second quantization module and the code printing facilities of SymPy can be used for this.
3. An implementation of CCSDT, and maybe even CCSDTQ in the spherical formulation of CCM requires angular momentum couplings of a large number of diagrams.

### 6.3.2 Application to other Nuclei

This work has focused much on the technical aspects that are required in order to do the calculations. Of the two papers, it is the application to  $^{24}\text{O}$  that has new physical implications of interest. Clearly, future work should in particular include the application to nuclei for which there is an interest in theoretical predictions. Potential future targets are the Ni isotopes and the Ca isotopes.

### 6.3.3 Tighter Connection with Reactions

An expression for *ab initio* radial overlap functions with CCM was derived in Chapter 3. However, numerical calculations of such functions reveal that a single particle basis of harmonic oscillator functions is not suitable to represent them. On the other hand, CCM can be used with any single particle basis, and in particular, it is possible to employ a Berggren basis [44, 50, 74, 73, 75, 102], which provides an excellent foundation for modelling systems with strong continuum coupling. By employing a single particle basis with correct asymptotic behaviour it is believed that well converged overlap functions can be calculated.

### 6.3.4 Detailed Analysis of the Center of Mass

A challenge that has plagued shell model like approaches to nuclear structure calculations for a long time, is the problem of spurious center of mass motion. The origin of the problem is that unlike a system of electrons in an atom, the nucleons are not subject to any external force that ties the particles to a heavy physical center. Since the center of mass is required to have a linear motion, i.e. a plane wave, this implies that the number of degrees of freedom in the system is less than the number of particles could indicate.

In a translation invariant model, such as a formulation with Jacobian coordinates, the wavefunction would be expressed in intrinsic coordinates that correspond to the correct number of freedoms in the system, and the center of mass motion would be correct. However, in a shell model like description, of a system with  $A$  particles we employ Slater determinants with  $A$  coordinates.

The centre of mass oscillations of Coupled-Cluster wave functions have been demonstrated to separate from the intrinsic wavefunction [45]. The separation is demonstrated by allowing the center of mass oscillation a frequency  $\tilde{\omega}$ , that may differ from the frequency that characterizes the single particle basis functions. By employing factorization, and determine the center of mass frequencies of both the  $A$  body solution and the  $A - 1$  body solution, one could investigate how the the overlap function as formulated in second quantization (See Chapter 3) can be made translation invariant. This in particular important if overlap functions calculated with CCM are employed in a reaction model for light nuclei.



# Bibliography

- [1] Sympy: Python library for symbolic mathematics, 2010. <http://www.sympy.org>.
- [2] ARFKEN, G. *Mathematical methods for physicists*, 2nd ed. Academic Press, New York, 1970.
- [3] BANG, J. M., GAREEV, F. G., PINKSTON, W. T., AND VAAGEN, J. S. One- and two-nucleon overlap functions in nuclear physics. *Phys. Rep.* 125 (1985), 253 – 399.
- [4] BARBIERI, C. Role of long-range correlations in the quenching of spectroscopic factors. *Phys. Rev. Lett.* 103 (2009), 202502.
- [5] BARBIERI, C., AND DICKHOFF, W. H. Spectroscopic factors in  $^{16}\text{O}$  and nucleon asymmetry. *Int. J. Mod. Phys. A* 24 (2009), 2060.
- [6] BARBIERI, C., AND HJORTH-JENSEN, M. Quasiparticle and quasihole states of nuclei around  $^{56}\text{Ni}$ . *Phys. Rev. C* 79 (2009), 064313.
- [7] BARTLETT, R. J., AND III, G. D. P. Molecular applications of coupled cluster and many-body perturbation methods. *Phys. Scr.* 21 (1980), 255.
- [8] BARTLETT, R. J., AND MUSIAL, M. Coupled-cluster theory in quantum chemistry. *Rev. Mod. Phys.* 79 (2007), 291–352.
- [9] BARTLETT, R. J., AND PURVIS, G. D. Many-body perturbation theory, coupled-pair many-electron theory, and the importance of quadruple excitations for the correlation problem. *Int. J. Quantum Chem.* 14 (1978), 561–581.
- [10] BECK, K. *Test-driven development: by example*. Addison-Wesley, Boston, Mass., 2003.
- [11] BEDAQUE, P., AND VAN KOLCK, U. Effective field theory for few-nucleon systems. *Annu. Rev. Nucl. Part. Sci.* 52 (2002), 339–396.
- [12] BISHOP, R., AND LÜHRMANN, K. Coupled clusters and the electron gas at metallic densities. *Physica B+C* 108, 1-3 (1981), 873 – 874.

- [13] BISHOP, R. F. An overview of coupled cluster theory and its applications in physics. *Theor. Chem. Acc.* 80 (1991), 95–148.
- [14] BISHOP, R. F., FLYNN, M. F., BOSCA, M. C., BUENDA, E., AND GUARDIOLA, R. Translationally invariant coupled cluster theory for simple finite systems. *Phys. Rev. C* 42, 4 (Oct 1990), 1341–1360.
- [15] BISHOP, R. F., AND LÜHRMANN, K. H. Electron correlations: I. ground-state results in the high-density regime. *Phys. Rev. B* 17, 10 (May 1978), 3757–3780.
- [16] BOCHEVAROV, A. D., AND SHERRILL, C. D. A general diagrammatic algorithm for contraction and subsequent simplification of second-quantized expressions. *J. Chem. Phys.* 121, 8 (2004), 3374–3383.
- [17] BRINK, D., AND SATCHLER, G. *Angular momentum*, 3rd ed. Clarendon Press, Oxford, 1993.
- [18] COESTER, F. Bound states of a many-particle system. *Nucl. Phys.* 7 (1958), 421 – 424.
- [19] COESTER, F., AND KÜMMEL, H. Short-range correlations in nuclear wave functions. *Nucl. Phys.* 17 (1960), 477 – 485.
- [20] COHEN, J. S. *Computer algebra and symbolic computation: elementary algorithms*. A. K. Peters, Natick, Mass., 2002.
- [21] CRAWFORD, T. D., AND SCHAEFER III, H. F. An introduction to coupled cluster theory for computational chemists. *Rev. Comp. Chem.* 14 (2000), 33.
- [22] DALGAARD, E., AND MONKHORST, H. J. Some aspects of the time-dependent coupled-cluster approach to dynamic response functions. *Phys. Rev. A* 28 (1983), 1217–1222.
- [23] DEAN, D. J., AND HJORTH-JENSEN, M. Toward coupled-cluster implementations in nuclear structure. P. Fallon, R. Clark, and A. M. Smith, Eds., vol. 656, AIP, pp. 197–204.
- [24] DEAN, D. J., AND HJORTH-JENSEN, M. Coupled cluster approach to nuclear physics. *Phys. Rev. C* 69 (2004), 054320.
- [25] EDMONDS, A. R. *Angular momentum in quantum mechanics*, 2nd ed. Princeton University Press, Princeton, N.J., 1996.
- [26] EMRICH, K. An extension of the coupled cluster formalism to excited states (i). *Nucl. Phys. A* 351, 3 (1981), 379 – 396.

- [27] ENGELS-PUTZKA, A. *An Efficient Implementation of Second Quantization-Based Many-Body Methods for Electrons and its Application to Coupled-Cluster with Arbitrary Excitation Level*. PhD thesis, University of Cologne, 2009.
- [28] ENTEM, D. R., AND MACHLEIDT, R. Accurate charge-dependent nucleon-nucleon potential at fourth order of chiral perturbation theory. *Phys. Rev. C* 68 (2003), 041001(R).
- [29] EPELBAUM, E., HAMMER, H.-W., AND MEISSNER, U.-G. Modern theory of nuclear forces. *Rev. Mod. Phys.* 81 (2009), 1773.
- [30] EPELBAUM, E., KREBS, H., LEE, D., AND MEISSNER, U. Lattice calculations for  $a = 3, 4, 6, 12$  nuclei using chiral effective field theory. *Eur. Phys. J. A* 45 (2010), 335–352.
- [31] EPELBAUM, E., KREBS, H., LEE, D., AND MEISSNER, U.-G. Lattice effective field theory calculations for  $a = 3, 4, 6, 12$  nuclei. *Phys. Rev. Lett.* 104 (2010), 142501.
- [32] EPELBAUM, E., NOGGA, A., GLÖCKLE, W., KAMADA, H., MEISSNER, U.-G., AND WITAŁA, H. Three-nucleon forces from chiral effective field theory. *Phys. Rev. C* 66 (2002), 064001.
- [33] FORSSÉN, C., NAVRÁTIL, P., ORMAND, W. E., AND CAURIER, E. Large basis ab initio shell model investigation of  $^9\text{Be}$  and  $^{11}\text{Be}$ . *Phys. Rev. C* 71, 4 (Apr 2005), 044312.
- [34] FURNSTAHL, R. J. Three-body interactions in many-body effective field theory. *Nucl. Phys. A* 737 (2004), 215.
- [35] FURNSTAHL, R. J., AND HAMMER, H. W. Are occupation numbers observable? *Phys. Lett. B* 531 (2002), 203.
- [36] FURNSTAHL, R. J., RUPAK, G., AND SCHÄFER, T. Effective field theory and finite-density systems. *Annu. Rev. Nucl. Part. Sci.* 58, 1 (2008), 1–25.
- [37] FURNSTAHL, R. J., AND SCHWENK, A. How should one formulate, extract and interpret 'non-observables' for nuclei? *J. Phys. G: Nucl. Part. Phys.* 37, 6 (2010), 064005.
- [38] GANDOLFI, S., PEDERIVA, F., FANTONI, S., AND SCHMIDT, K. E. Auxiliary field diffusion monte carlo calculation of nuclei with  $a \leq 40$  with tensor interactions. *Phys. Rev. Lett.* 99, 2 (Jul 2007), 022507.
- [39] GEERTSEN, J., RITTBY, M., AND BARTLETT, R. J. The equation-of-motion coupled-cluster method: Excitation energies of Be and CO. *Chem. Phys. Lett.* 164, 1 (1989), 57 – 62.

- [40] GOUR, J. R., PIECUCH, P., HJORTH-JENSEN, M., WŁOCH, M., AND DEAN, D. J. Coupled-cluster calculations for valence systems around  $^{16}\text{O}$ . *Phys. Rev. C* 74 (2006), 024310.
- [41] GREINER, W., NEISE, L., AND STÖCKER, H. *Thermodynamics and statistical mechanics*. Springer, New York, 1995.
- [42] HAGEN, G., DEAN, D. J., HJORTH-JENSEN, M., AND PAPENBROCK, T. Complex coupled-cluster approach to an ab-initio description of open quantum systems. *Phys. Lett. B* 656 (2007), 169.
- [43] HAGEN, G., DEAN, D. J., HJORTH-JENSEN, M., PAPENBROCK, T., AND SCHWENK, A. Benchmark calculations for  $^3\text{H}$ ,  $^4\text{He}$ ,  $^{16}\text{O}$ , and  $^{40}\text{Ca}$  with ab initio coupled-cluster theory. *Phys. Rev. C* 76, 4 (Oct 2007), 044305.
- [44] HAGEN, G., HJORTH-JENSEN, M., AND MICHEL, N. Gamow shell model and realistic nucleon-nucleon interactions. *Phys. Rev. C* 73, 6 (2006), 064307.
- [45] HAGEN, G., PAPENBROCK, T., AND DEAN, D. J. Solution of the center-of-mass problem in nuclear structure calculations. *Phys. Rev. Lett.* 103 (2009), 062503.
- [46] HAGEN, G., PAPENBROCK, T., DEAN, D. J., AND HJORTH-JENSEN, M. Medium-mass nuclei from chiral nucleon-nucleon interactions. *Phys. Rev. Lett.* 101 (2008), 092502.
- [47] HAGEN, G., PAPENBROCK, T., DEAN, D. J., AND HJORTH-JENSEN, M. Ab initio coupled-cluster approach to nuclear structure with modern nucleon-nucleon interactions. arXiv:1005.2627v1.
- [48] HAGEN, G., PAPENBROCK, T., DEAN, D. J., HJORTH-JENSEN, M., AND ASOKAN, B. V. Ab initio computation of neutron-rich oxygen isotopes. *Phys. Rev. C* 80 (2009), 021306(R).
- [49] HAGEN, G., PAPENBROCK, T., DEAN, D. J., SCHWENK, A., NOGGA, A., WŁOCH, M., AND PIECUCH, P. Coupled-cluster theory for three-body hamiltonians. *Phys. Rev. C* 76 (2007), 034302.
- [50] HAGEN, G., PAPENBROCK, T., AND HJORTH-JENSEN, M. Ab initio computation of the  $^{17}\text{F}$  proton halo state and resonances in  $a = 17$  nuclei. *Phys. Rev. Lett.* 104 (2010), 182501.
- [51] HANRATH, M., AND ENGELS-PUTZKA, A. An efficient matrix-matrix multiplication based antisymmetric tensor contraction engine for general order coupled cluster. *J. Chem. Phys.* 133, 6 (2010), 064108.

- [52] HEAD-GORDON, M., LEE, M., MASLEN, P., VAN VOORHIS, T., AND GWALTNEY, S. Tensors in electronic structure theory: Basic concepts and applications to electron correlation models. In *Modern Methods and Algorithms of Quantum Chemistry* (2000), vol. 3, pp. 593–638.
- [53] HEISENBERG, J. H., AND MIHAILA, B. Ground state correlations and mean field in  $^{16}\text{O}$ . *Phys. Rev. C* 59, 3 (Mar 1999), 1440–1448.
- [54] HELGAKER, T., KLOPPER, W., HALKIER, A., BAK, K., JØRGENSEN, P., AND OLSEN, J. Highly accurate ab initio computation of thermochemical data. In *Quantum-Mechanical Prediction of Thermochemical Data*, P. G. Mezey and J. Cioslowski, Eds., vol. 22 of *Understanding Chemical Reactivity*. Springer Netherlands, 2002, pp. 1–30.
- [55] HELGAKER, T., KLOPPER, W., AND TEW, D. P. Quantitative quantum chemistry. *Mol. Phys.* 106, 16 (2008), 2107–2143.
- [56] HELGAKER, T. U., OLSEN, J., AND JØRGENSEN, P. *Molecular electronic-structure theory*. John Wiley & Sons, Chichester, 2000.
- [57] HEYDE, K. L. *The nuclear shell model*. Springer-Verlag, Berlin, 1994.
- [58] HIRATA, S. Tensor contraction engine: Abstraction and automated parallel implementation of configuration-interaction, coupled-cluster, and many-body perturbation theories. *J. Phys. Chem. A* 107, 46 (2003), 9887–9897.
- [59] JANSSEN, C. L., AND SCHAEFER, H. F. The automated solution of second quantization equations with applications to the coupled cluster approach. *Theor. Chem. Acc.* 79 (1991), 1–42.
- [60] JENSEN, Ø., HAGEN, G., PAPENBROCK, T., DEAN, D. J., AND VAAGEN, J. S. Computation of spectroscopic factors with the coupled-cluster method. *Phys. Rev. C* 82 (2010), 014310.
- [61] KÁLLAY, M., AND GAUSS, J. Analytic second derivatives for general coupled-cluster and configuration-interaction models. *The Journal of Chemical Physics* 120, 15 (2004), 6841–6848.
- [62] KÁLLAY, M., AND SURJÁN, P. R. Higher excitations in coupled-cluster theory. *J. Chem. Phys.* 115, 7 (2001), 2945–2954.
- [63] KAMADA, H., NOGGA, A., GLÖCKLE, W., HIYAMA, E., KAMIMURA, M., VARGA, K., SUZUKI, Y., VIVIANI, M., KIEVSKY, A., ROSATI, S., CARLSON, J., PIEPER, S. C., WIRINGA, R. B., NAVRÁTIL, P., BARRETT, B. R., BARNEA, N., LEIDEMANN, W., AND ORLANDINI, G. Benchmark test calculation of a four-nucleon bound state. *Phys. Rev. C* 64 (2001), 044001.

- [64] KANUNGO, R., NOCIFORO, C., PROCHAZKA, A., AUMANN, T., BOUTIN, D., CORTINA-GIL, D., DAVIDS, B., DIAKAKI, M., FARINON, F., GEISSEL, H., GERNHÄUSER, R., GERL, J., JANIK, R., JONSON, B., KINDLER, B., KNÖBEL, R., KRÜCKEN, R., LANTZ, M., LENSKE, H., LITVINOV, Y., LOMMEL, B., MAHATA, K., MAIERBECK, P., MUSUMARRA, A., NILSSON, T., OTSUKA, T., PERRO, C., SCHEIDENBERGER, C., SITAR, B., STRMEN, P., SUN, B., SZARKA, I., TANIHATA, I., UTSUNO, Y., WEICK, H., AND WINKLER, M. One-neutron removal measurement reveals  $^{24}\text{O}$  as a new doubly magic nucleus. *Phys. Rev. Lett.* 102 (2009), 152501.
- [65] KOWALSKI, K., DEAN, D. J., HJORTH-JENSEN, M., PAPENBROCK, T., AND PIECUCH, P. Coupled cluster calculations of ground and excited states of nuclei. *Phys. Rev. Lett.* 92 (2004), 132501.
- [66] KREBS, H. Nuclear forces from effective field theory. *Few-Body Systems* (2010), 1–7.
- [67] KUCHARSKI, S. A., AND BARTLETT, R. J. Fifth-order many-body perturbation theory and its relationship to various coupled-cluster approaches. vol. 18 of *Advances in Quantum Chemistry*. Academic Press, 1986, pp. 281 – 344.
- [68] KÜMMEL, H., LÜHRMANN, K., AND ZABOLITZKY, J. Many-fermion theory in exps- (or coupled cluster) form. *Phys. Rep.* 36 (1978), 1.
- [69] KUO, T. T. S., SHURPIN, J., TAM, K. C., OSNES, E., AND ELLIS, P. J. A simple method for evaluating goldstone diagrams in an angular momentum coupled representation. *Annals of Physics* 132, 2 (1981), 237 – 276.
- [70] LAWSON, R. D. *Theory of the nuclear shell model*. Oxford studies in nuclear physics. Clarendon Press, Oxford, 1980. R. D. Lawson.
- [71] LEE, D. Lattice simulations for few- and many-body systems. *Progress in Particle and Nuclear Physics* 63, 1 (2009), 117 – 154.
- [72] MAHAUX, C., BORTIGNON, P. F., BROGLIA, R. A., AND DASSO, C. H. Dynamics of the shell model. *Phys. Rep.* 120, 1-4 (1985), 1 – 274.
- [73] MICHEL, N., NAZAREWICZ, W., AND PŁOSZAJCZAK, M. Continuum coupling and single-nucleon overlap integrals. *Nucl. Phys. A* 794, 1-2 (2007), 29 – 46.
- [74] MICHEL, N., NAZAREWICZ, W., PŁOSZAJCZAK, M., AND BENNACEUR, K. Gamow shell model description of neutron-rich nuclei. *Phys. Rev. Lett.* 89 (2002), 042502.

- [75] MICHEL, N., NAZAREWICZ, W., PLOSZAJCZAK, M., AND OKOLOWICZ, J. Gamow shell model description of weakly bound nuclei and unbound nuclear states. *Phys. Rev. C* 67 (2003), 054311.
- [76] MIHAILA, B. Continuum coupled-cluster expansion. *Phys. Rev. C* 68 (2003), 054327.
- [77] MIHAILA, B., AND HEISENBERG, J. H. Ground state correlations and mean field in  $^{16}\text{O}$ . ii. effects of a three-nucleon interaction. *Phys. Rev. C* 61 (2000), 054309.
- [78] MIHAILA, B., AND HEISENBERG, J. H. Microscopic calculation of the inclusive electron scattering structure function in  $^{16}\text{O}$ . *Phys. Rev. Lett.* 84 (2000), 1403–1406.
- [79] MOLINER, I., WALET, N. R., AND BISHOP, R. F. Translationally invariant coupled cluster method in coordinate space for nuclei. *J. Phys. G: Nucl. Part. Phys.* 28 (2002), 1209.
- [80] MONKHORST, H. J. Calculation of properties with the coupled-cluster method. *Int. J. Quantum Chem.* 12, S11 (1977), 421–432.
- [81] NAVRÁTIL, P., GUEORGUIEV, V. G., VARY, J. P., ORMAND, W. E., AND NOGGA, A. Structure of  $a = 10 - 13$  nuclei with two- plus three-nucleon interactions from chiral effective field theory. *Phys. Rev. Lett.* 99 (2007), 042501.
- [82] NAVRÁTIL, P., GUEORGUIEV, V. G., VARY, J. P., ORMAND, W. E., NOGGA, A., AND QUAGLIONI, S. Light nuclei from chiral EFT interactions. *Few-Body Systems* 43 (2008), 129.
- [83] NAVRÁTIL, P., QUAGLIONI, S., AND ROTH, R. Ab initio theory of light-ion reactions. *ArXiv e-prints* (Sept. 2010).
- [84] NAVRÁTIL, P., QUAGLIONI, S., STETCU, I., AND BARRETT, B. R. Recent developments in no-core shell-model calculations. *J. Phys. G: Nucl. Part. Phys.* 36, 8 (2009), 083101.
- [85] NAVRÁTIL, P., VARY, J. P., AND BARRETT, B. R. Large basis ab initio no-core shell model and its application to  $^{12}\text{C}$ . *Phys. Rev. C* 62 (2000), 054311.
- [86] NNDC. National nuclear data center. Information extracted from the NuDat 2 database, <http://www.nndc.bnl.gov/nudat2/>.
- [87] NOGGA, A., NAVRÁTIL, P., BARRETT, B. R., AND VARY, J. P. Spectra and binding energy predictions of chiral interactions for  $^7\text{Li}$ . *Phys. Rev. C* 73 (2006), 064002.

- [88] NOLLETT, K. M., PIEPER, S. C., WIRINGA, R. B., CARLSON, J., AND HALE, G. M. Quantum monte carlo calculations of neutron- $\alpha$  scattering. *Phys. Rev. Lett.* 99 (2007), 022502.
- [89] ORDÓÑEZ, C., RAY, L., AND VAN KOLCK, U. Two-nucleon potential from chiral lagrangians. *Phys. Rev. C* 53, 5 (May 1996), 2086–2105.
- [90] PALDUS, J., ČÍŽEK, J., AND SHAVITT, I. Correlation problems in atomic and molecular systems. iv. extended coupled-pair many-electron theory and its application to the  $bh_3$  molecule. *Phys. Rev. A* 5, 1 (Jan 1972), 50–67.
- [91] PALDUS, J., AND WONG, H. C. Computer generation of feynman diagrams for perturbation theory i. general algorithm. *Comput. Phys. Commun.* 6, 1 (1973), 1 – 7.
- [92] PIEPER, S. C. Quantum monte carlo calculations of light nuclei. *Nucl. Phys. A* 751 (2005), 516 – 532.
- [93] PIEPER, S. C., AND WIRINGA, R. B. Quantum monte carlo calculations of light nuclei. *Annu. Rev. Nucl. Part. Sci.* 51 (2001), 53–90.
- [94] QUAGLIONI, S., AND NAVRÁTIL, P. Ab initio many-body calculations of  $n-^3\text{H}$ ,  $n-^4\text{He}$ ,  $p-^3,^4\text{He}$ , and  $n-^{10}\text{Be}$  scattering. *Phys. Rev. Lett.* 101 (2008), 092501.
- [95] QUAGLIONI, S., AND NAVRÁTIL, P. Ab initio many-body calculations of nucleon-nucleus scattering. *Phys. Rev. C* 79 (2009), 044606.
- [96] REED, M., AND SIMON, B. *Methods of modern mathematical physics*, rev. and enl. ed. Academic Press, New York, 1980.
- [97] RILEY, K., HOBSON, M., AND BENCE, S. *Mathematical methods for physics and engineering*, 3rd ed. Cambridge University Press, Cambridge, 2006.
- [98] SATCHLER, G. R. Direct nuclear reactions. vol. 68 of *International series of monographs on physics*. Clarendon Press, Oxford, 1983.
- [99] SHALIT, A. D., AND TALMI, I. Nuclear shell theory. vol. 14 of *Pure and applied physics*. Academic Press, New York, 1963. Amos de-Shalit and Igal Talmi.
- [100] SHAVITT, I., AND BARTLETT, R. J. *Many-body methods in chemistry and physics: MBPT and coupled-cluster theory*. Cambridge University Press, Cambridge, 2009.
- [101] STANTON, J. F., AND BARTLETT, R. J. The equation of motion coupled-cluster method. a systematic biorthogonal approach to molecular excitation



- energies, transition probabilities, and excited state properties. *The Journal of Chemical Physics* 98, 9 (1993), 7029–7039.
- [102] TSUKIYAMA, K., HJORTH-JENSEN, M., AND HAGEN, G. Gamow shell-model calculations of drip-line oxygen isotopes. *Phys. Rev. C* 80 (2009), 051301.
- [103] VARSHALOVICH, D. A., MOSKALEV, A. N., AND KHERSONSKII, V. K. *Quantum theory of angular momentum : irreducible tensors, spherical harmonics, vector coupling coefficients, 3nj symbols*. World Scientific, Singapore, 1989. D. A. Varshalovich, A. N. Moskalev, V. K. Khersonskii.
- [104] ČÍŽEK, J. On the correlation problem in atomic and molecular systems. calculation of wavefunction components in ursell-type expansion using quantum-field theoretical methods. *J. Chem. Phys.* 45, 11 (1966), 4256–4266.
- [105] ČÍŽEK, J. On the use of the cluster expansion and the technique of diagrams in calculations of correlation effects in atoms and molecules. *Adv. Chem. Phys.* 14 (1969), 35.
- [106] WHITEHEAD, R., WATT, A., COLE, B., AND MORRISON, I. Computational methods for shell-model calculations. *Adv. Nucl. Phys.* 9 (1977), 123–173.
- [107] WLOCH, M., DEAN, D. J., GOUR, J. R., HJORTH-JENSEN, M., KOWALSKI, K., PAPENBROCK, T., AND PIECUCH, P. Ab initio coupled-cluster study of  $^{16}\text{O}$ . *Phys. Rev. Lett.* 94 (2005), 212501.

# **Appendices**

## Appendix A

# Angular Momentum Definitions

### A.1 The Wigner-Eckart Theorem

We write the Wigner-Eckart theorem as

$$\langle IN|T_m^{(j)}|JM\rangle = (JMjm|IN) \langle I||T^{(j)}||J\rangle . \quad (\text{A.1})$$

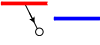
Here,  $(\cdot|\cdot)$  is a Clebsch-Gordan coefficient and  $\langle\cdot||\cdot||\cdot\rangle$  denotes the *reduced matrix element*.  $I$ ,  $j$  and  $J$  are angular momenta, and  $N$ ,  $m$  and  $M$  the respective projections.

## Appendix B

# Coupled Spectroscopic Factor Diagrams

Here we present the coupled version of all spectroscopic factor diagrams. The expressions for the coupled diagrams are complicated and not suitable for a table, so they have been organized in four different sections.

### B.1 Diagrams on the Form $\langle A - 1 | a_i | A \rangle$

$l^i r_0$  : 

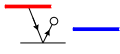
$$SF = -r_0 \cdot \delta_{J_{Am1}, j_i} \cdot \langle i \| L(J_{Am1}) \| \rangle \quad (\text{B.1})$$

$l_a^{ij} r_j^a$  : 

$$SF = - \sum_{J_{ij}} \cdot \frac{\sqrt{1+2 \cdot j_a} \cdot (1+2 \cdot J_{ij})}{\sqrt{1+2 \cdot J_{Am1}}} \cdot \langle a \| R(J_A) \| j \rangle \quad (\text{B.2})$$

$$\cdot \langle ij(i \curvearrowright j) \| L(J_{Am1}) \| a \rangle \cdot \left\{ \begin{matrix} J_A & J_{Am1} & j_i \\ J_{ij} & j_j & j_a \end{matrix} \right\}$$

### B.2 Diagrams on the Form $\langle A - 1 | a_a | A \rangle$

$l^i t_i^a r_0$  : 

$$SF = -r_0 \cdot \delta_{J_{Am1}, j_a} \cdot \delta_{J_{Am1}, j_i} \cdot \delta_{j_a, j_i} \cdot \langle a \| T(0) \| i \rangle \cdot \langle i \| L(J_{Am1}) \| \rangle \quad (\text{B.3})$$

$$l^i r_i^a : \text{Diagram with a red line above and a blue line below, connected by a vertical line with a circle at the top and a dot at the bottom.}$$

$$SF = -\sqrt{1+2 \cdot j_a} \cdot \delta_{J_{Am1}, j_i} \cdot \frac{\langle a \| R(J_A) \| i \rangle \cdot \langle i \| L(J_{Am1}) \| \rangle}{\sqrt{1+2 \cdot J_{Am1}}} \quad (\text{B.4})$$

$$\frac{1}{2} l_b^{ij} t_{ij}^{ab} r_0 : \text{Diagram with a red line above and a blue line below, connected by a vertical line with a circle at the top and a dot at the bottom, and a horizontal line to the right.}$$

$$SF = \frac{1}{2} r_0 \cdot (-1)^{J_{ij}+j_b-J_{Am1}} \cdot \frac{(1+2 \cdot J_{ij})}{1+2 \cdot J_{Am1}} \cdot \delta_{J_{Am1}, j_a} \cdot \delta_{M_{ab}, M_{ij}} \cdot \langle ab(a \curvearrowright b) \| T(0) \| ij(i \curvearrowright j) \rangle \cdot \langle ij(i \curvearrowright j) \| L(J_{Am1}) \| b \rangle \quad (\text{B.5})$$

$$l_b^{ij} t_i^a r_j^b : \text{Diagram with a red line above and a blue line below, connected by a vertical line with a circle at the top and a dot at the bottom, and a horizontal line to the right.}$$

$$SF = -\sum_{J_{ij}} \cdot \frac{\sqrt{1+2 \cdot j_b} \cdot (1+2 \cdot J_{ij})}{\sqrt{1+2 \cdot J_{Am1}}} \cdot \delta_{j_a, j_i} \cdot \langle a \| T(0) \| i \rangle \cdot \langle b \| R(J_A) \| j \rangle \cdot \langle ij(i \curvearrowright j) \| L(J_{Am1}) \| b \rangle \cdot \left\{ \begin{matrix} J_A & J_{Am1} & j_a \\ J_{ij} & j_j & j_b \end{matrix} \right\} \quad (\text{B.6})$$

$$\frac{1}{2} l_b^{ij} r_{ij}^{ab} : \text{Diagram with a red line above and a blue line below, connected by a vertical line with a circle at the top and a dot at the bottom, and a horizontal line to the right.}$$

$$SF = \frac{1}{2} \sum_{J_{ab} J_{ij}} \cdot (-1)^{1+J_A+J_{Am1}-j_a} \cdot \frac{\sqrt{1+2 \cdot J_{ij}} \cdot (1+2 \cdot J_{ab})}{2 \cdot \sqrt{1+2 \cdot J_{Am1}}} \cdot \langle ab(a \curvearrowright b) \| R(J_A) \| ij(i \curvearrowright j) \rangle \cdot \langle ij(i \curvearrowright j) \| L(J_{Am1}) \| b \rangle \cdot \left\{ \begin{matrix} J_{Am1} & J_A & j_a \\ J_{ab} & j_b & J_{ij} \end{matrix} \right\} \quad (\text{B.7})$$

### B.3 Diagrams on the Form $\langle A | a_a^\dagger | A-1 \rangle$

$$l_a^i r_i : \text{Diagram with a red line above and a blue line below, connected by a vertical line with a circle at the top and a dot at the bottom.}$$

$$SF = (-1)^{J_A+j_a-J_{Am1}} \cdot \delta_{J_{Am1}, j_i} \cdot \frac{\langle \| R(J_{Am1}) \| i \rangle \cdot \langle i \| L(J_A) \| a \rangle}{\sqrt{1+2 \cdot J_{Am1}}} \quad (\text{B.8})$$

$$\frac{1}{2}l_{ab}^{ij}r_{ij}^b : \text{Diagram with a red line and a blue line, with a loop on the blue line.}$$

$$SF = \frac{1}{2} \sum_{J_{ab}J_{ij}} \cdot (-1)^{J_{ab}-j_a-j_b} \cdot \frac{\sqrt{1+2 \cdot J_{ab}} \cdot \sqrt{1+2 \cdot J_{ij}} \cdot \sqrt{1+2 \cdot j_b}}{2 \cdot \sqrt{1+2 \cdot J_{Am1}}} \cdot \langle b \| R(J_{Am1}) \| ij(i \curvearrowright j) \rangle \cdot \langle ij(i \curvearrowright j) \| L(J_A) \| ab(a \curvearrowright b) \rangle \cdot \left\{ \begin{matrix} J_{Am1} & J_A & j_a \\ J_{ab} & j_b & J_{ij} \end{matrix} \right\} \quad (\text{B.9})$$

#### B.4 Diagrams on the Form $\langle A | a_i^\dagger | A-1 \rangle$

$$l^0 r_i : \text{Diagram with a red line and a blue line, with a loop on the blue line.}$$

$$SF = \frac{l_0 \cdot \delta_{J_{Am1}, j_i} \cdot \langle \| R(J_{Am1}) \| i \rangle}{\sqrt{1+2 \cdot j_i}} \quad (\text{B.10})$$

$$l_a^j r_{ij}^a : \text{Diagram with a red line and a blue line, with a loop on the blue line.}$$

$$SF = \sum_{J_{ij}} \cdot (-1)^{1+j_j-J_A-J_{Am1}-J_{ij}} \cdot \frac{\sqrt{1+2 \cdot J_{ij}} \cdot \sqrt{1+2 \cdot j_a} \cdot \sqrt{1+2 \cdot j_j}}{\sqrt{1+2 \cdot J_{Am1}}} \cdot \langle a \| R(J_{Am1}) \| ij(i \curvearrowright j) \rangle \cdot \langle j \| L(J_A) \| a \rangle \cdot \left\{ \begin{matrix} J_A & J_{Am1} & j_i \\ J_{ij} & j_j & j_a \end{matrix} \right\} \quad (\text{B.11})$$

$$-l_a^j t_i^a r_j : \text{Diagram with a red line and a blue line, with a loop on the blue line.}$$

$$SF = \frac{(-1)^{J_A-J_{Am1}-j_a}}{\sqrt{1+2 \cdot J_{Am1}}} \cdot \delta_{J_{Am1}, j_j} \cdot \delta_{j_a, j_i} \cdot \langle \| R(J_{Am1}) \| j \rangle \cdot \langle a \| T(0) \| i \rangle \cdot \langle j \| L(J_A) \| a \rangle \quad (\text{B.12})$$

$$-\frac{1}{2}l_{ab}^{jk}t_i^a r_{jk}^b : \text{Diagram}$$

$$SF = \frac{1}{2} \sum_{J_{ab} J_{jk}} \cdot (-1)^{J_{ab}+j_a-j_b} \cdot \frac{\sqrt{1+2 \cdot J_{ab}} \cdot \sqrt{1+2 \cdot J_{jk}} \cdot \sqrt{1+2 \cdot j_b}}{\sqrt{1+2 \cdot J_{Am1}}} \cdot \delta_{j_a, j_i} \cdot \langle a \| T(0) \| i \rangle \cdot \langle b \| R(J_{Am1}) \| jk(j \curvearrowright k) \rangle \cdot \langle jk(j \curvearrowright k) \| L(J_A) \| ab(a \curvearrowright b) \rangle \cdot \left\{ \begin{matrix} J_{Am1} & J_A & j_a \\ J_{ab} & j_b & J_{jk} \end{matrix} \right\} \quad (\text{B.13})$$

$$-\frac{1}{2}l_{ab}^{jk}t_{ik}^{ab} r_j : \text{Diagram}$$

$$SF = \frac{1}{2} \sum_{J_{ab} J_{jk}} \cdot (-1)^{1+J_{ab}-j_i-j_k} \cdot \frac{\sqrt{1+2 \cdot J_{ab}} \cdot (1+2 \cdot J_{jk})}{1+2 \cdot J_{Am1}} \cdot \delta_{J_{Am1}, j_j} \cdot \langle \| R(J_{Am1}) \| j \rangle \cdot \langle ab(a \curvearrowright b) \| T(0) \| ik(i \curvearrowright k) \rangle \cdot \langle jk(j \curvearrowright k) \| L(J_A) \| ab(a \curvearrowright b) \rangle \cdot \left\{ \begin{matrix} J_{Am1} & J_A & j_i \\ J_{ab} & j_k & J_{jk} \end{matrix} \right\} \quad (\text{B.14})$$

# Computation of spectroscopic factors with the coupled-cluster method

Ø. Jensen,<sup>1,\*</sup> G. Hagen,<sup>2</sup> T. Papenbrock,<sup>2,3</sup> D. J. Dean,<sup>2</sup> and J. S. Vaagen<sup>1</sup>

<sup>1</sup>*Department of Physics and Technology, University of Bergen, N-5007 Bergen, Norway*

<sup>2</sup>*Physics Division, Oak Ridge National Laboratory, Oak Ridge, Tennessee 37831, USA*

<sup>3</sup>*Department of Physics and Astronomy, University of Tennessee, Knoxville, Tennessee 37996, USA*

(Received 16 April 2010; published 19 July 2010)

We present a calculation of spectroscopic factors within coupled-cluster theory. Our derivation of algebraic equations for the one-body overlap functions are based on coupled-cluster equation-of-motion solutions for the ground and excited states of the doubly magic nucleus with mass number  $A$  and the odd-mass neighbor with mass  $A - 1$ . As a proof-of-principle calculation, we consider  $^{16}\text{O}$  as well as the odd neighbors  $^{15}\text{O}$  and  $^{15}\text{N}$  and compute the spectroscopic factor for nucleon removal from  $^{16}\text{O}$ . We employ a renormalized low-momentum interaction of the  $V_{\text{low-}k}$  type derived from a chiral interaction at next-to-next-to-leading order. We study the sensitivity of our results by variation of the momentum cutoff and then discuss the treatment of the center of mass.

DOI: [10.1103/PhysRevC.82.014310](https://doi.org/10.1103/PhysRevC.82.014310)

PACS number(s): 21.10.Jx, 21.60.De, 21.60.Gx, 31.15.bw

## I. INTRODUCTION

In the past two decades, *ab initio* nuclear structure calculations have led to the development and test of high-precision models with predictive power [1–3]. Recently, the application of effective field theory (EFT) [4–7] and renormalization-group techniques [8,9] has resulted in a model-independent approach to the nuclear interaction. These approaches have significantly deepened our understanding of nuclear forces and have also provided us with new technical means to simplify the solution of the nuclear many-body problem. The interactions from chiral EFT have been probed in light nuclei [10–13] and selected medium-mass nuclei using different techniques [14–16]. The focus of *ab initio* calculations is not only on observables such as binding energies, radii, and low-lying excitation spectra, but also on transition rates and more detailed spectroscopic information. Very recently, *ab initio* theory began to bridge the gap from nuclear structure to reactions [17–19]. The inclusion of continuum effects, for instance, is necessary for the description of weakly bound and unbound nuclei. Direct reactions such as stripping and pickup of a single nucleon are rather well understood within phenomenological approaches (see, e.g., Ref. [20]) but constitute a current frontier for *ab initio* theory.

The interpretation of direct reactions within a given model or Hamiltonian is based on spectroscopic factors [21,22]. The spectroscopic factor depends on wave function overlaps [see Eq. (16) for a definition] and provides useful information that relates nuclear structure within a given model (i.e., within a given Hamiltonian) to stripping and transfer reactions [21]. The spectroscopic factor is not an observable, as it depends on the employed Hamiltonian or model. In nuclear physics, the high-momentum parts of the interaction are unconstrained and modeled in different ways. Thus, the short-ranged part of the wave function is model dependent, and so is an overlap between wave functions. Therefore, the spectroscopic factor is

merely a theoretical quantity and cannot be measured [23,24]. However, the spectroscopic factor “provides a useful basis for the comparison of experiment and current nuclear models” [21]. Its purpose thus lies in understanding a direct reaction within a certain model or Hamiltonian, and this interpretation might be useful and interesting [25–29].

In this paper, we develop the technical tools to compute spectroscopic factors within the coupled-cluster method [30–34] (see Ref. [35] for a recent review of this method) and perform a proof-of-principle calculation for  $^{16}\text{O}$ . The computation of the spectroscopic factor within coupled-cluster theory is not trivial (i) because the method does not readily yield a many-body wave function and (ii) owing to details related to the translation invariance of the coupled-cluster wave function. However, the coupled-cluster method can employ modern nonlocal potentials [6–9], reaches medium-mass nuclei [14], and has been extended to treat weakly bound and unbound nuclei [17] that are of current experimental interest. This paper is structured as follows. Section II is dedicated to a summary of the employed coupled-cluster method. The theoretical computation of spectroscopic factors within coupled-cluster theory is presented in Sec. III. We present our results and a discussion of the center-of-mass treatment in Sec. IV. Section V reports our conclusions and an outlook.

## II. EQUATION-OF-MOTION AND COUPLED-CLUSTER THEORY FOR NUCLEI

In this section we introduce the Hamiltonian and coupled-cluster theory [30–34] for closed-shell and open-shell nuclei. Although our implementation of coupled-cluster theory has been presented elsewhere [14,35–38], we give a brief overview of the method, as some details are needed for the calculation of spectroscopic factors.

We consider the intrinsic nuclear  $A$ -body Hamiltonian,

$$\hat{H} = \hat{T} - \hat{T}_{\text{c.m.}} + \hat{V} = \sum_{1 \leq i < j \leq A} \frac{(\vec{p}_i - \vec{p}_j)^2}{2mA} + \hat{V}. \quad (1)$$

\*oyvind.jensen@uib.no



Here  $T$  is the kinetic energy,  $T_{\text{c.m.}}$  is the kinetic energy of the center-of-mass coordinate, and  $V$  is the two-body nucleon-nucleon interaction. In this paper we use low-momentum interactions  $V_{\text{low-}k}$  [9,39] with sharp cutoffs  $\lambda = 1.6, 1.8, 2.0$ , and  $2.2 \text{ fm}^{-1}$ , respectively. For simplicity, we neglect any contributions of three-nucleon forces, as we focus on a proof-of-principle calculation.

In coupled-cluster theory, one writes the ground-state many-body wave function as

$$|\psi_0\rangle = e^T |\phi_0\rangle. \quad (2)$$

Here,  $|\phi_0\rangle$  is a product state. The cluster operator  $T$  introduces correlations as a linear combination of particle-hole excitations,

$$T = T_1 + T_2 + \dots + T_A. \quad (3)$$

Here, the  $n$ -particle- $n$ -hole excitation operator is

$$T_n = \left(\frac{1}{n!}\right)^2 \prod_{v=1}^n \sum_{a_v, i_v} t_{i_1 \dots i_n}^{a_1 \dots a_n} a_{a_1}^\dagger \dots a_{a_n}^\dagger a_{i_n} \dots a_{i_1}. \quad (4)$$

We employ the standard convention that indices  $ijk \dots$  refer to orbits below Fermi level (holes), and indices  $abc \dots$  to orbits above Fermi level (particles). Approximations in coupled-cluster theory are introduced by truncating the cluster operator  $T$  at a certain particle-hole excitation level. In this work we truncate  $T$  at the two-particle-two-hole excitation level, that is,  $T \approx T_1 + T_2$ , which gives the coupled-cluster method with singles and doubles excitations (CCSD). This is the most commonly used approximation, as it provides a good compromise between computational cost, on the one hand, and accuracy, on the other.

Within the CCSD approximation, the computational cost is given by  $n_o^2 n_u^4$ , where  $n_o$  and  $n_u$  denote the number of occupied and unoccupied orbitals, respectively. The correlated ground-state solution is given by the amplitudes  $t_i^a$  and  $t_{ij}^{ab}$  that solve the nonlinear equations

$$\langle \phi_i^a | \bar{H} | \phi_0 \rangle = 0, \quad (5)$$

$$\langle \phi_{ij}^{ab} | \bar{H} | \phi_0 \rangle = 0. \quad (6)$$

Here, the bra states are particle-hole excitations of the reference Slater determinant, and  $\bar{H}$  denotes the similarity-transformed Hamiltonian,

$$\bar{H} = e^{-T} H e^T = (H e^T)_c. \quad (7)$$

The subscript  $c$  indicates that only fully connected diagrams give nonzero contributions. Once  $T$  is determined from the solution of the coupled-cluster equations (5) and (6), the correlated ground-state energy is given by

$$E_0 = \langle \phi_0 | \bar{H} | \phi_0 \rangle. \quad (8)$$

The CCSD approach is known to work particularly well for the ground state of nuclei with closed (sub-)shells, as a Slater determinant provides a reasonable first approximation. In this work we use the equation-of-motion (EOM) [35,40–43] method to solve for the ground and excited states of the closed-shell nucleus  $A$  and its odd neighbors with mass number  $A - 1$ .

In the EOM, the ground and excited states of a nucleus with mass number  $B$  are obtained by acting with an excitation

operator  $\Omega_\mu$  on the ground-state wave function of a nucleus with mass number  $A$ , that is,  $\psi_\mu^B = \Omega_\mu \psi_0^A$ . Here  $\mu$  denotes quantum numbers such as spin, parity, and isospin projection. Within the EOM approach, the ground-state wave function  $\psi_0^A$  denotes the coupled-cluster wave function  $e^T \phi_0$ . In this work we choose either  $B = A$ , in which case we solve the excited states of the closed-shell nucleus  $A$ , or  $B = A - 1$ , in which case we solve the ground and excited states of the  $A - 1$  neighboring nucleus. We refer to EOM with a particle removal operator as PR-EOM. To solve for the excited states of the closed-shell nucleus  $A$ , we define  $\Omega_\mu$  by the excitation operators,

$$R^A = r_0 + \sum_{ia} r_i^a a_i^\dagger a_a + \frac{1}{4} \sum_{ijab} r_{ij}^{ab} a_a^\dagger a_b^\dagger a_j a_i, \quad (9)$$

$$L^A = 1 + \sum_{ia} l_i^a a_i^\dagger a_a + \frac{1}{4} \sum_{ijab} l_{ab}^{ij} a_i^\dagger a_j^\dagger a_b a_a. \quad (10)$$

Here, we suppressed the index  $\mu$ , but it is understood that the operators  $R^A$  and  $L^A$  excite and de-excite states with quantum numbers  $\mu$ , respectively. For the ground and excited states of the nucleus with mass number  $A - 1$ , we define  $\Omega_\mu$  by the particle removal operators,

$$R^{A-1} = \sum_i r_i a_i + \frac{1}{2} \sum_{ija} r_{ij}^a a_a^\dagger a_j a_i, \quad (11)$$

$$L^{A-1} = \sum_i l_i^a a_i^\dagger + \frac{1}{2} \sum_{ija} l_{ij}^a a_a^\dagger a_j^\dagger a_a. \quad (12)$$

Again, we suppressed the index  $\mu$  labeling the quantum numbers. The operators  $R_\mu = R^A$  ( $R_\mu = R^{A-1}$ ) commute with the cluster operator  $T$ , and the unknowns  $r_i^a, r_{ij}^{ab}$  ( $r_i, r_{ij}^a$ ) solve the EOM,

$$[\bar{H}, R_\mu] |\phi_0\rangle = \omega_\mu R_\mu |\phi_0\rangle, \quad (13)$$

which defines an eigenvalue problem for the excitation operator  $R_\mu$  with eigenvalue  $\omega_\mu = E_\mu - E_0$ . It is clear from definitions (4) and (7) that  $\bar{H}$  is non-Hermitian; dual-space solutions need to be calculated explicitly. We obtain the de-excitation operators  $L_\mu = L^A, L^{A-1}$  by solving the left eigenvalue problem,

$$\langle \phi_0 | L_\mu \bar{H} = \langle \phi_0 | L_\mu \omega_\mu. \quad (14)$$

The right and left eigenvectors form a biorthogonal set and are normalized in the following way:

$$\langle \phi_0 | L_\mu R_{\mu'} | \phi_0 \rangle = \delta_{\mu\mu'}. \quad (15)$$

The EOM solution for the ground state of system  $A$  is identical to the CC solution, so that  $R_0^A = r_0 = 1$ . Reference [35] provides a detailed description of the EOM.

### III. OVERLAP FUNCTIONS AND SPECTROSCOPIC FACTORS FROM COUPLED-CLUSTER THEORY

The one-particle overlap function between two wave functions  $\Psi_{A-1}$  and  $\Psi_A$  of nuclei with mass number  $A - 1$

and  $A$ , respectively, is defined as [22]

$$O_{A-1}^A(\vec{x}) \equiv \sqrt{A} \int d^{3(A-2)} \xi \Psi_{A-1}^*(\vec{\xi}) \Psi_A(\vec{x}, \vec{\xi}). \quad (16)$$

Here  $\xi$  represent the  $3(A-2)$  translationally invariant position coordinates and the  $A-1$  spin coordinates of  $A-1$  particles present in both  $\Psi_{A-1}$  and  $\Psi_A$ , while  $\vec{x}$  labels the position and spin of the additional particle in the nucleus with mass number  $A$  with respect to the center of mass of the nucleus with mass number  $A-1$ . The isospin coordinate has been suppressed.

In our coupled-cluster approach, however, we do not employ coordinates with respect to the center of mass, as this would limit us to light systems [44]. For this reason, the overlap is associated with a specific nucleon represented by a second quantization operator,

$$O_{A-1}^A(\vec{x}) \equiv \langle A-1 | a(\vec{x}) | A \rangle. \quad (17)$$

Here,  $|A\rangle$  and  $|A-1\rangle$  denote eigenstates in the nucleus with mass  $A$  and  $A-1$ , respectively. A few comments regarding the center of mass are in order. First, Eq. (16) describes the removal of a particle with respect to the center of mass, while Eq. (17) simply removes a particle at position  $\vec{x}$ . In principle, the removal of a particle with respect to the center of mass can be expanded in terms of single-particle annihilation and creation operators with the leading term being of the form of Eq. (17) [45]. Such an expansion is in powers of  $1/A$  and we thus consider its leading term. Second, the states  $|A\rangle$ ,  $|A-1\rangle$  need to factorize into a product of an intrinsic wave function and a center-of-mass wave function. In Sec. IV we show that this is indeed the case. This factorization is caused by the usage of the intrinsic Hamiltonian (1) and the employment of a sufficiently large model space [46]. In small spaces, one needs to explicitly remove spurious center-of-mass effects [28,47].

In Eq. (17)  $|A\rangle$  typically denotes the ground state, while  $|A-1\rangle$  is the ground state or an excited state. Our formalism will be kept general and is not limited to these cases. The radial overlap function  $O_{A-1}^A(lj; r)$  is derived by expanding  $\vec{x}$  in terms of partial waves,

$$a(\vec{x}) = (-)^{j-m} \sum_{ljm} \tilde{a}_{lj-m}(r) Y_{ljm}(\hat{x}). \quad (18)$$

Here,  $Y_{ljm}(\hat{x})$  is the spin-orbital spherical harmonic,

$$Y_{ljm}(\hat{x}) = [Y_l(\hat{r}) \otimes \chi_{1/2}(\sigma)]_{jm},$$

$Y_l(\hat{r})$  is the spherical harmonic of rank  $l$  and  $\chi_{1/2}(\sigma)$  is a fermionic spin function. The orbital angular momentum quantum number is denoted  $l$ , while  $j$  and  $m$  denote the rank and projection, respectively, of  $Y_{ljm}(\hat{x})$  as a spherical tensor. The hat denotes unit vectors, that is,  $\hat{x} \equiv \vec{x}/|\vec{x}|$ . We have also introduced the spherical annihilation operator  $\tilde{a}_{ljm}(r) = (-)^{j+m} a_{lj-m}(r)$ . The radial overlap is now given by the reduced matrix element and the overlap becomes<sup>1</sup>

$$O_{A-1}^A(\vec{x}) = \sum_j (-)^{j-m} (J_A M_A j - m | J_{A-1} M_{A-1}) \times O_{A-1}^A(lj; r) Y_{ljm}(\hat{x}). \quad (19)$$

Here,  $(\cdot | \cdot)$  denotes a Clebsch-Gordan coefficient. The overlap is now expressed by a radial function associated with each tensorial component  $Y_{ljm}(\hat{x})$ ,

$$O_{A-1}^A(lj; r) \equiv \langle A-1 | \tilde{a}_{lj}(r) | A \rangle = (-)^{j-m} \frac{\langle A-1 M_{A-1} | a_{ljm}(r) | A M_A \rangle}{(J_A M_A j - m | J_{A-1} M_{A-1})}. \quad (20)$$

This equation also defines the reduced matrix elements we employ.

The norm of the radial overlap function is the spectroscopic factor

$$S_{A-1}^A(lj) = \int dr r^2 |O_{A-1}^A(lj; r)|^2. \quad (21)$$

The overlap functions can be expressed in an energy basis by inserting the expansions

$$a_{ljm}^\dagger(r) = \sum_n a_{nljm}^\dagger \phi_{nlj}(r), \quad (22)$$

$$a_{ljm}(r) = \sum_n a_{nljm} \phi_{nlj}^*(r), \quad (23)$$

where  $n$  is the nodal quantum number and  $\phi_{nlj}(r)$  is the radial single-particle wave function associated with the orbits  $nljm$ . While  $a_{ljm}^\dagger(r)$  represents the creation of a particle at radial distance  $r$ ,  $a_{nljm}^\dagger$  represents the action of populating a single-particle orbit.

Assuming orthogonality of the single-particle wave functions, the spectroscopic factor is written as

$$S_{A-1}^A(lj) = \sum_n |\langle A-1 | \tilde{a}_{nlj} | A \rangle|^2 = \sum_n \frac{|\langle A-1 | a_{nljm} | A \rangle|^2}{(J_A M_A j - m | J_{A-1} M_{A-1})^2}. \quad (24)$$

Here we used the Wigner-Eckhart theorem for the reduced matrix elements. Equation (24) is our starting point, as we work in an uncoupled ( $m$ -scheme) basis. Using the EOM-CCSD solutions for the right and left eigenvalue problems for the  $A$  and the  $A-1$  systems, and employing the ground-state solutions for system  $A$ , Eq. (24) takes the form

$$S_{A-1}^A(lj) = \sum_n \frac{\langle \phi_0 | L_0^A \overline{a_{nljm}^\dagger} R_\mu^{A-1} | \phi_0 \rangle \langle \phi_0 | L_\mu^{A-1} \overline{a_{nljm}} R_0^A | \phi_0 \rangle}{(J_A M_A j - m | J_{A-1} M_{A-1})^2}. \quad (25)$$

This gives the equation for the spectroscopic factors as defined within coupled-cluster theory. We note that this equation is unambiguously and uniquely defined in terms of the left and right eigenstates of the nuclei with mass numbers  $A$  and  $A-1$ . This is clear, as the spectroscopic factor is given by the absolute value squared of the one-body overlap matrix element, so any ambiguity related to the normalization condition (15) is removed.

In Eq. (25) we have introduced the similarity-transformed creation and annihilation operators,

$$\overline{a_p^\dagger} = e^{-T} a_p^\dagger e^T, \quad (26)$$

$$\overline{a_p} = e^{-T} a_p e^T. \quad (27)$$

<sup>1</sup>Many authors use an alternative definition derived from  $\langle A | a^\dagger(\vec{x}) | A-1 \rangle$ .

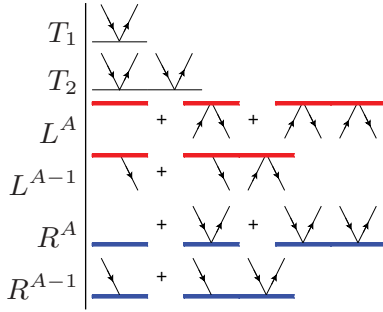


FIG. 1. (Color online) Left: Algebraic symbols for the particle-hole excitation operators and particle removal operators. Right: Corresponding diagrammatic representations. Arrows pointing up (down) represent particle (hole) orbits with implicit summation indices  $a, b, c, \dots$  ( $i, j, k, \dots$ ).

Using the Baker-Campbell-Hausdorff commutator expansion, we can derive algebraic expressions for  $\overline{a_p^\dagger}$  and  $\overline{a_p}$  in terms of the “bare” creation and annihilation operators  $a_p^\dagger$  and  $a_p$  and the particle-hole excitations amplitudes  $t_i^a$  and  $t_{ij}^{ab}$ ,

$$\overline{a_p^\dagger} = a_p^\dagger - \sum_b t_p^b a_b^\dagger - \frac{1}{2} \sum_{jbc} t_{pj}^{bc} a_b^\dagger a_c^\dagger a_j, \quad (28)$$

$$\overline{a_p} = a_p + \sum_i t_i^p a_i + \frac{1}{2} \sum_{ijc} t_{ij}^{pc} a_c^\dagger a_j a_i. \quad (29)$$

These equations can also be given in diagrammatic form, which provides a convenient bookkeeping system for the available Wick contractions in the expressions.

The coupled-cluster diagrams are similar to Goldstone diagrams. An algebraic Wick contraction corresponds to the diagrammatic connection of two directed lines, but the interpretation rules are slightly different. We refer the reader to Refs. [35] and [48] for a complete introduction to the diagrammatic approach. Here we only present the few concepts necessary to introduce the novel extensions of the formalism used in the context of spectroscopic factors.

Diagrammatic representations of the excitation and particle-removal operators  $T$ ,  $L_\mu$ , and  $R_\mu$  are displayed in Fig. 1. Lines with arrows pointing up (down) represent particle (hole) orbits. These lines have implicit indices  $a, b, c, \dots$  ( $i, j, k, \dots$ ) that are summed over. We suppress both the summation symbol and the dummy indices for a cleaner notation.

We have to deal with diagrams that represent operators with an index that is not being summed over. Such a creation (annihilation) operator is represented by a directed line pointing out from (into) a small circular vertex. The corresponding diagrams are displayed in the upper half of Fig. 2. Equations (28) and (29) can be reproduced diagrammatically as displayed in the lower half of Fig. 2. The possible Wick contractions between the creation and annihilation operators  $a_p^\dagger$  and  $a_p$  and the cluster operators  $T_1$  and  $T_2$  depend on whether the index  $p$  denotes an orbital above or below the Fermi surface. The small circular vertices distinguish the index fixed by the operator and is not summed over. In practice, the circle prevents an accidental connection of the operator line,

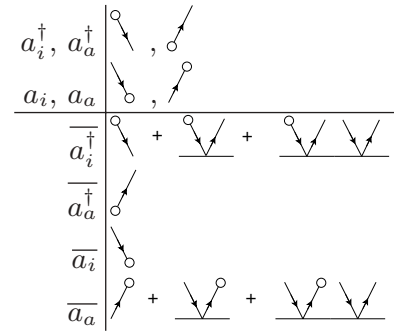


FIG. 2. Diagrammatic representation of the “bare” and the similarity-transformed second quantization operators. The horizontal bars represent the cluster operators  $T_1$  and  $T_2$ , as displayed in Fig. 1.

which would have introduced an erroneous Wick contraction when the spectroscopic factor diagrams are written down.

The overall sign of a diagram is determined according to standard rules [48]. The negative sign of the second and third terms in Eq. (28) is reflected in the  $\overline{a_i^\dagger}$  diagrams by the internal hole lines that connect the small open circle with the  $T$  operators. To determine the overall sign correctly for the spectroscopic factor diagrams, a sequence of directed lines ending or starting in a small circular vertex must be counted as a loop.

The diagrams in Figs. 1 and 2 are the basic building blocks for computation of the spectroscopic factor. We compute the matrix elements of the overlap function as products of the components  $R_\mu$ ,  $L_\mu$ , and either  $\overline{a_p^\dagger}$  or  $\overline{a_p}$ . The only nonvanishing contributions to the spectroscopic factor come from the diagrams in which all directed lines can be connected. These diagrams and the corresponding algebraic interpretation are shown in Fig. 3. We assume an implicit summation over repeated indices.

The computational cost of the spectroscopic factor diagrams has the very gentle scaling  $n_o^2 n_u^2$ , so the cost is completely dominated by the coupled-cluster and EOM calculations. In the case that  $|A\rangle$  is the ground state of the closed-shell nucleus, we have  $r_i^a = 0 = r_{ij}^{ab}$ , and several diagrams vanish.

#### IV. RESULTS

In this section we present our results for the calculation of the spectroscopic factor using *ab initio* coupled-cluster theory. We study the spectroscopic factor of nucleon removal from  $^{16}\text{O}$  by calculating the one-body overlap functions of  $^{16}\text{O}$  with the odd-mass neighbors  $^{15}\text{O}$  and  $^{15}\text{N}$  using the (PR-)EOM-CCSD approach to the ground and excited states of the  $A - 1$  nuclei. The CCSD approximation is used to calculate the ground state of  $^{16}\text{O}$ .

Our model space is spanned by oscillator states. We label the model space with the largest principal quantum number  $N$  that is included in the single-particle basis, so that the maximum single-particle energy is  $E_N = (N + \frac{3}{2})\hbar\omega$ , and the number of major oscillator shells is  $N + 1$ . In Fig. 4 we show the convergence of the ground state of  $^{16}\text{O}$  with increasing size of the model space for a wide range of oscillator frequencies  $\hbar\omega$ , using  $V_{\text{low-}k}$  with momentum cutoff  $\lambda = 2.0 \text{ fm}^{-1}$ . In Fig. 5

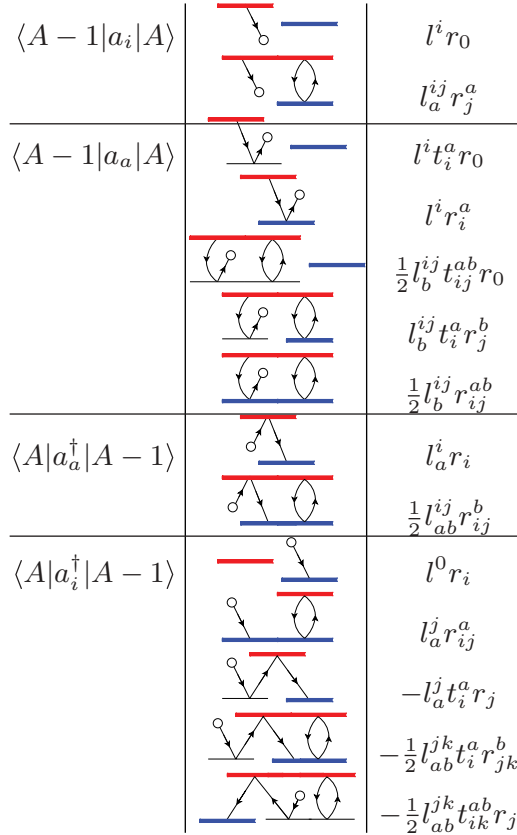


FIG. 3. (Color online) Diagrammatic representation of the overlap expressions; repeated indices imply a summation. If the closed-shell system is in the ground state, diagrams involving either  $r_i^a$  or  $r_{ij}^{ab}$  vanish. The individual components of these diagrams are explained in the captions to Figs. 1 and 2.

we show the convergence of the ground-state energies of  $^{15}\text{O}$  and  $^{15}\text{N}$  relative to the ground-state energy of  $^{16}\text{O}$ .

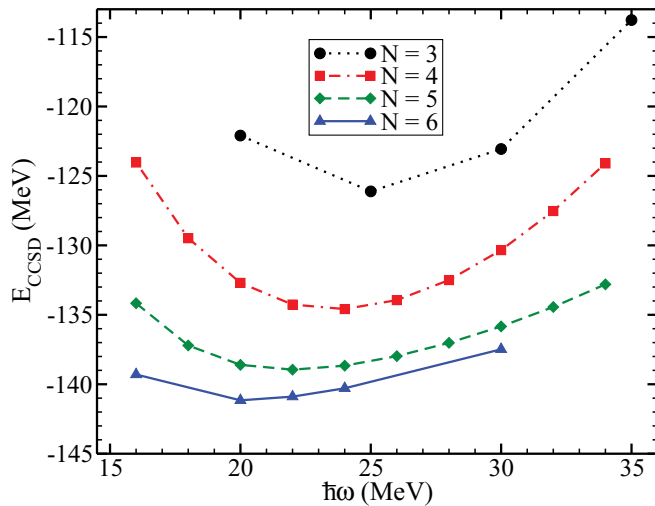


FIG. 4. (Color online) Convergence of the ground-state energy (within the CCSD) of  $^{16}\text{O}$  using a low-momentum potential with cutoff  $\lambda = 2.0 \text{ fm}^{-1}$  for increasing model space size  $N = 2n + l$  and as a function of the oscillator spacing  $\hbar\omega$ .

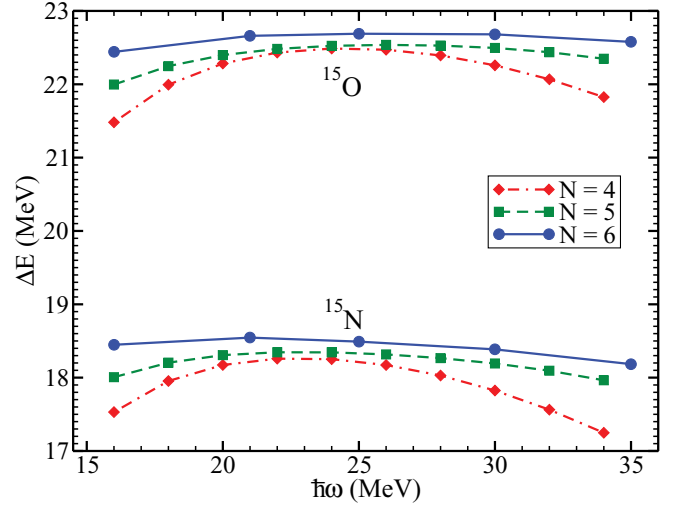


FIG. 5. (Color online) Convergence of the ground-state energies (within the PR-EOM-CCSD) of  $^{15}\text{O}$  and  $^{15}\text{N}$  relative to the ground-state energy of  $^{16}\text{O}$  using a low-momentum potential with cutoff  $\lambda = 2.0 \text{ fm}^{-1}$  for increasing model space size and as a function of the oscillator spacing  $\hbar\omega$ .

Our results shown in Figs. 4 and 5 show a weak dependence on  $\hbar\omega$  in the largest model space. We estimate that our results for the ground-state energies are converged within a few mega-electron volts in our largest model. We note that the CCSD ground state for  $^{16}\text{O}$  is overbound by  $\sim 15 \text{ MeV}$  compared to experiment and that the  $A = 15$  nuclei lack about 6 MeV of binding energy with respect to  $^{16}\text{O}$ . However, the energy difference between the ground state of  $^{15}\text{O}$  and that of  $^{15}\text{N}$  is  $\sim 4 \text{ MeV}$ , which is very close to the experimental value of 3.5 MeV. The main deficiency of our calculation is the omission of three-nucleon forces. The leading-order contributions of these forces are isospin symmetric [49], and it seems that this is the reason for the relatively good reproduction of the energy difference between the two  $A = 15$  nuclei.

The  $\hbar\omega$  dependence provides some information about how the finite size of the model space affects the solutions. For high values of  $\hbar\omega$ , the model space includes high-momentum states beyond the momentum cutoff  $\lambda$  of the interaction but is not sufficiently extended in position space to accommodate a nucleus. For small values of  $\hbar\omega$ , the model space is sufficiently wide in position space for the extension of the nucleus but does not contain sufficient high-momentum modes to resolve the cutoff  $\lambda$  of the interaction. Close to the minimum, in the largest model spaces considered, a good compromise is realized.

We also studied the energy levels using  $V_{\text{low-}k}$  for various momentum cutoffs in the range  $\lambda = 1.6\text{--}2.2 \text{ fm}^{-1}$ . The calculated ground-state energies for  $^{16}\text{O}$ ,  $^{15}\text{O}$ , and  $^{15}\text{N}$  are sensitive to the cutoff, implying that induced three-body forces and short-ranged forces of higher rank would contribute significantly to the calculated energies.

Let us turn to the spectroscopic factor for nucleon removal from  $^{16}\text{O}$ . Figure 6 shows the spectroscopic factor, Eq. (25),

$$\text{SF}(1/2^-) \equiv S_{15}^{16}(l=1, j=1/2), \quad (30)$$



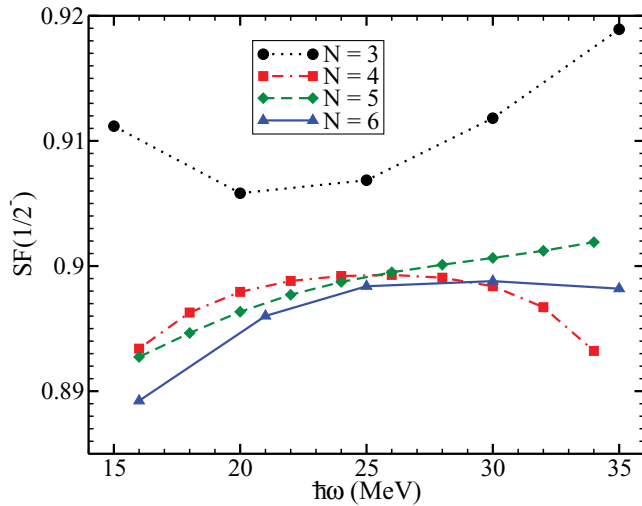


FIG. 6. (Color online) Spectroscopic factor  $SF(1/2^-)$  for proton removal from  $^{16}\text{O}$  as a function of the oscillator spacing  $\hbar\omega$  for different model spaces consisting of  $(N + 1)$  oscillator shells and a low-momentum interaction with cutoff  $\lambda = 2.0 \text{ fm}^{-1}$ .

for the removal of a proton with quantum numbers  $J^\pi = 1/2^-$  from  $^{16}\text{O}$  using a low-momentum interaction  $V_{\text{low-}k}$  with a cutoff  $\lambda = 2.0 \text{ fm}^{-1}$ . Evidently, the spectroscopic factor is well converged and depends very weakly on the size of the model space and the oscillator frequency  $\hbar\omega$ . It varies less than 1% over a wide range of oscillator frequencies. The spectroscopic factor  $SF(1/2^-)$  for neutron removal from  $^{16}\text{O}$  is almost identical to the  $SF(1/2^-)$  for proton removal. Recall that isospin is approximately conserved in light nuclei.

The dependence on momentum cutoff  $\lambda$  is displayed in Fig. 7. Note that the spectroscopic factor increases with decreasing cutoff. This is expected, as upon lowering of the cutoff the system becomes less correlated, the product state  $|\phi_0\rangle$  becomes an increasingly good approximation, and the

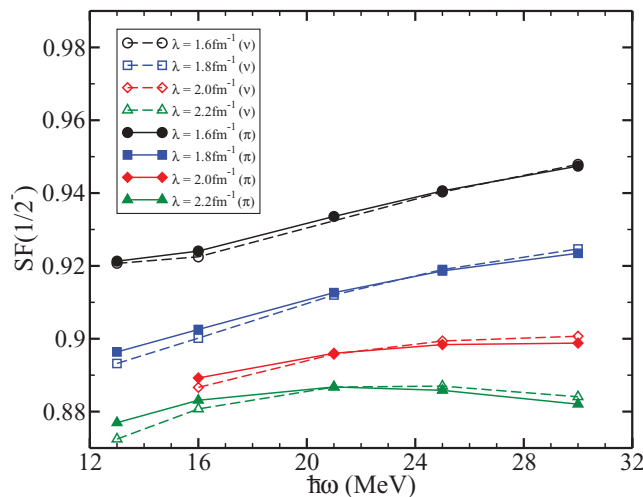


FIG. 7. (Color online) Spectroscopic factor  $SF(1/2^-)$  for neutron and proton removal as a function of the oscillator spacing  $\hbar\omega$  for nucleon-nucleon interactions with different cutoffs in a model space with  $N = 6$ .

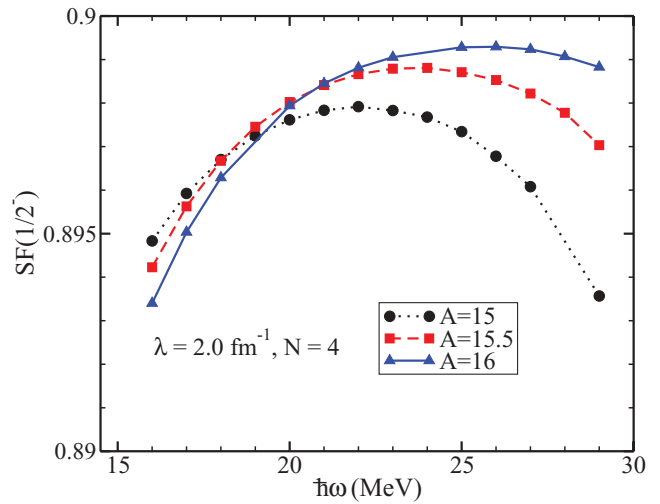


FIG. 8. (Color online) Spectroscopic factor  $SF(1/2^-)$  for proton removal from  $^{16}\text{O}$  as a function of the oscillator spacing  $\hbar\omega$  computed for different values of the mass number  $A$  employed in the intrinsic Hamiltonian, Eq. (1). The model space consists of  $N + 1 = 5$  oscillator shells, and the momentum cutoff of the nucleon-nucleon interaction is  $\lambda = 2.0 \text{ fm}^{-1}$ .

single-particle picture becomes more and more valid. Note also that isospin is approximately a good quantum number, as the spectroscopic factors for proton and neutron removal are almost identical.

Let us also study the center-of-mass problem. The intrinsic Hamiltonian, Eq. (1), depends on the mass number  $A$  of the nucleus, and the calculation of the spectroscopic factor requires us to employ identical Hamiltonians for nuclei with mass numbers  $A$  and  $A - 1$ . This constitutes a dilemma, as no choice of actual value for the parameter  $A$  can satisfy the parent and daughter nuclei simultaneously. It is thus necessary to investigate how strongly the spectroscopic factor depends on this value. Figure 8 shows the spectroscopic factor (in a model space  $N = 4$  for a momentum cutoff  $\lambda = 2.0 \text{ fm}^{-1}$  for different values of the mass number  $A$  of the intrinsic Hamiltonian. The dependence on  $A$  is very weak, and it is similar in size to the dependence on the parameters of the model space.

For an *intrinsic* Hamiltonian, the coupled-cluster wave function of a closed-shell nucleus factorizes into an intrinsic part and a Gaussian for the center of mass coordinate [46]. Following the procedure in Ref. [46], we confirmed that this factorization is present for the ground states of  $^{15}\text{O}$  and  $^{15}\text{N}$  in the largest model space we considered. We found that this factorization even takes place if the value  $A = 16$  for the mass number is employed in the intrinsic Hamiltonian, Eq. (1), for computation of the nuclei  $^{15}\text{O}$  and  $^{15}\text{N}$ . These results suggest that our approach to calculating spectroscopic factors within the coupled-cluster method is practically free of any center-of-mass contamination. In particular, it is not necessary to employ the corrections [28,47] that are caused by wave functions with spurious center-of-mass excitations.

So far, we have focused on the spectroscopic factors for removal of a  $J^\pi = 1/2^-$  proton and neutron from  $^{16}\text{O}$ . We finally also compute the spectroscopic factor for removal of a  $J^\pi = 3/2^-$  proton and a (deeply bound)  $J^\pi = 1/2^+$

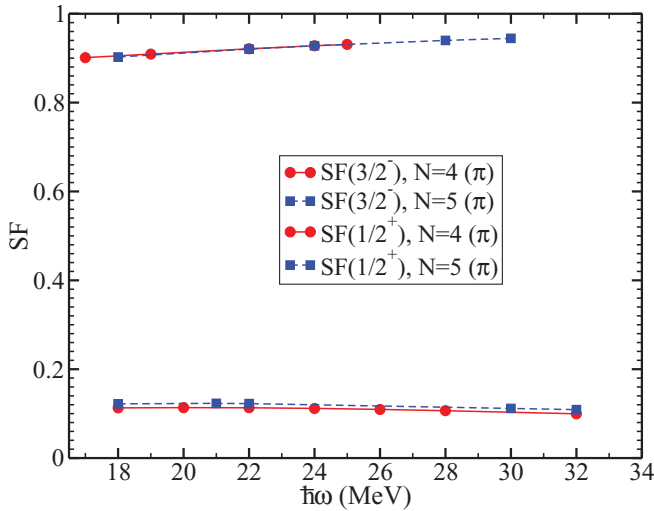


FIG. 9. (Color online) Spectroscopic factors  $SF(3/2^-)$  and  $SF(1/2^+)$  for proton removal from  $^{16}\text{O}$  as a function of the oscillator spacing  $\hbar\omega$ . The employed model spaces have  $N + 1$  oscillator shells, and the momentum cutoff of the nucleon-nucleon interaction is  $\lambda = 2.0 \text{ fm}^{-1}$ .

proton from  $^{16}\text{O}$ . The result is shown in Fig. 9 for different model spaces. As before, the results are well converged with respect to the size of the model space and display only a mild dependence on the oscillator frequency. We find that the spectroscopic factor  $SF(3/2^-)$  is similar in size to  $SF(1/2^-)$ . This is an interesting result. Barbieri and Dickhoff [25] also found, in their computation of spectroscopic factors, that  $SF(1/2^-) \approx SF(3/2^-)$  for nucleon removal from  $^{16}\text{O}$ . As expected, the spectroscopic factor of the  $J^\pi = 1/2^+$  state is very small. The removal of a deeply bound  $J^\pi = 1/2^+$  proton from  $^{16}\text{O}$  yields a highly excited state of  $^{15}\text{N}$  that is a rather complex superposition of many  $n$ -particle- $(n + 1)$ -hole states and thus has little overlap with a one-hole state.

## V. CONCLUSION AND OUTLOOK

We have extended the coupled-cluster method for the computation of spectroscopic factors. To this purpose, we derived diagrammatic and algebraic expressions of the one-body overlap functions based on EOM methods for the ground and excited states of the closed-shell nucleus with mass number  $A$  and the neighboring nuclei with mass number  $A - 1$ . We implemented the equations in an uncoupled  $m$  scheme and presented proof-of-principle calculations of the spectroscopic factor for proton and neutron removal from  $^{16}\text{O}$ . The calculated spectroscopic factors are well converged in model spaces consisting of six oscillator shells for low-momentum nucleon-nucleon interactions. Within the coupled-cluster approach, the same intrinsic Hamiltonian has to be employed in the nuclei with mass numbers  $A$  and  $A - 1$ . We found that the spectroscopic factor is insensitive to the actual value of the mass number that is employed in the intrinsic Hamiltonian.

We plan to implement the computation of the spectroscopic factor also in a spherical formulation of nuclear coupled-cluster theory. This will allow us to employ much larger model spaces, and we plan to apply the techniques to physically interesting nuclei, such as  $^{22,24}\text{O}$ ,  $^{48,52}\text{Ca}$ , and  $^{56,78}\text{Ni}$ .

## ACKNOWLEDGMENTS

We acknowledge discussions with C. Barbieri, E. Bergli, R. J. Furnstahl, and M. Hjorth-Jensen. Ø.J. thanks the University of Oslo and Oak Ridge National Laboratory (ORNL) for hospitality. This research was partly funded by Norwegian Research Council Project NFR 171247/V30 and by the US Department of Energy under Grant Nos. DE-FG02-96ER40963 (University of Tennessee) and DE-FC02-07ER41457 (SciDAC UNEDF). This research used resources of the National Center for Computational Sciences at ORNL.

- 
- [1] P. Navrátil, J. P. Vary, and B. R. Barrett, *Phys. Rev. C* **62**, 054311 (2000).
  - [2] S. C. Pieper and R. B. Wiringa, *Annu. Rev. Nucl. Part. Sci.* **51**, 53 (2001).
  - [3] A. Nogga, A. Kievsky, H. Kamada, W. Glockle, L. E. Marcucci, S. Rosati, and M. Viviani, *Phys. Rev. C* **67**, 034004 (2003).
  - [4] C. Ordóñez, L. Ray, and U. van Kolck, *Phys. Rev. C* **53**, 2086 (1996).
  - [5] P. Bedaque and U. van Kolck, *Annu. Rev. Nucl. Part. Sci.* **52**, 339 (2002).
  - [6] E. Epelbaum, H.-W. Hammer, and U.-G. Meißner, *Rev. Mod. Phys.* **81**, 1773 (2009).
  - [7] D. R. Entem and R. Machleidt, *Phys. Rev. C* **68**, 041001(R) (2003).
  - [8] S. K. Bogner, T. T. S. Kuo, and A. Schwenk, *Phys. Rep.* **386**, 1 (2003).
  - [9] S. K. Bogner, R. J. Furnstahl, and A. Schwenk, *Prog. Part. Nucl. Phys.* **65**, 94 (2010).
  - [10] P. Navrátil, V. G. Gueorguiev, J. P. Vary, W. E. Ormand, and A. Nogga, *Phys. Rev. Lett.* **99**, 042501 (2007).
  - [11] P. Navrátil, V. G. Gueorguiev, J. P. Vary, W. E. Ormand, A. Nogga, and S. Quaglioni, *Few-Body Syst.* **43**, 129 (2008).
  - [12] P. Navrátil, S. Quaglioni, I. Stetcu, and B. R. Barrett, *J. Phys. G: Nucl. Part. Phys.* **36**, 083101 (2009).
  - [13] E. Epelbaum, H. Krebs, D. Lee, and U.-G. Meißner, *arXiv:1003.5697v1*.
  - [14] G. Hagen, T. Papenbrock, D. J. Dean, and M. Hjorth-Jensen, *Phys. Rev. Lett.* **101**, 092502 (2008).
  - [15] C. Barbieri, *Phys. Rev. Lett.* **103**, 202502 (2009).
  - [16] S. Fujii, R. Okamoto, and K. Suzuki, *Phys. Rev. Lett.* **103**, 182501 (2009).
  - [17] G. Hagen, D. J. Dean, M. Hjorth-Jensen, and T. Papenbrock, *Phys. Lett. B* **656**, 169 (2007).
  - [18] K. M. Nollert, S. C. Pieper, R. B. Wiringa, J. Carlson, and G. M. Hale, *Phys. Rev. Lett.* **99**, 022502 (2007).
  - [19] S. Quaglioni and P. Navrátil, *Phys. Rev. Lett.* **101**, 092501 (2008).

- [20] P. G. Hansen and J. A. Tostevin, *Annu. Rev. Nucl. Part. Sci.* **53**, 219 (2003).
- [21] M. F. Macfarlane and J. B. French, *Rev. Mod. Phys.* **32**, 567 (1960).
- [22] J. M. Bang, F. G. Gareev, W. T. Pinkston, and J. S. Vaagen, *Phys. Rep.* **125**, 253 (1985).
- [23] R. J. Furnstahl and H. W. Hammer, *Phys. Lett. B* **531**, 203 (2002).
- [24] R. J. Furnstahl and A. Schwenk, [arXiv:1001.0328v1](#).
- [25] C. Barbieri and W. H. Dickhoff, *Int. J. Mod. Phys. A* **24**, 2060 (2009).
- [26] A. Polls, M. Radici, S. Boffi, W. H. Dickhoff, and H. Mütter, *Phys. Rev. C* **55**, 810 (1997).
- [27] W. J. W. Geurts, K. Allaart, W. H. Dickhoff, and H. Mütter, *Phys. Rev. C* **53**, 2207 (1996).
- [28] D. Van Neck, M. Waroquier, A. E. L. Dieperink, S. C. Pieper, and V. R. Pandharipande, *Phys. Rev. C* **57**, 2308 (1998).
- [29] A. Fabrocini and G. Co', *Phys. Rev. C* **63**, 044319 (2001).
- [30] F. Coester, *Nucl. Phys.* **7**, 421 (1958).
- [31] F. Coester and H. Kümmel, *Nucl. Phys.* **17**, 477 (1960).
- [32] J. Čížek, *J. Chem. Phys.* **45**, 4256 (1966).
- [33] J. Čížek, *Adv. Chem. Phys.* **14**, 35 (1969).
- [34] H. Kümmel, K. Lührmann, and J. Zabolitzky, *Phys. Rep.* **36**, 1 (1978).
- [35] R. J. Bartlett and M. Musiał, *Rev. Mod. Phys.* **79**, 291 (2007).
- [36] D. J. Dean and M. Hjorth-Jensen, *Phys. Rev. C* **69**, 054320 (2004).
- [37] G. Hagen, D. J. Dean, M. Hjorth-Jensen, T. Papenbrock, and A. Schwenk, *Phys. Rev. C* **76**, 044305 (2007).
- [38] G. Hagen, T. Papenbrock, D. J. Dean, M. Hjorth-Jensen, and B. Velamuri Asokan, *Phys. Rev. C* **80**, 021306(R) (2009).
- [39] S. K. Bogner, T. T. S. Kuo, and A. Schwenk, *Phys. Rep.* **386**, 1 (2003).
- [40] K. Kowalski, D. J. Dean, M. Hjorth-Jensen, T. Papenbrock, and P. Piecuch, *Phys. Rev. Lett.* **92**, 132501 (2004).
- [41] J. R. Gour, P. Piecuch, M. Hjorth-Jensen, M. Wloch, and D. J. Dean, *Phys. Rev. C* **74**, 024310 (2006).
- [42] J. Geertsen, M. Rittby, and R. J. Bartlett, *Chem. Phys. Lett.* **164**, 57 (1989).
- [43] D. J. Rowe, *Rev. Mod. Phys.* **40**, 153 (1968).
- [44] R. F. Bishop, M. F. Flynn, M. C. Bosca, E. Buendia, and R. Guardiola, *Phys. Rev. C* **42**, 1341 (1990).
- [45] B. Mihaila and J. H. Heisenberg, *Phys. Rev. C* **60**, 054303 (1999).
- [46] G. Hagen, T. Papenbrock, and D. J. Dean, *Phys. Rev. Lett.* **103**, 062503 (2009).
- [47] A. E. L. Dieperink and T. D. Forest, *Phys. Rev. C* **10**, 543 (1974).
- [48] T. D. Crawford and H. F. Schaefer III, *Rev. Comp. Chem.* **14**, 33 (2000).
- [49] E. Epelbaum, A. Nogga, W. Glöckle, H. Kamada, Ulf-G. Meißner, and H. Witała, *Phys. Rev. C* **66**, 064001 (2002).

# Closed-shell properties of $^{24}\text{O}$ with *ab initio* coupled-cluster theory

Ø. Jensen,<sup>1</sup> G. Hagen,<sup>2,3</sup> M. Hjorth-Jensen,<sup>4</sup> and J. S. Vaagen<sup>1</sup>

<sup>1</sup>*Department of Physics and Technology, University of Bergen, N-5007 Bergen, Norway*

<sup>2</sup>*Physics Division, Oak Ridge National Laboratory, Oak Ridge, TN 37831, USA*

<sup>3</sup>*Department of Physics and Astronomy, University of Tennessee, Knoxville, TN 37996, USA*

<sup>4</sup>*Department of Physics and Center of Mathematics for Applications, University of Oslo, N-0316 Oslo, Norway*

We present an *ab initio* calculation of spectroscopic factors for neutron and proton removal from  $^{24}\text{O}$  using the coupled-cluster method and the chiral nucleon-nucleon interaction at next-to-next-to-next-to-leading order with a cutoff of 500-MeV. In order to account for coupling to the scattering continuum we use a Berggren single-particle basis that treats bound, resonant, and continuum states on equal footing. We report neutron removal spectroscopic factors for the  $^{23}\text{O}$  states  $J^\pi = 1/2^+$ ,  $5/2^+$ ,  $3/2^-$  and  $1/2^-$ , and proton removal spectroscopic factors for the  $^{23}\text{N}$  states  $1/2^-$  and  $3/2^-$ . Our calculations support the accumulated experimental evidence that  $^{24}\text{O}$  is a closed-shell nucleus.

PACS numbers: 21.10.Jx, 21.60.De, 21.10.Pc, 31.15.bw, 24.10.Cn

*Introduction* The study of nuclei far from stability is a leading direction in nuclear physics, experimentally and theoretically. It represents a considerable intellectual challenge to our understanding of the stability of matter itself, with potential implications for the synthesis of elements. An important aspect of this research direction is to understand how magic numbers and shells appear and evolve with increasing numbers of neutrons or protons. The structure and properties of barely stable nuclei at the limits of stability, have been demonstrated to deviate dramatically from the established patterns for ordinary, stable nuclei. For an overview, see [1] and references therein. One of the striking features of nuclei close to the drip line is the adjustment of shell gaps, giving rise to different *magic numbers* [2]. The way shell closures and single-particle properties evolve as functions of the number of nucleons, forms one of the greatest challenges to our understanding of the basic features of nuclei, and thereby the stability of matter.

The chain of oxygen isotopes up to  $^{28}\text{O}$  is particularly interesting since these are the heaviest nuclei for which the drip line is well established. Two out of four stable even-even isotopes exhibit a doubly magic nature, namely  $^{22}\text{O}$  ( $Z=8, N=14$ ) and  $^{24}\text{O}$  ( $Z=8, N=16$ ). Several experiments [3–12] bring evidence that  $^{24}\text{O}$  is the last stable oxygen isotope. This is rather remarkable, in particular if one considers the fact that the addition of a single proton on top of the  $Z=8$  closed shell brings the drip line of the fluorine isotopes to  $^{31}\text{F}$ . Recent measurements [5] also suggest that  $^{24}\text{O}$  has a closed neutron shell. The isotopes  $^{25-28}\text{O}$  are all believed to be unstable towards neutron emission, even though  $^{28}\text{O}$  is a doubly magic nucleus within the standard shell-model picture. This indicates that the magic number at the neutron drip line for the oxygen isotopes is not at  $N=20$  but rather at  $N=16$ .

Although spectroscopic factors are not observable quantities [15, 16], they can be used to address shell closure properties within the context of a given model. Experimentally, spectroscopic factors are defined as the ratio of the observed reaction rate with respect to the same

rate, calculated with a particular reaction model and assuming a full occupation of the relevant single-particle states. The spectroscopic factors are then interpreted as the occupancy of specific single-particle states. Theoretically however, spectroscopic factors measure what fraction of the full wave function can be parameterized in terms of a correlated state (normally chosen to be a given closed-shell core) and an independent single-particle or single-hole state. Large deviations from the values predicted by an independent-particle model, point to a strongly correlated system.

Kanungo *et al* [5] reported measurements of one-neutron removal from  $^{24}\text{O}$ , and an extraction of spectroscopic factors. They used an eikonal reaction model and Woods-Saxon overlap functions, that were calculated with a well depth adjusted to reproduce the one-neutron separation energies. The results were compared with shell model predictions using the fitted *sd*-shell USDB interaction [13] and the SDPF-M interaction [14]. The theoretical calculations corroborate the large *s*-wave probability found in the experimental analysis, implying thereby that  $^{24}\text{O}$  is indeed a doubly magic nucleus.

The aim of this work is to add further theoretical evidence and support to these claims. We present spectroscopic factors for neutron and proton removal from  $^{24}\text{O}$  as predicted by the *ab initio* coupled-cluster method with the chiral nucleon-nucleon interaction by Entem and Machleidt [17] at next-to-next-to-next-to-leading order ( $\text{N}^3\text{LO}$ ). Our calculations are performed in a large single-particle basis which includes bound and continuum single-particle states. The above mentioned theoretical calculations of Refs. [13, 14] involve only fitted effective interactions tailored to small shell-model spaces, such as the *sd* or the *sd-pf* shells only.

The virtue of *ab initio* methods applied to nuclear physics is to reduce the model dependence of computed results. By means of a recipe for systematic improvements, one can distinguish between parameters of technical and physical character. Whereas the result may be expected to depend on physical parameters, it should be insensitive to the technical parameters as systematic



improvements are included. Ultimately, a converged *ab-initio* result may provide a rigorous test of the nuclear interaction model and the corresponding physical parameters. Since our single-particle basis contains continuum states, and therefore represents the correct asymptotical behaviour, we are able to generate radial overlap functions for drip-line nuclei. This paves the way for neutron-knockout reactions with fully *ab initio* structure information. This rapid communication should be considered a milestone on this path.

After these introductory remarks, we briefly expose our calculational formalism in the next section. Following that, our results are presented, while conclusions and perspectives are drawn in the final section.

*Hamiltonian and Method* The aim of this section is to give a short overview of the steps in our calculations. The nucleon-nucleon interaction [17], the coupled-cluster method [18–28] and the application to spectroscopic factors [29] have been presented in great detail elsewhere. Here we give only a brief summary of the concepts that enter the calculations leading to the results presented in this article.

We use an intrinsic  $A$ -nucleon Hamiltonian

$$\hat{H} = \hat{T} - \hat{T}_{\text{cm}} + \hat{V}. \quad (1)$$

Here  $\hat{T}$  is the kinetic energy,  $\hat{T}_{\text{cm}}$  is the kinetic energy of the center-of-mass coordinate, and  $\hat{V}$  is the two-body nucleon-nucleon interaction. Coupled-cluster calculations starting from this Hamiltonian have been shown to generate solutions that are separable into a gaussian center-of-mass wave function and an intrinsic wave function, see details in Refs. [27, 30].

The nucleon-nucleon interaction we use is the  $N^3\text{LO}$  potential of Entem and Machleidt [17]. The derivation of the interaction is based on chiral effective field theory, see for example Refs. [31–34] for recent reviews and details. The interaction includes terms up to next-to-next-to-next leading order in the momentum and is characterized by a momentum cut-off  $\Lambda = 500$  MeV. Other parameters which enter the interaction model are fitted to reproduce two-nucleon scattering data and properties of the deuteron. Although the interaction has a cut-off  $\Lambda = 500$  MeV, it still contains high momentum modes, and one typically need model spaces which comprise about 20 major oscillator shells in order to reach convergence for the ground states of selected oxygen and calcium isotopes, see for example Refs. [27, 35] for a discussion. However, exploiting the spherical symmetry of the interaction and our coupled-cluster formalism, we can use model spaces that are large enough so that there is no need for a subsequent renormalization of the interaction.

Short-range nucleon properties are not modelled explicitly, but are instead represented by contact terms in the interaction. The contact terms are subject to the fitting procedure, so the short range dynamics will be sensitive to the momentum cut-off. Since we are neglecting many-body forces like three-body forces or more complicated terms, our results will in general depend, less or

more, on the chosen cut-off of the nucleon-nucleon interaction model. Quantities that are sensitive to the short-range part of the wavefunctions, such as spectroscopic factors, may depend strongly on the chosen cut-off. This is why even *ab initio* calculations of spectroscopic factors must be considered as model dependent. Our results may be fully converged in terms of a given Hamiltonian and its parameters at a given level of many-body physics, however, employing another nucleon-nucleon interaction may lead to slightly different results since many-body terms beyond those represented by a two-body interaction can be very important. This is discussed in detail in Ref. [35].

The many-body wave function used to model the closed-shell nucleus  $^{24}\text{O}$  is written on the form

$$|\psi_0\rangle = \exp T |\phi_0\rangle. \quad (2)$$

Here,  $|\phi_0\rangle$  is an antisymmetric product state for all  $A$  nucleons. We use a Hartree-Fock solution for the reference state, as detailed in for example Ref. [27]. These Hartree-Fock solutions were built from the standard harmonic oscillator (HO) basis combined with Woods-Saxon (WS) single particle states for selected partial waves in order to properly reproduce effects of the continuum. The role of the continuum is expected to be important close to the drip line, as seen in Refs. [26, 36–38]. For this purpose we use a Berggren representation [39] for the neutron  $s_{1/2}$ ,  $d_{3/2}$ , and  $d_{5/2}$  partial waves. This representation generalizes the standard completeness relation to the complex energy plane. In the Berggren basis, bound, resonant, and non-resonant continuum states are treated on an equal footing. The Berggren ensemble has been successfully used within the Gamow shell model, see for example Ref. [37] for a recent review, and in *ab initio* coupled-cluster calculations of energies and lifetimes in Refs. [26, 28]. The Berggren basis is constructed by diagonalizing a one-body Hamiltonian with a spherical Woods-Saxon potential in a spherical plane-wave basis defined on a discretized contour in the complex momentum plane. We employ a total of 30 Gauss-Legendre mesh points along the contour for each of the  $s_{1/2}$ ,  $d_{3/2}$ , and  $d_{5/2}$  neutron partial waves. With 30 discretized single-particle states our results for the above single-particle states become independent of the choice of contour. For the choice of interaction that we use, the  $1/2^+$  and  $5/2^+$  states are fairly well bound with respect to  $^{22}\text{O}$  [27, 42], therefore it is sufficient to use a contour along the real energy axis. For all other partial waves, the basis functions are those of the spherical harmonic oscillator.

The cluster operator  $T$  introduces correlations as a linear combination of particle-hole excitations

$$T = T_1 + T_2 + \dots + T_A. \quad (3)$$

Here,  $T_n$  represents an  $n$ -particle- $n$ -hole excitation operator. The coupled-cluster solution for  $^{24}\text{O}$  is obtained as a set of amplitudes that defines  $T$ . The variable  $A$  denotes the number of particles in the system.

For the coupled-cluster singles and doubles approximation (CCSD) employed here,  $T$  is truncated at the level

of double excitations,

$$T = T_1 + T_2. \quad (4)$$

An important property of the coupled-cluster method is that the method is *size-extensive* even when  $T$  is truncated. This is due to the fact that only linked diagrams enter the equation, and it means that the energy scales correctly with system size, i.e. linearly for  $A \rightarrow \infty$ . Another important property that follows from the size-extensivity, is that the relative error related to the truncation of  $T$  is constant for increasing system size.

The calculation of spectroscopic factors follows the recipe detailed in Ref. [29]. However, the difference from Ref. [29] is that, all terms that contribute to the spectroscopic factors have been expressed in terms of reduced matrix elements in an angular momentum coupled basis. This allows us to handle a much larger set of single-particle states.

Left and right solutions for  $^{23}\text{O}$  are calculated with particle-removal equations-of-motion (PR-EOM-CCSD) using the CCSD ground state solution of  $^{24}\text{O}$  as the reference state. We refer the reader to Refs. [20, 26, 41] for details about the equation-of-motion approach combined with coupled-cluster theory.

We define the spectroscopic factors in the spherical coupled-cluster formalism as,

$$S_{A-1}^A(lj) = \sum_n \langle L_{\mu}^{A-1}(J_{A-1}) | \bar{a}_{nlj} | R_{\nu}^A(J_A) \rangle \times \langle R_{\mu}^{A-1}(J_{A-1}) | \bar{a}_{nlj} | L_{\nu}^A(J_A) \rangle^*, \quad (5)$$

where we have used the similarity transformed spherical annihilation operator, defined as

$$\bar{a}_{nljm} = e^{-T} \tilde{a}_{nljm} e^T \quad (6)$$

$$= (-1)^{j+m} e^{-T} a_{nlj-m} e^T. \quad (7)$$

Here,  $n$  and  $l$  are single particle nodal and orbital quantum numbers, and  $j, m$  labels the single particle angular momentum magnitude and projection. The isospin coordinate has been suppressed. Closed expressions for the similarity transformed operators are given in Ref. [29]. The states  $|R_{\nu}^A(J_A)\rangle$  and  $\langle L_{\nu}^A(J_A)|$  represent the right and left EOM-CCSD solutions for an  $A$ -body system with total angular momentum  $J_A$ . Similarly,  $|R_{\mu}^{A-1}(J_{A-1})\rangle$  and  $\langle L_{\mu}^{A-1}(J_{A-1})|$  are PR-EOM-CCSD solutions for the  $A-1$ -body system. The labels  $\mu$  and  $\nu$  are included to distinguish excited states. In the spherical formulation of EOM-CCSD, the solutions are spherical tensors [27], and the spectroscopic factor depends on the rank, but not on the projection of the EOM-CCSD states. In order to derive the coupled expressions, a Racah algebra module was developed for the open source computer algebra system SymPy[43]. More details about these calculations can be found in Ref. [40].

**Results** In Fig. 1 we plot the spectroscopic factors for removing a neutron in the  $s_{1/2}$  and  $d_{5/2}$  partial waves

of  $^{24}\text{O}$  as a function of the harmonic oscillator frequency  $\hbar\omega$ . The ground state  $1/2^+$  and excited  $5/2^+$  state in  $^{23}\text{O}$  were calculated within the PR-EOM-CCSD approximation starting from a Gamow-Hartree-Fock (GHF) basis with 30 mesh points for each of the  $s_{1/2}, d_{3/2}$  and  $d_{5/2}$  neutron partial waves and 17 major oscillator shells for the protons and remaining neutron partial waves. The spectroscopic factors are well converged with respect to the model space size. To investigate the role of continuum on the spectroscopic factors, we compare with a calculation done in a pure harmonic oscillator basis of 17 major shells.

We find that the effect of the continuum is small. This is expected, since our calculations of the  $1/2^+$  and  $5/2^+$  single particle states in  $^{24}\text{O}$  are rather well bound with respect to the neutron emission threshold. (See Ref. [27] for more details.) We do however see a small reduction of the spectroscopic factors with continuum included. The reduction of spectroscopic factors will be enhanced for states closer to the scattering threshold and this is also related to the Wigner cusp [44]. Although, the effect of continuum on the spectroscopic factors is marginal in the cases we consider, the effect is crucial in order to obtain the correct asymptotic behaviour of the overlap functions for one-neutron removal. It is the asymptotic normalization coefficient (ANC), which is calculated from the tail of the radial overlap function that enters the exact reaction amplitudes. It is arguably the physical relevant quantity to calculate for reactions [45].

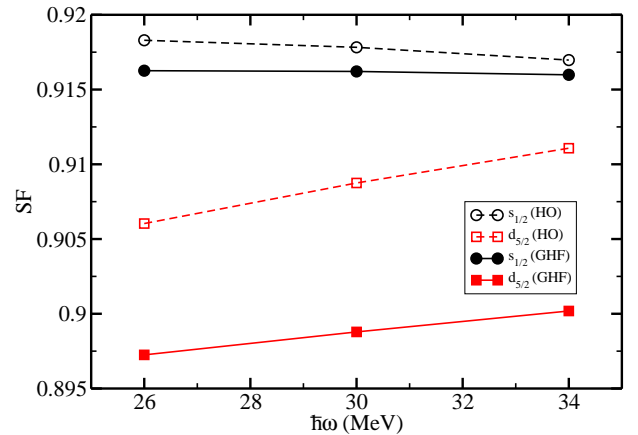


FIG. 1: (Color online) Normalized spectroscopic factors plotted against  $\hbar\omega$  for  $J^\pi = 1/2^+$  and  $5/2^+$  one-neutron removal from  $^{24}\text{O}$ . The continuum states included in the Berggren-basis calculation, leads only to a small reduction compared with the harmonic oscillator values. The dependence on the oscillator spacing  $\hbar\omega$  is very weak in both calculations. The inclusion of the continuum structure also gives a small, but visible, improvement in the  $\hbar\omega$  dependence.

In Fig. 2 we show our calculations of the spectroscopic factors for removing either a neutron or a proton in the  $p_{3/2}$  and  $p_{1/2}$  partial waves of  $^{24}\text{O}$ . The corresponding  $1/2^-$  and  $3/2^-$  states in  $^{23}\text{O}$  are highly excited, and we

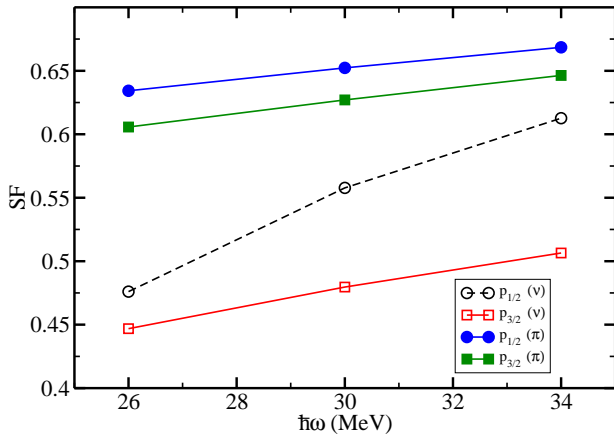


FIG. 2: (Color online) Normalized spectroscopic factors plotted against  $\hbar\omega$  for  $J^\pi = 1/2^-$  and  $3/2^-$  one-proton (pi in the figure) and one-neutron (nu in figure) removal from  $^{24}\text{O}$ . Results are for the Berggren basis only. The Berggren basis leads only to a small reduction compared with the harmonic oscillator values. The dependence on the oscillator spacing  $\hbar\omega$  is very weak in both calculations.

expect that correlations beyond  $2h - 1p$  are important. From Fig. 2 we see that the  $1/2^-$  and  $3/2^-$  states in both  $^{23}\text{O}$  and  $^{23}\text{N}$  can not be interpreted as simple one-hole states in  $^{24}\text{O}$ . The stronger dependence on the harmonic oscillator frequency  $\hbar\omega$  also indicates that we are missing many-body correlations beyond the  $2h - 1p$  level in our PR-EOM-CCSD computations of the  $1/2^-$  and  $3/2^-$  states in  $^{23}\text{O}$  and  $^{23}\text{F}$ .

Our results for spectroscopic factors and energies for the  $J^\pi = 1/2^+, 5/2^+, 3/2^-, 1/2^-$  states in  $^{23}\text{O}$  and the  $J^\pi = 1/2^-, 3/2^-$  states in  $^{23}\text{N}$  are presented in Table I. We present the values that were calculated with harmonic oscillator frequency  $\hbar\omega = 30\text{MeV}$ . The theoretical results obtained with the *sd*-shell USDB interaction [13] are 1.810 for the neutron  $1/2^+$  state and 5.665 for the neutron  $5/2^+$  state. The corresponding numbers for the SDFP-M interaction [14] are 1.769 and 5.593 for the  $1/2^+$  and  $5/2^+$  states, respectively. The corresponding energy differences for these two states are 2.586 MeV and 2.593 MeV for the SDFP-M interaction and the USDB interaction, respectively. As can be seen from Table I, our spacing is only 0.35 MeV. Since the other theoretical calculations, performed within small model-spaces, predict rather large spectroscopic factors, the *d*-wave state  $5/2^+$  should have been seen in the experiment of Kanungo *et al* [5]. The lack of such an observation supports the interpretation that this state is unbound, and this contradicts our findings here. The spectroscopic factors are however in good agreement with other theoretical calculations and the experimentally extracted value for the  $1/2^+$  state. We speculate that missing three-nucleon forces can play an important role regarding the shell gap between the  $1/2^+$  and  $5/2^+$  single particle states in  $^{24}\text{O}$ . We note, that it is the shell gap between the  $1/2^+$  and

the  $3/2^+$  states together with other quantities such as spectroscopic factors and *E2* transitions that determine the shell gap and magicity of the  $N = 16$  neutron number in  $^{24}\text{O}$ .

		PR-EOM-CCSD		Experiment	
		E	SF	E	SF
$^{23}\text{O}$	$1/2^+$	0.0	1.832	0.0	$1.71 \pm 0.19$
	$5/2^+$	0.35	5.393		
	$3/2^-$	12.4	1.919		
	$1/2^-$	13.4	1.116		
$^{23}\text{N}$	$3/2^-$	20.7	2.609		
	$1/2^-$	21.8	1.254	22.33	

TABLE I: Energies for states in  $^{23}\text{O}$  and  $^{23}\text{N}$  and corresponding spectroscopic factors (SF) for the removal of a particle from  $^{24}\text{O}$ . The reported coupled-cluster results are at the level of singles and doubles (CCSD), and are calculated with  $\hbar\omega = 30\text{MeV}$ . Experimental values are taken from Ref. [5].

Compared with the experimental results Table I, we note that the experimental error bars are typically orders of magnitude larger than the dependence on technical parameters displayed in Figs. 1 and 2.

However, there is still a considerable model dependence inherent in the calculation of spectroscopic factors. First of all, our calculations have been performed at the level of the singles and doubles approach, meaning that all correlations up to the level of two-particle-two-hole excitations are included to infinite order. Some selected higher *n*-particle-*n*-hole correlations are also included. The inclusion of triples correlations, that is the admixture of three-particle-three-hole correlations to infinite order, could change our results at the level of at most 10% for the various energies, as demonstrated in for example Refs. [20, 26, 27]. The effect of triples correlations on the ground state of nucleus *A* and  $3h - 2p$  excitations in the PR-EOM-CCM calculations of the *A* - 1 nucleus, on spectroscopic factors remains to be investigated. The largest uncertainty in our calculations is however the effect of three-body interactions arising in chiral perturbation theory. A recent analysis by Otsuka *et al* [42] demonstrates in shell-model calculations constrained by the degrees of freedom of the *sd*-shell, that three-body interactions are important in order to obtain the experimental trend in binding energies for the oxygen isotopes. Three-body interactions, included as density dependent corrections to the two-body interactions for the *sd*-shell, result in  $^{25}\text{O}$  as unbound with respect to  $^{24}\text{O}$ . This is however still an unsettled topic. A similar effect can be obtained at the level of two-body effective interactions by including higher-lying single-particle excitations in many-body perturbation theory.

The role of such three-body interactions in our calculations of spectroscopic factors and single-particle energies is a topic for future investigations.

*Conclusion and Outlook* We have computed single-

particle energies and spectroscopic factors for hole states in  $^{24}\text{O}$  using coupled-cluster theory at the level of singles and doubles correlations. The role of resonant and non-resonant continuum states has also been included in our investigations. For the hole states the major influence of the continuum states is to give final single-particle energies and spectroscopic factors which are almost independent of the chosen oscillator energy. The single-particle energies disagree with theoretical calculations that employ fitted interactions, however, our lack of many-body interactions beyond the two-body level may influence the final result. The spectroscopic factors for protons and neutrons obtained with *ab initio* coupled-cluster calculations support the emerging consensus that  $^{24}\text{O}$  is a doubly magic nucleus. In future work we plan to investigate the application of *ab initio* radial overlap functions to neutron knock-out reactions on drip line nuclei, thereby

removing a level of model dependence, also from the reaction analysis.

### Acknowledgments

Useful discussions with Gustav R. Jansen are acknowledged. This work was supported by the U.S. Department of Energy, under Grant Nos. DE-FG02-96ER40963 (University of Tennessee), and DE-FC02-07ER41457 (UN-EDF SciDAC). This research used computational resources of the National Center for Computational Sciences and the Notur project in Norway. ØJ and MHJ acknowledge support from the Research Council of Norway.

- 
- [1] M. Thoennessen, Rep. Prog. Phys. **67**, 1187 (2004).
  - [2] A. Ozawa *et al*, Phys. Rev. Lett. **84**, 5493 (2000).
  - [3] M. Fauerbach *et al*, Phys. Rev. C **53**, 647 (1996).
  - [4] D. Guillemaud-Mueller *et al*, Phys. Rev. C **41**, 937 (1990).
  - [5] R. Kanungo *et al*, Phys. Rev. Lett. **102**, 152501 (2009).
  - [6] M. Langevin *et al*, Phys. Lett. **150**, 71 (1985).
  - [7] H. Sakurai *et al*, Phys. Lett. **448**, 180 (1999).
  - [8] O. Tarasov *et al*, Phys. Lett. B **409**, 64 (1997).
  - [9] M. Thoennessen *et al*, Phys. Rev. C **68**, 044318 (2003).
  - [10] M. Stanoiu *et al*, Phys. Rev. C **69**, 034312 (2004).
  - [11] C. R. Hoffman *et al*, Phys. Lett. B **672**, 17 (2009).
  - [12] W. N. Catford *et al*, Phys. Rev. Lett. **104**, 192501 (2010).
  - [13] B. A. Brown and W. A. Richter, Phys. Rev. C **74**, 034315 (2006).
  - [14] Y. Utsuno, T. Otsuka, T. Mizusaki, and M. Honma, Phys. Rev. C **60**, 054315 (1999); Y. Utsuno, T. Otsuka, T. Glasmacher, T. Mizusaki, and M. Honma, Phys. Rev. C **70**, 044307 (2004).
  - [15] Furnstahl, R. J., and Hammer, H. W. Phys. Lett. B **531** (2002), 203.
  - [16] Furnstahl, R. J., and Schwenk, A. J. Phys. G **37**, 6 (2010), 064005.
  - [17] D. R. Entem and R. Machleidt, Phys. Rev. C **68**, 041001(R) (2003).
  - [18] J. Čížek, Adv. Chem. Phys. **14**, 35 (1969).
  - [19] J. Čížek, J. Chem. Phys. **45**, 4256 (1966).
  - [20] R. J. Bartlett and M. Musiał, Rev. Mod. Phys. **79**, 291 (2007).
  - [21] F. Coester, Nucl. Phys. **7**, 421 (1958).
  - [22] F. Coester and H. Kümmel, Nucl. Phys. **17**, 477 (1960).
  - [23] D. J. Dean and M. Hjorth-Jensen, Phys. Rev. C **69**, 054320 (2004).
  - [24] G. Hagen, T. Papenbrock, D. J. Dean, and M. Hjorth-Jensen, Phys. Rev. Lett. **101**, 092502 (2008).
  - [25] G. Hagen, T. Papenbrock, D. J. Dean, M. Hjorth-Jensen, and B. V. Asokan, Phys. Rev. C **80**, 021306(R) (2009).
  - [26] G. Hagen, T. Papenbrock, and M. Hjorth-Jensen, Phys. Rev. Lett. **104**, 182501 (2010).
  - [27] G. Hagen, T. Papenbrock, D. J. Dean, and M. Hjorth-Jensen, Phys. Rev. C **82**, 034330 (2010).
  - [28] G. Hagen, D. J. Dean, M. Hjorth-Jensen, and T. Papenbrock, Phys. Lett. B **656**, 169 (2007).
  - [29] Ø. Jensen, G. Hagen, T. Papenbrock, D. J. Dean, and J. S. Vaagen, Phys. Rev. C **82**, 014310 (2010).
  - [30] G. Hagen, T. Papenbrock, and D. J. Dean, Phys. Rev. Lett. **103**, 062503 (2009).
  - [31] P. Bedaque and U. van Kolck, Annu. Rev. Nucl. Part. Sci. **52**, 339 (2002).
  - [32] E. Epelbaum, H.-W. Hammer, and U.-G. Meißner, Rev. Mod. Phys. **81**, 1773 (2009).
  - [33] E. Epelbaum, H. Krebs, D. Lee, and U.-G. Meißner, Eur. Phys. J. A **45**, 335 (2010).
  - [34] E. Epelbaum, A. Nogga, W. Glöckle, H. Kamada, U.-G. Meißner, and H. Witała, Phys. Rev. C **66**, 064001 (2002).
  - [35] M. Hjorth-Jensen, D. J. Dean, G. Hagen, and S. Kvaal, J. Phys. G **37**, 064035 (2010).
  - [36] K. Tuskijama, M. Hjorth-Jensen and G. Hagen, Phys. Rev. C **80**, 051301 (2000).
  - [37] N. Michel, W. Nazarewicz, M. Płoszajczak, and T. Vertse, J. Phys. G **36**, 013101 (2009).
  - [38] A. Volya and V. Zelevinsky, Phys. Rev. C **74**, 064314 (2006).
  - [39] T. Berggren, Nucl. Phys. A **109**, 265 (1968).
  - [40] Ø. Jensen, PhD thesis, University of Bergen (2010), unpublished.
  - [41] J. R. Gour, P. Piecuch, M. Hjorth-Jensen, M. Włoch, and D. J. Dean, Phys. Rev. C **74**, 024310 (2006).
  - [42] T. Otsuka, T. Suzuki, J. D. Holt, A. Schwenk, and Y. Akaishi, Phys. Rev. Lett. **105**, 032501 (2010).
  - [43] SymPy Development Team (2010), SymPy: Python library for symbolic mathematics, [www.sympy.org](http://www.sympy.org)
  - [44] Michel, N., Nazarewicz, W., and Płoszajczak, M. Phys. Rev. C **75**, 031301 (2007).
  - [45] A. M. Mukhamedzhanov and A. S. Kadyrov, arXiv:1005.3788v1 (2010).